Robustness and Performance Enhancement in Smart Antenna Systems through Novel Beamforming Techniques

Thesis submitted in the fulfillment of the requirement for the degree of

DOCTOR OF PHILOSOPHY

by

DIKSHA THAKUR

DEPARTMENT OF ELECTRONICS & COMMUNICATION ENGINEERING

JAYPEE UNIVERSITY OF INFORMATION TECHNOLOGY

WAKNAGHAT-173234, DISTRICT-SOLAN, H.P., INDIA

August 2024

Contents

DECLARATION BY THE SCHOLAR

I hereby declare that the work reported in the Ph.D. thesis entitled "**Robustness and Performance Enhancement in Smart Antenna Systems through Novel Beamforming Techniques**" at **Jaypee University of Information Technology, Waknaghat, Solan (H.P.) India**, is an authentic record of my work carried out under the supervision of **Dr. Vikas Baghel** and **Dr. Salman Raju Talluri**. I have not submitted this work elsewhere for any other degree or diploma. I am fully responsible for the contents of my Ph.D. Thesis.

Diksha Thakur
(Enrollment No.: 186004)
Department of Electronics and Communication Engineering
Jaypee University of Information Technology,
Waknaghat, Solan, H.P., 173234, INDIA

Date:16/08/2024

SUPERVISORS CERTIFICATE

This is to certify that the work reported in the Ph.D. thesis entitled **"Robustness and Performance Enhancement in Smart Antenna Systems through Novel Beamforming Techniques"**, submitted by **Diksha Thakur** at **Jaypee University of Information Technology, Waknaghat,** is a bonafide record of her original work carried out under our supervision. This work has not been submitted elsewhere for any other degree or diploma.

Dr. Vikas Baghel
Assistant Professor (SG)
Department of Electronics &
Communication Engineering
Jaypee University of Information
Technology
Waknaghat, Solan, H.P., 173234, India

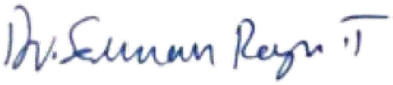

Dr. Salman Raju Talluri
Assistant Professor (SG)
Department of Electronics &
Communication Engineering
Jaypee University of Information
Technology
Waknaghat, Solan, H.P., 173234, India

Date:16/08/2024

Acknowledgement

I express my gratitude and dedicate all accomplishments to the Almighty GOD for the strength, wisdom, and perseverance bestowed upon me during this research and throughout my life.

I am delighted to express my sincere appreciation to my supervisors, Dr. Vikas Baghel and Dr. Salman Raju Talluri, who generously provided me with the opportunity to work under their guidance. I am grateful to both of them for their patience, unwavering support, positive outlook, ongoing discussions, timely advice, and freedom throughout this course.

I would like to express my heartfelt gratitude to the Vice-chancellor Prof. (Dr.) Rajendra Kumar Sharma, the Dean of Academic Research Prof. (Dr.) Ashok Kumar Gupta and the JUIT administrations for furnishing the necessary amenities and infrastructure that facilitated the completion of this research work.

I am deeply grateful for the generous cooperation of Dr. Rajiv Kumar, Head of the Department of Electronics and Communication Engineering, throughout the course of this research. My sincere appreciation goes out to all the members of the DPMC, including Prof. Dr. P.B. Barman, Dr. Sunil Dutt Sharma, and Dr. Naveen Jaglan , for their assistance, constructive feedback, and invaluable suggestions at every stage of this study. I also want to convey my heartfelt thanks to all the faculty members of the Department of Electronics and Communication Engineering for their support.

I am immensely grateful to my family members for their unwavering love and support throughout this journey. My success is attributed to the dedication and encouragement

of my parents, Mr. Suresh Thakur and Mrs. Kanta Thakur. Above all, I want to express my gratitude to my mother-in-law Mrs. Rajana, my husband Mr. Vishal Dhiman and my daughter Divisha, for their exceptional belief, love, and for creating the supportive environment that allowed me to complete this research work.

I express gratitude to my colleagues and friends, Garima Thakur, Vishakha Thakur, and Ratish, who have provided assistance in various ways. I treasure the time I spent in the Department of Electronics and Communication Engineering at JUIT, Waknaghat.

Finally, I extend my sincere gratitude to all those individuals from the bottom of my heart who contributed to the realization of this thesis.

Diksha Thakur

List of Acronyms

Sr. No.	Acronym	Full form
1	ADCs	Analog to digital convertors
2	BW	Beamwidth
3	BWFM	Beamwidth between first minimas
4	CMT	Covariance matrix taper
5	DSP	Digital signal processing
6	DOA	Direction of arrival
7	IF	Improvement factor
8	INCM	Interference-plus-noise covariance matrix
9	INR	Interference-to-noise ratio
10	LHCP	Left-hand circular polarization
11	MSE	Mean square error
12	MVDR	Minimum variance distortionless response
13	OD	Orthogonal diagonalization
14	OPSO	Orthogonal particle swarm optimization
15	OSINR	Output SINR
16	PGRCB	Proximal gradient based RCB
17	PSO	Particle swarm optimization
18	RHCP	Right-hand circular polarization
19	RCB	Robust Capon beamformer
20	ROI	Region of interest
21	ROIs	Regions of interest
22	SA	Sparse array
23	SCB	Standard Capon beamformer
24	SCB-DB	SCB-dual beam
25	SINR	Signal-to-interference-noise ratio
26	SNR	Signal-to-noise ratio

Sr. No.	Acronym	Full form
27	SLL	Sidelobe level
28	SOCP	Signal-to-interference-noise ratio
29	SOI	Signal of interest
30	TDL	Tapped delay line
31	ULAs	Uniform linear arrays
32	VSP	Vector space projection

List of Figures

List of Tables

Abstract

Beamforming is a technique used to process signals received by an array of antennas. It amplifies signals coming from desired directions while reducing the strength of signals coming from undesired directions. The algorithms used to perform real-time beamforming are called adaptive beamformers. The adaptive beamforming algorithms are sensitive to certain circumstances, such as the steering vector errors, small samples for parameter estimation, non-stationary interference signals, increase sidelobe level (SLL), multiple desired signals, etc. The errors in the steering vector arise from various factors, including mismatch in the direction of arrival (DOA) of signal of interest (SOI), perturbation in propagation medium, sensor position uncertainty, imperfect antenna array calibration etc. Therefore, to overcome these problems, robust adaptive beamformers are required. In this work, various robust beamformers have been developed to enhance the efficacy of beamforming algorithms in different scenarios. The foremost cause of the steering vector error is DOA mismatch, so the true direction of the desired signal is estimated iteratively through proximal gradient approach. The regularization function is utilized to modify a hyper-parameter for each iteration and also guarantees that the estimated direction is sufficiently close to the actual direction in case of large DOA mismatch. In a moving interference environment, traditional algorithms become ineffective as the interferences may shift outside the null created by the beamforming algorithm. Expan- ding the nulls effectively resolves the issue of moving interferences. The process of null widening involves modifying the steering vector by introducing a taper matrix of imaginary interferences alongside the original one. Hence, an algorithm is developed for moving interferences along with DOA mismatch. To address the DOA mismatch, the approach is to maximize the signal-to-interference-noise ratio (SINR) output while adhering to specific constraints on the response levels within the region of interest (ROI). A bi-objective optimization problem has been formulated for dual desired signals and SLL control in the vicinity of the two desired signals. To accomplish the bi-objective, standard Capon beamformer (SCB) is modified by incorporating a limited number of constraints into it. The proposed algorithm can form dual beams for

receiving the two SOIs simultaneously amidst interference and noise , while also regulating the SLL to a predefined level. This work is geared towards designing the sparse arrays with only 50% antenna elements of the full array. The resulting sparse array undergoes further analysis, considering additional constraints to enhance the performance of the SCB in terms of mitigating SLL, addressing grating lobes, and minimizing mutual coupling. This work also explored the area of evolutionary computing. The algorithms such as orthogonal particle swarm optimization (OPSO) and particle swarm optimization (PSO) have been utilized for beamforming. Mean square error (MSE) based novel objective function is developed for the implementation of wideband beamforming. Frequency invariant beampatterns are obtained with OPSO and PSO over the 200MHz bandwidth.The simulation results clearly demonstrate that the proposed techniques are better than the current techniques in terms of various performance metrics.

Chapter 1

Introduction

Smart antennas [1, 2] have maintained their popularity over the years due to the continuous advancements in wireless technology. The phrase "smart antenna" typically describes an array of antenna elements [3] that is associated to an advanced signal processor. Here, the signal processor refers to an adaptive algorithm used for processing the signals received on the array of antenna [4]. The primary objective of adaptive algorithms is to boost the SOI while suppressing the interferences along with the noise at the array output [5]. This process is commonly referred to as "beamforming".

The process of beamforming is accomplished by multiplying the signals received with adjustable weights that are determined using different adaptive beamforming algorithms. Adaptive algorithms are employed to dynamically adjust these weights to achieve desired performance characteristics such as maximizing signal strength, minimizing interference, or tracking a moving target. The weight vector is applied to the antenna elements to form the desired beam pattern. The weight vector in adaptive beamforming algorithms consists of both amplitude and phase components for each antenna element. These components are crucial for controlling the direction and shape of the antenna array's radiation pattern.

The amplitude of each antenna element affects the strength of the signals received or transmitted by each element. By varying the amplitudes, the overall beam pattern

can be shaped to amplify signals from desired directions while minimizing interference and noise from undesired directions. The phase of the signal at each antenna element shifts the phase relationship between elements. By controlling the phase, the system can direct the beam towards a specific target or direction, enhancing signal reception and transmission in that direction. The pictorial representation of the smart antenna system [6] is depicted in Figure 1.1. To practically implement the adaptive algorithms and control the array weights, several components and technologies are required:

- Antenna Elements: The individual radiating elements that form the array. These can be dipole, patch, or any other suitable type of antenna.
- RF front end: Each antenna element has its own RF chain, which includes amplifiers, phase shifters, and variable attenuators. The adaptive weights are applied within these RF chains to control the amplitude and phase of the signals.
- Digital signal processing (DSP) Unit: This unit is critical for real-time signal processing and execution of adaptive algorithms. It includes:
  - Analog to digital convertors (ADCs) : Convert the analog signals received by the antenna elements into digital form for processing.
  - DSP: High-performance DSP are used to execute the adaptive algorithms in real-time. These processors calculate the optimal weights based on the incoming signal data and the desired beam pattern.
- Feedback Mechanism: A feedback loop is established between the antenna array and the DSP unit. The system continuously monitors the received signals and dynamically updates the weights based on the output of the adaptive algorithm. This real-time feedback ensures that the antenna array can adapt to changing signal environments, maintaining optimal performance.

In literature, numerous adaptive algorithms are employed to compute beamforming weights in a dynamic signal environment, ensuring that the wireless system's performance is maintained. However, the traditional beamforming algorithms often suffer from

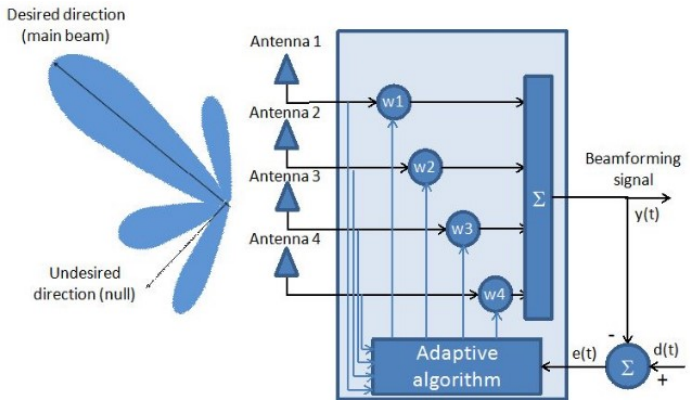

Figure 1.1: Smart Antenna System

substantial performance degradation due many situations such as mismatches in the signal steering vector, limited snapshot number, existence of the target signal within the training snapshots, mobile interferences, etc [7, 8]. Thus, robust beamformers are required to obtain good performance in these situations. In the literature, diverse robust beamformers have been presented based on different techniques such as diagonal loading and its variants, eigen space based methods, uncertainty based techniques, reconstruction based methods, etc. These different approaches are described in the next section.

1.1 Literature review

Various robust beamforming methods are reviewed in this section. These robust techniques are applied on the SCB which is also known as minimum variance distortionless response (MVDR).

1.1.1 Diagonal loading and its variants

Diagonal loading has been a prominent technique to improve the robustness against a small number of samples and mismatches in the signal steering vector. In the diagonal loading, the covariance matrix has been modified to achieve robustness, and the modification has been done by incorporating a weighted identity matrix into it [9].

The primary purpose of diagonal loading is to determine the scaling factor, referred to as the loading level, by which scaling is performed. The diagonal loading technique has been formulated in [10] by placing additional limits to the weight vector's norm, and the covariance matrix has diagonally loaded with an appropriate multiple of the identity matrix. In the work by [11], an additional constraint has been introduced to the disparity between the weight vector and the desired weight vector, leading to the derivation of diagonal loading. However, there is no relation between the loading level and the uncertainty set of the steering vector. Therefore, a sophisticated diagonal loading-based approach has been proposed in [12], where the loading value has been calculated with the uncertainty bound of the steering vector. But in reality , it has been very difficult to obtain the uncertainty bounding value, and therefore the calculation of the loading level also became challenging. Moreover, the algorithm will not be robust if the uncertainty set parameter has not been chosen correctly. A robust adaptive beamformer has been presented in [13] that calculates the loading level dynamically. This method, on the other hand, requires iterations and will place a computing load on an adaptive beamformer. So, a less computationally complex method has been proposed in [14] to calculate the loading value.

The authors of [15] have employed only single snapshot for DOA estimation [16] which can subsequently be employed in a beamforming algorithm. A constant modulus-based robust beamformer has been proposed in [17] to achieve robust adaptive beamforming. The loading value has been determined by utilizing the constant modulus property of the desired signal. A few diagonal loading techniques have been presented in the literature that are fully automatic [18], [19]. To find the diagonal loading level, they do not need any user parameter. Some variable loading techniques have also been proposed in the literature. In the variable loading approach, the loading has been done in such a way that the loading factor only provides for the lower eigenvalues of the covariance matrix. A simple less complex variable loading adaptive beamformer has been described in [20] and the loading factor has been determined in an ad-hoc manner.

To further improve the performance, a low-complexity variable loading beamformer in [21] that dynamically changes the value of the loading level with the practical

scenario. To generalize the diagonal loading technique, a robust beamformer has been proposed that is based on tridiagonal loading. The diagonal loading has been realized by regularizing the covariance matrix with the tridiagonal Toeplitz matrix. Recently, the mismatch in the signal steering vector has been rectified using the diagonal loading method [22]. Instead of using any uncertain parameters which are very hard to estimate practically, the suggested methodology determined the loading factor from the optimization problem of weight vector calculation.

1.1.2 Eigen-space based methods

When the performance of conventional beamformers has been degraded due to errors in the sample covariance matrix. The errors in the sample covariance matrix mainly occurred because of a small number of snapshots available for its calculation and the perturbation errors occur due to various reasons such as discrepancy between the presumed and actual signal steering vectors, pointing error in the direction of SOI, imperfect calibration of the sensor array, etc. To mitigate the effects of these errors, another class of robust beamformers have been presented which are known as eigen-space based beamformers. In this method, the signal plus interference subspace has estimated from the sample covariance matrix and then the actual steering vector has estimated by projecting the presumed steering vector on the estimated subspace [23]. This approach was initially introduced in [24], where the weight vector is computed using the signal plus interference subspace. It has been demonstrated that this technique converges more rapidly compared to the conventional beamformer.
[25] illustrated a signal subspace-based robust beamformer against steering vector errors mainly due to look direction error. The proposed methodology has been analyzed with and without the steering vector error. From the analysis, it has been noticed that it enhances performance in the presence of errors while providing the best performance when the errors are absent. The proposed technique can be applied as long as the sample covariance matrix can be divided into signal and noise subspaces. The effect of pointing error on the conventional sample matrix inversion

beamformer and the eigen-space-based beamformer has been studied in [26]. The output SINR of both the considered beamformers has been evaluated to examine their performance in the presence of pointing error. A robust adaptive beamformer against array imperfections has been provided in [27] and the mentioned goal has been achieved by determining the proper steering vector orthogonal to the noise subspace. Another projection method described in [28] has been used to provide robustness by modifying the presumed steering vector. The modification has again been done by projecting the presumed vector onto the subspace associated with the principal eigenvectors of the covariance matrix. However, the described eigenspace-based beamformers do not improve the array's ability to receive the SOI. As it is already known, even a little pointing error might cause a significant performance reduction. An effective solution for steering vector errors has been offered in [29] that utilizes the signal subspace technique. The suggested method has reduced level of computational complexity compared to the current beamformers since it uses subarrays to calculate the signal subspace and estimate the actual steering vector instead of the original array. To further improve the robustness in the case of eigen-space-based beamformers, an algorithm has been presented in [30]. Firstly, the signal plus interference subspace has been constructed using an eigen decomposition, and then the constructed signal subspace has been employed for the calibration of the presumed steering vector. Numerous simulations have demonstrated the viability of the suggested method.

It is already known that pointing error may lead to performance deterioration of the eigen-space-based beamformers, and the robustness against pointing error has been presented in the described literature. However, when the pointing errors are large, the SOI may be considered interference, and instead of enhancing it, the beamformer can suppress it. So, to deal with large pointing errors, a generalized eigen-space-based beamformer has been given in [31]. A full array has been utilized to calculate the actual steering vector and signal subspace. Now, to handle the large steering vector mismatch and in situations of low signal-to-noise ratio (SNR), a modified approach has been developed in [32]. Firstly, the covariance matrix has been estimated from the received data, and then the signal subspace has been evaluated from the eigenvectors of the estimated covariance matrix. Finally, the weight vector has been calculated

with the estimated covariance matrix and the signal subspace. Another different approach has been presented in [33] named vector space projection (VSP), which is employed for the elimination of pointing errors. Moreover, the power of SOI has been evaluated in a single step using the covariance fitting approach. Although the eigen-space beamformers provide robustness against steering vector errors, the performance of most of the beamformers deteriorates in situations of low SNR. So, an algorithm has been suggested in [34] that provides optimum performance in the case of a low SNR scenario. The estimation of the new steering vector has been done by the eigen decomposition method and solved by quadratically constrained quadratic programming, which increases the computational complexity. Recently, an approach has been presented in [35] that approximates the eigen-space projection beamformer. The accurate steering vector of SOI has been estimated by orthogonally projecting the presumed signal steering vector onto the signal subspace.

It is described that eigen-space-based beamformers have many advantages as they offer robustness against various factors of steering vector errors. Nonetheless, it has many shortcomings, such as performance degradation in low SNR scenarios, prior knowledge of the number of sources, performance degradation in cases of unknown dimensions or incorrect dimensions of subspaces, etc.

1.1.3 Uncertainty set constraint based methods

Uncertainty involves scenarios in which there is incomplete or imprecise knowledge about the steering vector. The method based on uncertainty set constraints is widely recognized as a prominent approach in robust adaptive beamforming. In this category of robust beamforming, the steering vector of the SOI is estimated by incorporating spherical or ellipsoidal uncertainty constraints on the signal steering vector. The actual signal steering vector is represented as the summation of the assumed steering vector and the uncertainty set.

A beamforming approach grounded in worst-case performance optimization has been introduced in both [36] and [37]. The beamformer offers robustness against an

unknown signal steering vector by employing the spherical constraints in the mathematical modeling of the algorithm. In the optimization problem, the output interference plus noise power have been minimized while forcing the magnitude response of the signal steering vector to be distortionless. The problem has been formulated using second order cone programming (SOCP) and solved using the interior point method. But the worst case optimization based methods are not able to provide closed form solutions as they have used SOCP, moreover, they do not provide easy online execution. To have simpler closed form solutions, another worst case based beamformer has been suggested in [13]. The proposed approach has provided a general approach that can be applied to single rank as well as higher rank signal models. The generalization has been executed by designing the SOI's uncertainty using the covariance matrix instead of the steering vector.

The efficacy of considered worst case based algorithms can be further enhanced by extending these for non-stationary interferences. So, a new approach has been explained in [38] which provides robustness against steering vector uncertainties along with robustness to rapidly moving interferences. The steering vector uncertainties have been dealt by using worst case optimization of [36] and to ensure nulling of non-stationary interferences, the tapering of the covariance matrix has been done. To enhance the robustness of worst case based technique an additional constraint has been added to the norm of the steering vector in [39]. The other parameters and the preliminary insights needed for the proposed method are the same as that of the worst case approach. The proposed approach consists of two constraints in the optimization problem hence named a doubly constrained robust beamformer and due to the additional constraint, It has offered an improved estimation of the steering vector

In [40] and [41] ellipsoidal uncertainty has been employed instead of spherical uncertainty to deal with steering vector errors. The weight vector in [40] has been evaluated by minimizing the total output power subject to the condition that the gain for each response in the defined ellipsoid must be greater than one. The SOCP has been employed as the optimization problem for the calculation of the optimum weight vector, and further, the optimization problem has been solved by the Lagrange

multiplier. The formulation used in [41] has been similar to the doubly constrained robust beamformer of [39] but spherical uncertainty has been replaced by ellipsoidal uncertainty. The advantage of using ellipsoidal uncertainty over spherical one is that it can provide a more realistic depiction of the uncertainty.

A different approach has been investigated in [42] which assumed that the mismatch vector is random in nature. In worst-case-based approaches, the assumption is made that the mismatch vector is deterministically norm-bounded. Consequently, in the proposed approach, the optimization needs to be formulated in probabilistic terms. For the formulation of the probabilistic optimization problem, various parameters have to be known, including the presumed steering vector, type of probability distribution, variance, and non-outage probability. In comparison to the worst case base approach, the prior known parameters of this approach are easy to determine. The proposed method has improved robustness by rejecting errors whose probability is low while providing robustness for errors with a high probability.

In [43] a robust approach has been provided to rectify the errors in the steering vector. The formulation of the optimization problem involves maximizing the output SINR to estimate the discrepancy between the true and assumed signal steering vector. The difference has been evaluated for each iteration, and it has been utilized to correct the signal steering vector.

The methods outlined assume only steering vector errors, yet the array may be subject to a range of other imperfections, including sensor location errors, sensor phase mismatches, and sensor gain mismatches. So, to provide robustness against all the stated errors, the reformulation of the worst case based approach has been done in [44] using semidefinite programming. Based on some ideas of [45] and the worst case method, a new algorithm has been obtained. The optimization problem has a regularized semidefinite relaxation form, and robustness has been managed through the regularization parameter. Till now, the error in the steering vector has been eliminated by various distinct approaches, and the theoretical covariance matrix has not been estimated. But the covariance matrix has been estimated in [46] by employing the shrinkage method, and the estimated matrix has been used to rectify the error of the presumed steering matrix.

The presented findings do not discuss the ability to withstand significant discrepancies in steering vectors. To address substantial deviations in steering vectors, it is necessary to expand the size of the uncertainty sphere, resulting in a degradation of performance for robust beamformers in terms of output SINR. Therefore, to overcome the large steering vector mismatches, robust adaptive beamformers have been depicted in [47] and [48]. In the [47], an adaptive uncertainty level has been used, and in each iteration, the uncertainty level of the sphere has been changed according to the mismatch in the signal steering vector. Along with this, one more approach based on flat ellipsoidal constraints to model the steering vector mismatch has been presented. In [48], the SOI's steering vector has been calculated iteratively by employing a small sized uncertainty sphere as well as a small flat ellipsoid. The proposed mythologies have been mostly confined to the case of uniform linear arrays (ULAs). The uncertainty based beamformers can also be applied to arbitrary array geometries, which have been suggested in [49]. The robustness against array imperfections has been achieved by applying magnitude constraints, and the solution has been obtained by solving a series of convex subproblems.

Most of the explained techniques utilize some prior knowledge about the steering vectors, amount of uncertainty, non-outage probability, etc. There is a need for a beamformer that utilizes as little prior knowledge as possible prior knowledge to achieve robustness. Thus, a beamformer has been suggested in [50] that requires very small and imprecise prior information and even provides robustness by maintaining an acceptably high output SINR. In the proposed technique, it has been assumed that the SOI is located inside the known angular sector, and that sector is free from interferences.

A novel approach has been presented in [51] to correct the deterministic errors in the estimated signal steering vector. The convex optimization [52] method has been utilized for the estimation purpose and the eigen decomposition has been done to separate the signal and noise subspaces. Moreover, to deal with uncertainties in the covariance matrix and optimizing the performance of the worst case approach, a new error bound has been suggested by employing the estimated signal steering vector. Different from the suggested approaches, a new method has been developed in [53]

to improve the performance in the case of a mismatch in the signal steering vector. Usually, maximizing the output SINR has been considered the objective function, but in the proposed approach, the objective function has been formed by minimizing the sum of the estimated actual signal steering vector projections on the noise subspace. Further, the constraints in the optimization problem have been added according to the angular sector of the SOI and array geometries.

The sensitivity of a robust beamformer is a parameter that is used to examine its sensitivity to enduring errors. In [54] a general scenario has been considered by assuming that the signals have been disturbed by the correlated random errors. The random error covariance has been calculated by inverting the sample covariance matrix, and Euclidean uncertainty has been used to provide the beamformer with the minimum sensitivity to random errors. Further, the problem has been solved by the Lagrange multiplier. To manage the main beam in the beampattern of robust adaptive beamformer has been presented in [55]. The signal steering vector and sample covariance matrix uncertainties have been considered to formulate the problem. The proposed method proved through the simulations that it can control the main beam precisely for arbitrary steering vector error.

Some of the suggested beamformers utilize specific optimization toolboxes in order to solve the formulated optimization problems for the estimation of the steering vector. Besides this, the effectiveness of almost all the beamformers relies on ad-hoc parameters, which are very challenging to compute in a real situation. Various improvements have been made using the uncertainty based technique, though their performance deterioration occurred in the high SNR scenario because of the presence of a desired signal component in the covariance matrix.

1.1.4 INCM reconstruction

To eliminate the SOI from the covariance matrix, a new technique has been developed called interference plus noise covariance matrix (INCM) reconstruction. The interference-plus-noise covariance matrix has been reformed in [56] by integrating

the product of the Capon spatial spectrum and the signal steering vector component over an angular region devoid of SOI. Subsequently, the estimation of the actual signal steering vector has been performed using the reconstructed INCM. Finally, the optimal weight vector has been determined by utilizing the estimated signal steering vector. The robust performance has been achieved at the expense of increased computational burden due to the integration function. The performance of the algorithm proposed in [56] has been improved further in [57]. As the steering vector is not known prior, the algorithm of [56] used the interference angular sector as well as the signal steering vector for the reconstruction. So, in [57] firstly the DOA of SOI and interferences have been estimated before reconstruction, and the steering vectors have been estimated using the robust Capon beamformer (RCB) approach [12]. Then, the INCM matrix was obtained by employing the estimated steering vectors. A different shrinkage based technique has been developed in [58] that determines the signal steering vector by utilizing the cross correlation between array observation data and the output of the beamformer. Then the INCM has been calculated by subtracting the covariance matrix of SOI from the received data matrix. The proposed approach offers low computational complexity, but it can work for lower interference powers. The reconstructed INCM has been obtained in [59] by employing the compressive sensing approach. The proposed approach used sparsely distributed sources with the assumption that the DOA of the source signals has been known prior. In [60], the component of SOI has been removed from the covariance matrix by using the average of noise eigen values instead of signal eigen values in the correlation coefficient. The developed method provided robustness against large steering vector mismatches by estimating the signal steering vector before reconstruction. However, this method has been valid only when the interference-to-noise ratio (INR) is not in the vicinity of SNR.

In most of the previously proposed methods, the region over which the integration took place for the reconstruction was the complement of the SOI's region. In [61], the integral region has been reduced by employing low-resolution DOA estimation methods, and the reconstruction has been done by imposing the annulus uncertainties constraints on the interference steering vectors. But it has been a challenging task

to obtain the exact region for integration. To further reduce the computational complexity of [56] a novel INCM reconstruction method based on the sampling of the spatial spectrum has been developed in [62]. The taper matrix has been utilized in the covariance matrix to enhance the robustness of the beamformer. The computational complexity of the proposed method has been reduced, but it has a little performance degradation.

To reconstruct the INCM and examine the efficiency of reconstruction, a parameter has been defined in [63] that is known as the improvement factor (IF). A relationship has been established between SNR and the IF, i.e., when the SNR is low, reconstruction has not been required to achieve robustness, but when the SNR is high, reconstruction has to be performed after the estimation of the signal steering vector. In [64], a novel method has been devised to extract the SOI from the covariance matrix. To calculate the interference steering vector, the intersection of two subspaces has been done, and the corresponding power has been determined by the Capon spectrum. The two subspaces include the signal plus interference subspace and the interference subspace only. The coprime array configuration has been utilized in [65] for the estimation of DOA as well as for the power estimation. Then, the reconstruction was done using the estimated DOA and the corresponding powers. As the coprime array configuration has a larger aperture as compared to ULA, therefore, using an equal number of elements as that of ULA, the coprime array has improved resolution along with less computation burden.

In [66], the efficacy of various reconstruction based algorithms has been analyzed. The effect of the estimation of interference power on robustness has been studied, and based upon that, a simple approach has been presented to estimate the power of interference.

1.2 Research gaps

Robust adaptive beamforming algorithms are employed to improve smart antenna system performance. However, when reviewing both traditional and state-of-the-art

algorithms, several research gaps become apparent which are as follows:

1. The effectiveness of existing algorithms diminishes significantly in cases where there is a substantial disparity in the DOA of the SOI. Thus, there is a need to create robust algorithms capable of addressing such significant DOA mismatches.

2. The current body of research on adaptive beamforming algorithms has primarily concentrated on individually mitigating DOA mismatch or mobile interferences, rather than providing a holistic solution that effectively combats both of these critical factors simultaneously. To fulfil this research gap in view, there is a need to develop a robust algorithm capable of addressing these dual challenges cohesively.

3. Most adaptive beamforming algorithms have traditionally focused on a single desired signal at a given time. However, in numerous applications, there is a requirement to simultaneously monitor multiple SOIs. Therefore, the need arises for advanced technique capable of effectively handling such multi-source scenarios.

4. In the literature, both traditional and recent beamforming techniques have predominantly centred around ULAs. Nevertheless, as a means to streamline system complexity, the utilization of sparse arrays offers a viable alternative to ULAs. Thus, investigating the incorporation of sparse arrays into beamforming methodologies holds great promise in terms of mitigating hardware demands and augmenting performance across a wide spectrum of applications.

5. In literature, while evolutionary algorithms have found applications in beamforming, their utilization in the context of wideband beamforming has been relatively scarce. Therefore, there is a pressing need to improve the performance of wideband beamforming by integrating evolutionary algorithms with novel objective functions.

1.3 Motivation

The main aim of adaptive beamforming algorithms is to enhance the performance of a system. The overall performance can be influenced by both external environmental factors and internal factors. External environmental factors include environmental uncertainties such as SOI direction mismatch, source wavefront distortion, signal fading, signal scattering, fast variations in propagation channel or medium, and sometimes the performance deterioration is caused due to the antenna array itself, such as inaccurate array calibration or distorted antenna shape, which are known as internal factors.

In today's rapidly evolving world of communication, it is essential to prioritize accuracy when it comes to estimating parameters. The array signal processing field is completely dependent on estimating parameters such as DOA of SOI, steering vector estimation, covariance matrix estimation, etc.

To minimize the impact of inconsistency and maintain the accuracy of estimating parameters, it is essential to develop innovative approaches and algorithms that focus on maximizing the performance of the system.

1.4 Objectives

There are several areas identified where further investigation is needed. In light of these gaps, following objectives have been formulated.

1. To develop a robust adaptive beamforming algorithm capable of mitigating the adverse effects of large DOA mismatch.

2. To develop an adaptive beamforming algorithm for robustness against moving interferences along with DOA mismatch.

3. To develop an adaptive algorithm to efficiently control the SLL in dual beams scenario to enhance the overall performance of beamforming.

4. To analyse and design sparse arrays for improvements in the beamformer performance.

5. To develop a novel objective function for evolutionary algorithms to implement wideband beamforming.

1.5 Thesis organisation

The structure of this thesis is as follows. In the chapter 1, a brief overview of the thesis topic and review of literature are described. All the remaining work that has been presented is listed as follows.

1. **To develop a robust adaptive beamforming algorithm capable of mitigating the adverse effects of large DOA mismatch.**
   The proximal gradient method is employed to develop a novel optimization for robust beamforming. By estimating the true direction of SOI, the suggested method effectively mitigates the impact of DOA mismatch while suppressing interfering signals. The iterative estimation of the true SOI direction is integrated as a hyper-parameter within a regularization function.

2. **To develop an adaptive beamforming algorithm for robustness against moving interferences along with DOA mismatch.**
   The formulation of the interference steering matrix entails the use of a taper matrix, designed to broaden the nulls. Deriving this taper matrix requires introducing artificial interferences in proximity to the existing ones. Furthermore, to ensure the beamformer's resilience against DOA mismatch, the magnitude within the ROI is restricted to unity. The proposed beamforming solution is computed using semi-definite techniques and resolved utilizing Matlab's CVX toolbox.

3. **To develop an adaptive algorithm to efficiently control the SLL in dual beams scenario to enhance the overall performance of beamforming.**

The traditional SCB has been remodelled by including a single constraint in its optimization problem. This modification ensures that both beams are accurately directed towards the dual desired signals even in the presence of interference and noise. Moreover, to control the SLL, constraints are introduced into the optimization problem.

4. **To analyse and design sparse arrays for improvements in the beamformer performance.**

   The optimal positions of antenna elements in sparse array (SA) are ascertained through SINR maximization criteria. Subsequently, an analysis is presented, introducing supplementary constraints to enhance the beamforming algorithm's performance using sparse arrays. Simulation results corroborate that sparse arrays subject to these conditions outperform unconstrained arrays, exhibiting superior performance in terms of sidelobe levels and grating lobes.

5. **To develop a novel objective function for evolutionary algorithms to implement wideband beamforming.**

   Evolutionary algorithms such as OPSO and PSO are used to calculate the optimum weights for wideband beamforming. To enhance wideband beamforming's effectiveness, a novel objective function is introduced. The MSE serves as a fitness function and measures the dissimilarity between the array pattern derived from uniform weights and that achieved through OPSO/PSO. This ensures that nulls and main lobe positions are maintained in the designated direction for every specified frequency.

Chapter 2

Robust Beamforming for Large DOA Mismatch

2.1 Introduction

Array signal processing is essential in many different fields such as radar, wireless communication, sonar, and antenna arrays. Adaptive beamforming [67] is one of the most important aspects of array signal processing and is capable of receiving the desired signal amid noise and interference. Capon beamforming is a technique that offers remarkable resolution and interference nulling ability. Despite that, this method can be applied only if the desired signal is known correctly [68, 69]. Due to the disparity between the presumed and actual/true angle of the desired signal, the performance of the beamformer deteriorates, and there is a need for robustness. So, there are various methods in the literature to improve the performance of SCB. Diagonal loading is a renowned approach for robustness against steering vector errors and small sample size. In the basic diagonal loading approach, the covariance matrix is modified by incorporating the weighted identity matrix into it [9]. The factor by which the identity matrix is weighted is called the loading level or loading factor. There are many approaches described in [12, 14, 18, 70, 71] to calculate the appropriate loading level to achieve robustness. However, in practical situations, it is very challenging to

determine the accurate loading level. In [12], the signal steering vector is estimated to prevent any mismatches in the RCB. The optimization problem has been reformulated by employing ellipsoidal uncertainty in it. The performance of the beamformer relies on the selected uncertainty bounding value, and obtaining the exact bounding value as that of actual uncertainty is very difficult in real situations. When the bounding value is smaller than the current uncertainty, then optimization conditions will not be fulfilled. The interferences nulling capability reduces in cases of large chosen uncertainty as compared to the actual amount. The most challenging task is to determine the uncertainty value in the actual situations. The Bayesian approach [72] has been employed with RCB in [73] to cope with large DOA mismatches. RCB has been used to estimate the signal steering vector, and further, the weights have been calculated by the Bayesian method. Many parameters have been defined for the execution of the presented beamformer, and the parameters are environment dependent. Therefore, for each scenario,the parameters should be redefined, which makes it a little more complex, and choosing several parameter values leads to performance tradeoffs. The robustness is achieved against incomplete and erroneous knowledge about the steering vector in recently presented algorithms [50, 74]. The estimation of the signal steering vector has been executed by reformulating the optimization problem, and particular toolboxes have been used to obtain the solution. Most of the described robust beamformers utilize some specific parameters that are challenging to determine in a practical situation. Moreover, various adaptive beamformers do not solve the optimization problem analytically rather use some specific toolboxes, which increases the computation burden. A novel beamformer has been presented in [75] which estimates the signal steering vector by eigen decomposition approach. However, it is assumed that the number of signals are known in advance and desired signal's strength is relatively low compared to the strength of interfering signals, which limits its practicality.

The foremost objective of an adaptive beamformer is to improve the quality of the desired signal with nullifying the interferences. For enhancing the quality of the desired signal its direction of incidence should be known accurately because by directing more power towards wrong direction of the desired signal degrades the

performance of the beamformer. The essential parameter to examine the performance of a robust adaptive beamformer is output SINR. The accurate estimation of the desired signal's direction leads to enhancement of output SINR. In this chapter, a proximal gradient based approach has been proposed, which reduces the impact of DOA mismatches. The precise direction of the desired signal has been iteratively determined using a hyper-parameter incorporated into a regularization function. The performance of the suggested method has been improved by nullifying the interferences along with the estimation of actual SOI.

2.2 Signal model

It is considered that P farfield source signals are incident on the M element ULA. Assume that the desired signal impinges on the array from θ_o direction and the remaining $P-1$ interference signals are incident from $\theta_1, \theta_2 ... \theta_{P-1}$ directions. At a particular instant (k), the array output [38] can be illustrated as

$$\boldsymbol{x}(k) = s_o(k)\boldsymbol{a}(\theta_o) + \sum_{i=1}^{P-1} s_i(k)\boldsymbol{a}(\theta_i) + \boldsymbol{n}(k), \quad k = 1, 2, \ldots, K \tag{2.2.1}$$

In the equation 2.2.1, $s_o(k)$, $s_i(k)$ and $\boldsymbol{n}(k)$ represent the desired signal, i^{th} interference signal and noise, respectively. The assumed noise is white and has a zero mean. The steering vector for the angle θ is denoted by $\boldsymbol{a}(\theta)$.
When there are M elements in an antenna array spaced half a wavelength apart, the representation of the steering vector is as follows:

$$\boldsymbol{a}(\theta) = [1, e^{j\pi \sin(\theta)}, ..., e^{j\pi(M-1)\sin(\theta)}]^T \tag{2.2.2}$$

Now, for the $\boldsymbol{x}(k)$ received vector, the covariance matrix can be calculated by utilizing the expectation operator, i.e.,

$$\boldsymbol{R} = E[\boldsymbol{x}(k)\boldsymbol{x}(k)^H] \tag{2.2.3}$$

where $(.)^H$ denotes the Hermitian. However, the covariance matrix $\boldsymbol{R}$ is not available in the actual scenario, and the sample covariance can be calculated as

$$\hat{\boldsymbol{R}} = \frac{1}{K}\sum_{k=1}^{K} \boldsymbol{x}(k)\boldsymbol{x}(k)^H \tag{2.2.4}$$

The SCB can be determined by reducing the total output power while constraining the beamformer's response towards the presumed direction of the desired signal θ_p to unity. The overall power of the received signal $\boldsymbol{x}(k)$ is determined as follows:

$$\mathrm{E}\{|\boldsymbol{w}^H\boldsymbol{x}(k)|^2\} = \boldsymbol{w}^H\boldsymbol{R}\boldsymbol{w} \tag{2.2.5}$$

So, mathematical formulation of SCB is given as

$$\min_{\boldsymbol{w}} \ \boldsymbol{w}^H\hat{\boldsymbol{R}}\boldsymbol{w}, \quad s.t.\ \boldsymbol{w}^H\boldsymbol{a}(\theta_p) = 1 \tag{2.2.6}$$

2.3 Proposed proximal gradient based robust beamformer

SCB provides good resolution and superior interference rejection ability in the absence of a mismatch condition. However, if the presumed direction of SOI (θ_p) is deviated from the actual direction (θ_o) then the performance of SCB degrades severely. So, the SCB is altered by constraining the total array power to direction $\theta \in [-\pi/2, \pi/2]$ and the proximal gradient method is used to update the direction iteratively. The modified optimization problem is formulated as

$$\min_{\boldsymbol{w}} \ \boldsymbol{w}^H\hat{\boldsymbol{R}}\boldsymbol{w}, \quad s.t.\ \boldsymbol{w}^H\boldsymbol{a}(\theta) = 1 \tag{2.3.1}$$

The constrained problem of equation 2.3.1 can be converted to a single goal problem by using the Lagrange multiplier technique, which is provided as

$$f(\theta) = \boldsymbol{w}^H \hat{\boldsymbol{R}} \boldsymbol{w} + \lambda(1 - \boldsymbol{w}^H \boldsymbol{a}(\theta)) \tag{2.3.2}$$

The single optimization problem is solved w.r.t. $\boldsymbol{w}$ to yield the Lagrange multiplier λ_θ and the optimum weight vector $\boldsymbol{w}_\theta$ for the direction θ.

$$\lambda_\theta = \frac{1}{\boldsymbol{a}(\theta)^H \hat{\boldsymbol{R}}^{-1} \boldsymbol{a}(\theta)} \tag{2.3.3}$$

$$\boldsymbol{w}_\theta = \frac{\hat{\boldsymbol{R}}^{-1} \boldsymbol{a}(\theta)}{\boldsymbol{a}(\theta)^H \hat{\boldsymbol{R}}^{-1} \boldsymbol{a}(\theta)} \tag{2.3.4}$$

For the direction θ the minimum array output power is calculated by utilizing the equations (2.3.2-2.3.4).

$$f_{min}(\theta) = \boldsymbol{w}_\theta^H \hat{\boldsymbol{R}} \boldsymbol{w}_\theta = \frac{1}{\boldsymbol{a}(\theta)^H \hat{\boldsymbol{R}}^{-1} \boldsymbol{a}(\theta)} \tag{2.3.5}$$

It should be noted that when the θ lies proximate to the actual direction of SOI θ_o then there is an increase in $f_{min}(\theta)$ which in turn improves the output SINR. This motivates to develop a new function in terms of θ that maximizes the $f_{min}(\theta)$ and adjust θ to determine the actual direction of SOI. Hence, a new function is expressed as a combination of the initial function $f(\theta)$ and a regularization function $r(\theta)$. The regularization function is utilized for adjusting the hyper-parameter θ, moreover, it assures that the determined direction must be in enough proximity to the tune direction of SOI. For the formulation of the described function some assumptions are made that are the unknown actual direction of SOI belongs to an angular sector $\Theta = [\theta_{min}, \theta_{max}]$ and the interferences are not situated in the given angular sector. For the separation of desired signal from interference signals, a matrix $\tilde{C}$ is used, which is given as

$$\tilde{C} = \int_{\tilde{\Theta}} \boldsymbol{a}(\phi) \boldsymbol{a}(\phi)^H d\phi \tag{2.3.6}$$

In equation 2.3.6, $\tilde{\Theta}$ includes all the angles except the angles of set Θ and $\boldsymbol{a}(\phi)$ is the steering vector corresponds to angle ϕ. Now, to formulate the optimization problem equations (2.3.2), (2.3.5) and (2.3.6) are used

$$\underset{\theta}{minimize} \quad F(\theta) = \boldsymbol{a}(\theta)^H \hat{\boldsymbol{R}}^{-1} \boldsymbol{a}(\theta) + \boldsymbol{a}(\theta)^H \tilde{C} \boldsymbol{a}(\theta) \tag{2.3.7}$$

$$= \frac{1}{f(\theta)|_{\boldsymbol{w}_\theta, \lambda_\theta}} + r(\theta) \tag{2.3.8}$$

Due to the convex and differentiable nature of $f(\theta)$, simple and convex $r(\theta)$ moreover, $f(\theta)$, $\boldsymbol{w}$ and θ are linked only through a constraint, thus, the proximal gradient approach is utilized to resolve the problem. The θ is evaluated for each iteration using the proximal gradient approach and the update for a particular iteration is given as:

$$\theta^{j+1} = \boldsymbol{prox}_{\delta^j, r} \left(\theta^j + \delta^j \left[\nabla_\theta f(\theta) \right]_{\theta = \theta^j} \right) \tag{2.3.9}$$

where δ^j is the step size whose value is chosen greater than zero, i.e., $\delta^j > 0$ and ∇ is the gradient operator. Initially, the value of step size is chosen randomly, and it is updated with every iteration according to approach mentioned in [76]. The proximal operator $\boldsymbol{prox}$ given in equation (2.3.9) is defined as

$$\boldsymbol{prox}_{\delta, r}(\varphi) = \underset{\theta \in [-\frac{\pi}{2}, \frac{\pi}{2}]}{\arg\min} \left(\delta r(\theta) + \frac{1}{2} (\theta - \varphi)^2 \right) \tag{2.3.10}$$

Now, the gradient of j^{th} iteration can be computed by :

$$g^j = \left[\nabla_\theta f(\theta) \right]_{\theta = \theta^j} = \left[\frac{d}{d\theta} \left(\boldsymbol{w}^H \hat{\boldsymbol{R}} \boldsymbol{w} + \lambda (1 - \boldsymbol{w}^H \boldsymbol{a}(\theta)) \right) \right]_{\theta = \theta^j}$$

$$= -j\pi\lambda_{\theta^j} \cos(\theta^j) \left(\boldsymbol{w}_{\theta^j}^H \left(\boldsymbol{u} \circ \boldsymbol{a}(\theta^j) \right) \right) \tag{2.3.11}$$

In the equation 2.3.11, $\boldsymbol{u} = [0, 1, 2, ..., M-1]^T$, $\circ$ indicate Hadamard product.

Further, the issue of the number of received samples is addressed because they are used to determine the sample covariance matrix. The estimation of the sample covariance matrix can be inaccurate because of the small snapshot number that deteriorates the effectiveness with regard to the output SINR of the beamformer. So, to enhance the output SINR, the optimum weight vector is determined by using the diagonal loading method. The weight vector for the proposed proximal gradient based RCB (PGRCB) is given as

$$\hat{\boldsymbol{w}} = \frac{(\hat{\boldsymbol{R}} + \rho \boldsymbol{I})^{-1}\boldsymbol{a}(\hat{\theta})}{\boldsymbol{a}(\hat{\theta})^{H}(\hat{\boldsymbol{R}} + \rho \boldsymbol{I})^{-1}\boldsymbol{a}(\hat{\theta})} \tag{2.3.12}$$

where ρ is the loading level and $\hat{\theta}$ is the estimated direction of the desired signal. The diagonal loading value is determined by scaling the estimated power of the desired signal in [70] but the value becomes very large as the number of snapshots increases in case of no mismatch condition, which deteriorates the performance of beamformer. In the suggested beamformer, the estimated direction of the desired signal is approximately the same as the actual direction. Therefore, the HKB approach will not be the appropriate method. So, the diagonal loading value is calculated according to [10] and no scaling is performed on the estimated power of SOI.

$$\rho = \boldsymbol{w}_{\theta^J}^{H}\hat{\boldsymbol{R}}\boldsymbol{w}_{\theta^J}$$

$$= \frac{1}{\boldsymbol{a}(\hat{\theta})^{H}\hat{\boldsymbol{R}}^{-1}\boldsymbol{a}(\hat{\theta})} \tag{2.3.13}$$

where $\boldsymbol{w}_{\theta^J}$ depicts the weight vector for J^{th} iteration. The whole method is summarized in an algorithm which is depicted in Algorithm 1.

Input: Sample covariance matrix $\hat{\boldsymbol{R}}$, Number of array elements M, Presumed DOA of SOI θ_p, DOA uncertainty range $[-\Delta, \Delta]$;

Initial: DOA $\theta^1 = \theta_p$, angular sector $\Theta^1 = [\theta_p - \Delta, \theta_p + \Delta]$, step size δ^1, number of iterations J;

for $j = 1, 2, \ldots, J$ **do**

  Compute the steering vector $\boldsymbol{a}(\theta^j)$ equation (2.2.2);

  Compute matrix $\tilde{C}$ associated with angular sector Θ^j equation (2.3.6);

  Compute minimization function $F(\theta^j)$ equation (2.3.7);

  Compute the Lagrange multiplier λ_{θ^j} equation (2.3.3);

  Compute the weight vector $\boldsymbol{w}_{\theta^j}$ equation (2.3.4);

  Compute the gradient g^j equation (2.3.11);

  Compute the gradient step $\varphi^j = \theta^j + \delta^j g^j$;

  Compute the proximal operator $\theta^{tent} = \boldsymbol{prox}_{\delta^j, r}(\varphi^j)$ equation (2.3.10);

  Repeat steps 4-6 to compute $F(\theta^{tent})$;

  if $F(\theta^{tent}) \leq F(\theta^j)$ **then**

    Update DOA, angular sector and increase step size: ;

    $\theta^{j+1} \leftarrow \theta^{tent}$;

    $\Theta^{j+1} \leftarrow [\theta^{tent} - \Delta, \theta^{tent} + \Delta]$;

    $\delta^{j+1} \leftarrow 1.2\delta^j$;

    quit if $|(\theta^{j+1} - \theta^j)/\delta^j| + |g^{j+1} - g^j| \leq \varepsilon$;

  else

    Reject updates and decrease step size:;

    $\theta^{j+1} \leftarrow \theta^j$;

    $\Theta^{j+1} \leftarrow \Theta^j$;

    $\delta^{j+1} \leftarrow \frac{1}{2}\delta^j$;

  end

end

Output: Estimated DOA of SOI: $\hat{\theta} \leftarrow \theta^{j+1}$;

Optimum weight vector: $\hat{\boldsymbol{w}}$ equation (2.3.12);

Algorithm 1: PGRCB algorithm

2.4 Simulation results and discussions

Several simulations are implemented to illustrate the performance of the proposed beamformer. To validate the superiority and effectiveness of the proposed PGRCB, it is compared with some standard as well as state-of-the-art algorithms that are SCB,RCB [12], MVDR2012 [50], and MVDR2019 [74] . In the simulations, ULA of 10 elements that are uniformly placed at a distance of half-wavelength w.r.t. each other is utilized. Two interferences are assumed to incident on the array from -20° and 60° with an equal interference-to-noise ratio (INR) of 30 dB.
The proposed PGRCB is configured to have a total of 100 iterations set as $J = 100$. The step size for each iteration is chosen as $\delta^1 = 0.1$. A small value of step size is chosen because more iterations will be required to converge in the case of a larger value. Different scenarios have been considered to examine the performance of the PGRCB. For each scenario, final results are obtained by averaging the 500 independent simulation runs. The parameter uncertainty value for RCB is set to $\epsilon = 6$ and the range of uncertainty for the other considered algorithm is $[-6^\circ, 6^\circ]$.

2.4.1 Precise knowledge of DOA for SOI

Firstly, it is assumed there is no mismatch in the DOA of SOI. The actual and presumed DOAs of SOI are identical $\theta_o = \theta_p = 0^\circ$. The effectiveness of the considered beamforming algorithms is evaluated by the parameter output SINR. Input SNR and snapshot number are varied, and their effect on output SINR is studied. The effect of input SNR and snapshot number on output SINR is illustrated in Figure 2.1 and Figure 2.2, respectively. In Figure 2.1, input SNR is varied with a fixed number of snapshots $K = 100$, and from the figure it can be seen that for the entire range of input SNR, the proposed PGRCB provides better output SINR in comparison to the tested beamforming algorithms. It can also be noticed that even for the higher range of input SNR, the output SINR degrades severely in the cases of MVDR2012 and MVDR2019.

Figure 2.2 depicts the effect of a change in snapshot number on the output SINR. It is

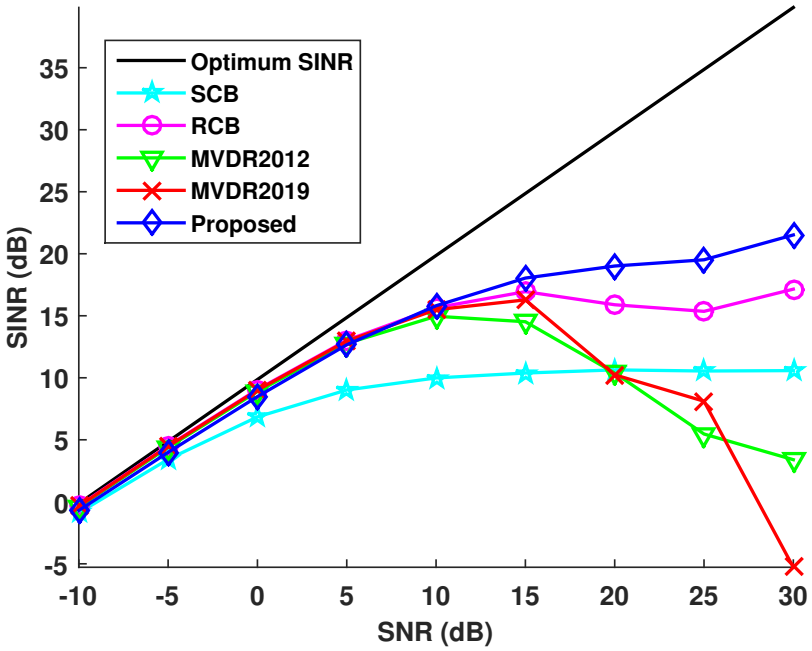

Figure 2.1: Output SINR performance against input SNR with $K = 100$

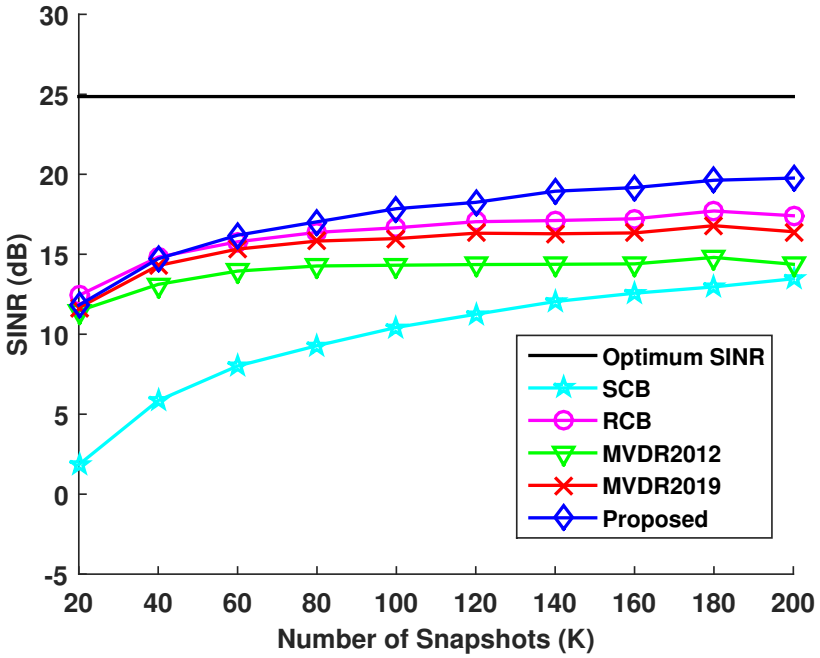

Figure 2.2: Output SINR performance against snapshot number with SNR = 15 dB

evident from the figure that the best performance among all the tested beamformers is given by the proposed PGRCB. However, the SINR of conventional SCB deteriorated, particularly at lower snapshot numbers.

2.4.2 Mismatch in the DOA for SOI

In this case, mismatch is considered the DOA of SOI. The presumed DOA of SOI impinges on the array from $\theta_p = 0°$. However, the direction of actual SOI is incident on the array from some other direction, which is not the same as the presumed direction. So, in the proposed algorithm, the actual DOA of SOI is considered to be random in nature and is evenly distributed in the range $[-6°, 6°]$. For every trial, the DOA of SOI is changed while being kept the same for each snapshot. The simulation results for this scenario are shown in Figure 2.3 and Figure 2.4. The performance

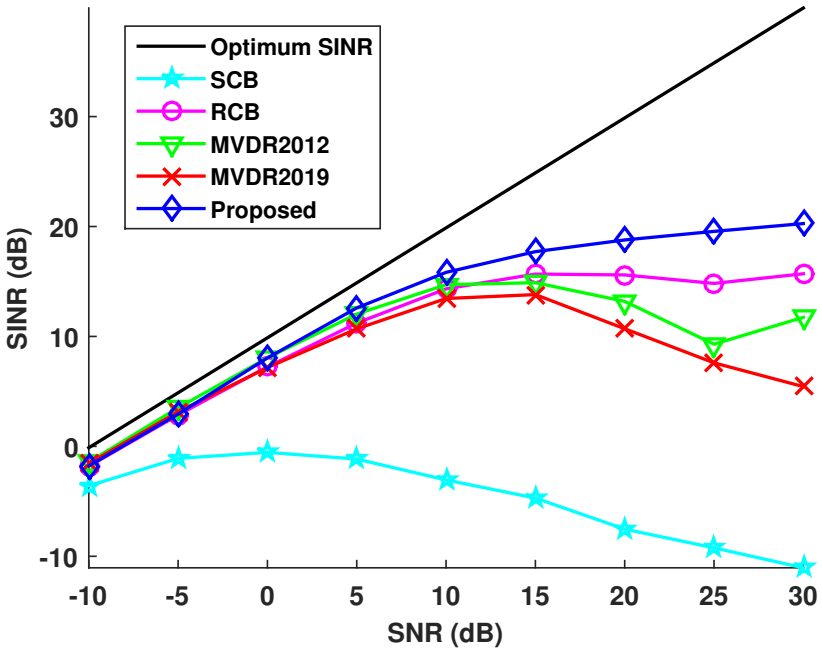

Figure 2.3: Output SINR performance against input SNR with $K = 100$ in mismatch scenario

of output SINR is analyzed in the mismatch situation by changing the input SNR while keeping the number of snapshots fixed at a constant value of $K = 100$ and

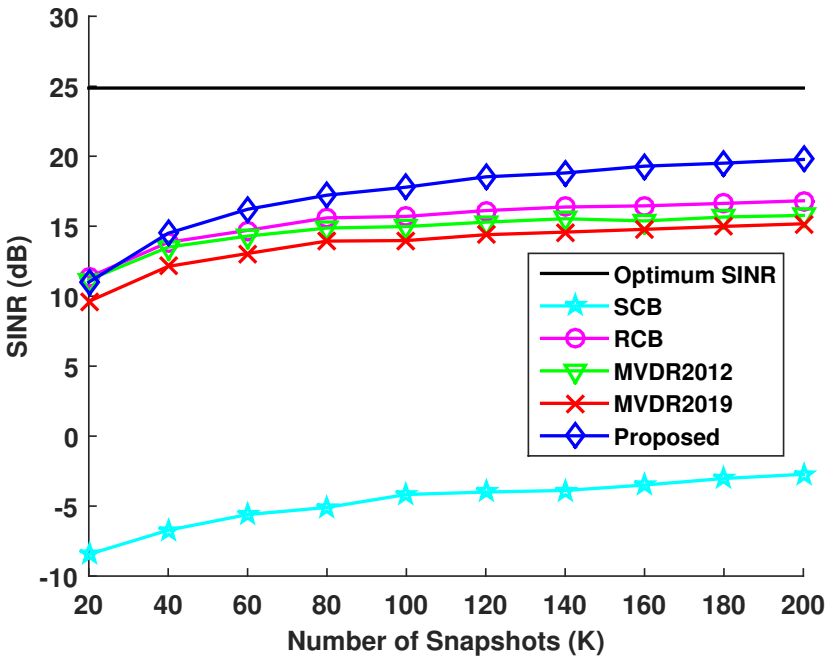

Figure 2.4: Output SINR performance against snapshot number with SNR = 15 dB in mismatch scenario

the results are illustrated in the Figure 2.3. From the figure, it can be seen that the proposed PGRCB provides nearly identical results for both mismatch and no mismatch scenario. So, it can be said that it is robust against mismatch in the DOA of SOI. Additionally, the performance of the suggested beamformer surpasses that of other examined beamformers across the entire input SNR range. However, the conventional SCB is not able to provide robustness against mismatch in the DOA of SOI as the output SINR deteriorates dramatically . Now, the performance parameter SINR is evaluated by varying the snapshot number with fixed input SNR of 15 dB and the results are depicted in the Figure 2.4. From where it is observed that the proposed PGRCB is more robust because it maintains higher output SINR as compared to all other tested beamformers.

2.4.3 Large DOA mismatch

To investigate the robustness against large DOA mismatch, the range of DOA mismatch is taken from $[0°, 10°]$. The performance parameters, such as output SINR and estimate of SOI power, are evaluated by uniformly varying the DOA mismatch angle from 0° to 10° with SNR=15 dB and snapshots $K = 100$. The performance of output SINR against the DOA mismatch angle is illustrated in Figure 2.5. It is clear from the figure that the proposed beamformer can handle the large DOA mismatch as it maintains the output SINR for the whole range of mismatch angles. However, the other beamformers, such as RCB, MVDR2012, and MVDR2019, work well only for small mismatches.

Now, the power of SOI is estimated under the large mismatch scenario, and the results are depicted in Figure 2.6. From there, it is evident that the proposed technique accurately estimates the power in comparison to all the examined beamformers. RCB also estimates the power accurately, but only for small DOA mismatches. While all the other beamformers are failed to estimate the DOA of SOI in the large mismatch case.

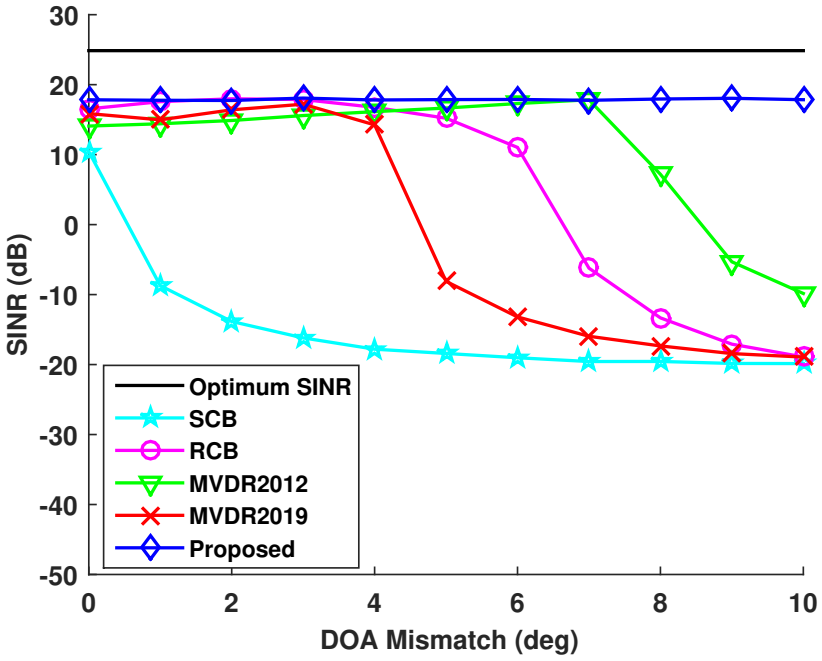

Figure 2.5: Output SINR performance against SOI mismatch angle

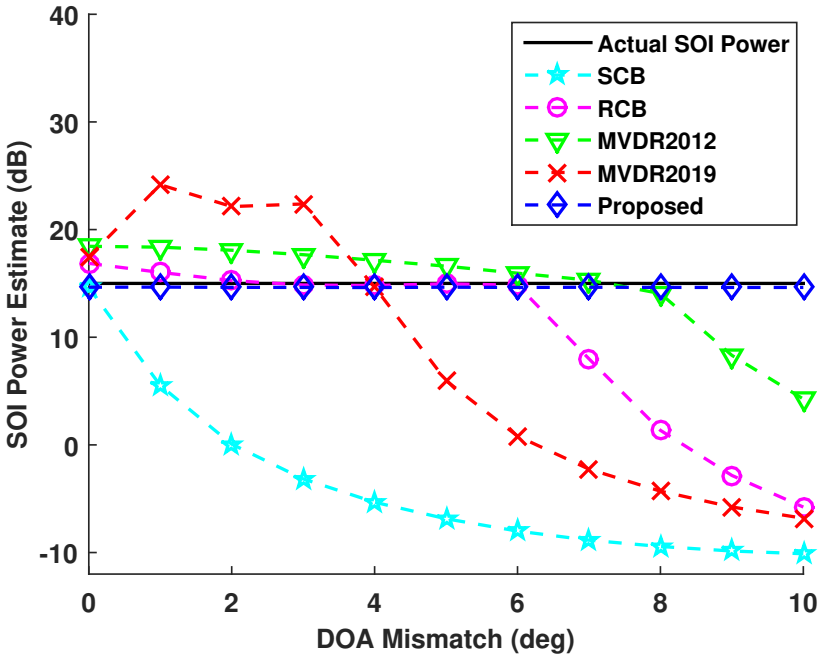

Figure 2.6: SOI power estimation performance against SOI mismatch angle

2.4.4 Deviation in the estimation of DOA of SOI

The proposed algorithm estimates the actual DOA of SOI along with robustness against mismatches. The performance of DOA estimation is investigated by calculating the error in estimation. The input SNR and snapshot number are varied to evaluate the error in estimation, and the corresponding results are shown in Figure 2.7 and Figure 2.8, respectively. From Figure 2.7, it can be seen that there is negligible error for each presumed DOA of SOI θ_p. Moreover, the error vanishes as the input SNR increases.

Now, the error is also evaluated for a different number of snapshots, which is given in Figure 2.8. The figure makes it abundantly evident that as the snapshots rises, the error dies out for each considered presumed angle.

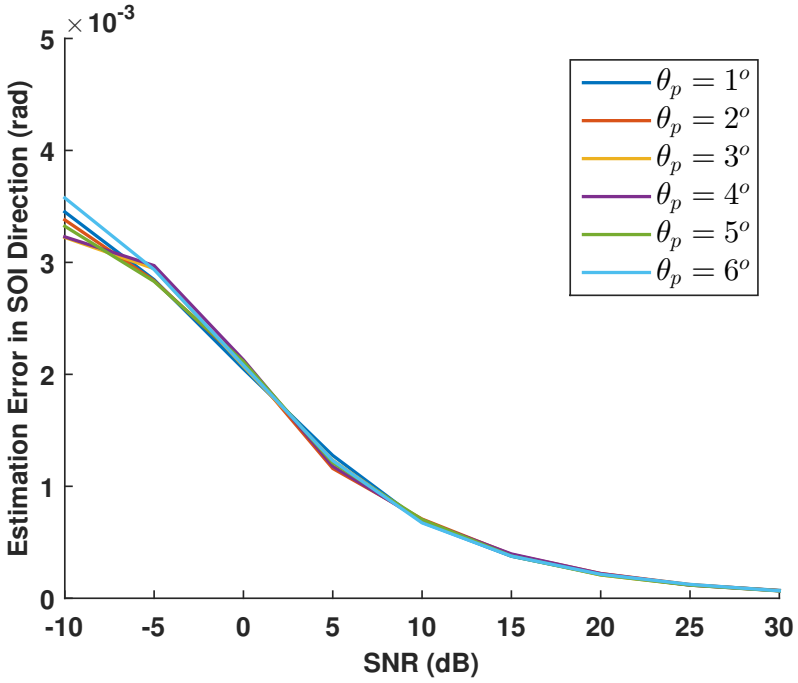

Figure 2.7: Deviation in estimated DOA of SOI with variable input SNR.

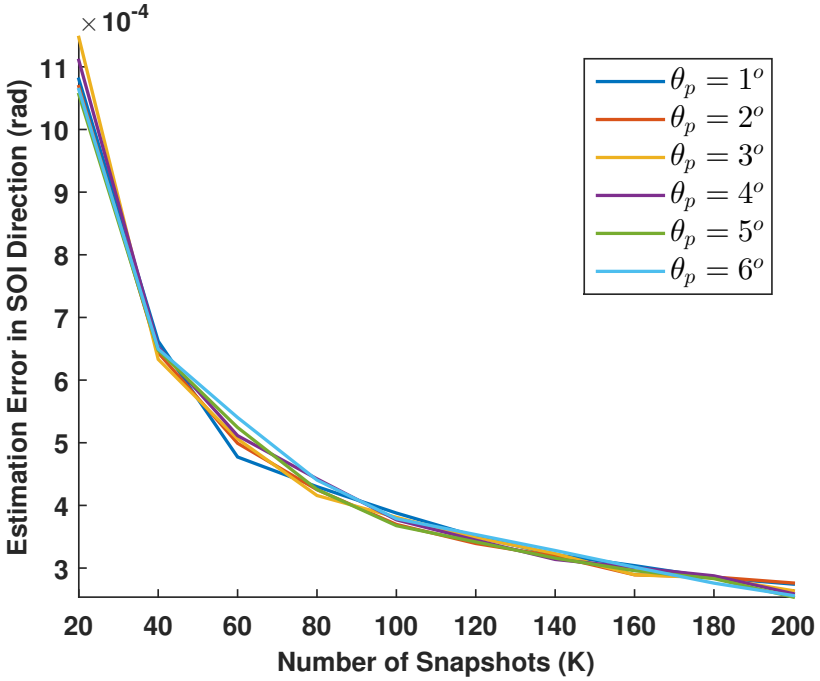

Figure 2.8: Deviation in estimated DOA of SOI with variable snapshot number

2.5 Conclusion

In this chapter, a simple robust beamforming algorithm is developed that is based on the proximal gradient method. Firstly, the beamforming problem is parameterized and further solved by a hyper-parameter, which is regulated by the proximal gradient method. The proposed algorithm estimates the accurate DOA of SOI along with the power of SOI. The robustness against large DOA mismatches is achieved by acquiring the optimal weight vector. The simulation results demonstrate that the proposed beamformer is more robust to large mismatches as compared to the standard and state-of-the-art algorithms.

Chapter 3

Robust Beamforming for DOA Mismatch and Moving Interference

3.1 Introduction

Due to rapid advancements in wireless communications, researchers have shown a keen interest in adaptive beamforming. It is a versatile and efficient technology for boosting the SOI while simultaneously suppressing noise and interfering signals. The most classical adaptive beamformer has been developed by Capon [69] that provides outstanding performance in terms of resolution and interference suppression ability. Since the Capon beamformer is highly susceptible to various factors such as DOA mismatch, a small number of snapshots for steering vector estimation, moving interfering signals, imperfect antenna array calibration,etc. It is necessary to make the beamformer robust so that its performance can be improved against the above-mentioned factors. A review of various robust beamformers has been presented in [77–80] that improves the capon beamformer's performance in various scenarios.

To tackle the problem of DOA mismatch, diagonal loading techniques have been given in [9, 14, 17, 18, 81, 82]. These techniques addressed the problem of DOA mismatch quite effectively, at the expense of a reduction in interference suppression

capability. Further, [83] and [12] handled the SOI's uncertainties by employing ellipsoidal constraints in the steering vector. However, the loading value is dependent on the amount of uncertainty, which is difficult to obtain in reality. To deal with large DOA mismatches, magnitude constraints have been utilized in [55, 84]. Despite significant mismatches, the main beam's beamwidth and direction were kept in check, but they did not consider the desired signal is the received data.

Further, to make the beamformer robust against moving interferences, various methods have been illustrated in [85–95]. For these quickly moving interferences, the null broadening method has received a lot of attention [96]. Multi-parametric quadratic programming has utilized in [85] to control the null width. In [91–93] the expansion of null is executed via covariance matrix taper (CMT). The aforementioned techniques address DOA mismatch and non-stationary interferences independently but do not concurrently offer robustness against these two key problems. Consequently, a new robust beamformer has been developed to suppress the moving interferences while also being resilient against DOA mismatch.

Thus, this chapter is divided into the different sections below:
The mathematical model of SCB and the proposed formulation for null widening along with DOA mismatch are illustrated in sections 3.2 and 3.3, respectively. It is followed by simulation results, which is elucidated in section 3.4. Finally, the chapter is concluded in section 3.5.

3.2 Signal model

It is considered that P number of signals are incident on antenna array of M elements, which are positioned at half wavelength spacing. There is only one SOI, and the remaining $P-1$ are interference signals. The steering vector for angle θ is calculated as

$$\boldsymbol{a}(\theta) = [1, e^{j\pi \sin(\theta)}, ..., e^{j\pi(M-1)\sin(\theta)}]^T \tag{3.2.1}$$

The SOI and the steering vector for DOA θ_o are represented by s_o and $\boldsymbol{a}(\theta_o)$, respectively. For i^{th} interference signal s_i, the steering vector is denoted as $\boldsymbol{a}(\theta_i)$. The $P-1$ interference signals impinge on the array from $\theta_1, \theta_2 ... \theta_{P-1}$ directions. The mathematical expression of the received data in the presence of noise $\boldsymbol{n}$ on the antenna array at a particular instant k [80] is given as:

$$\boldsymbol{x}(k) = s_o(k)\boldsymbol{a}(\theta_o) + \sum_{i=1}^{P-1} s_i(k)\boldsymbol{a}(\theta_i) + \boldsymbol{n}(k), \quad k = 1, 2, \ldots, K \tag{3.2.2}$$

The covariance matrix is calculated from the received signal vector $\boldsymbol{x}(k)$ given by

$$\boldsymbol{R} = E[\boldsymbol{x}(k)\boldsymbol{x}(k)^H] \tag{3.2.3}$$

Where E is the expectation. Theoretically, the covariance matrix can be represented as the summation of SOI covariance matrix and INCM.

$$\begin{aligned} \boldsymbol{R}_t &= \boldsymbol{R}_s + \boldsymbol{R}_{i+n} \\ &= \sigma_o^2 \boldsymbol{a}(\theta_o)\boldsymbol{a}^H(\theta_o) + \sum_{i=1}^{P-1} \sigma_i^2 \boldsymbol{a}(\theta_i)\boldsymbol{a}^H(\theta_i) + \sigma_n^2 \boldsymbol{I} \end{aligned} \tag{3.2.4}$$

In the equation 3.2.4, σ_o^2 , σ_i^2 and σ_n^2 represent the power of SOI, i^{th} interference signal, and noise, respectively. However, in the real environment, the covariance matrix is determined from the received snapshots at the antenna array. The expression of the covariance matrix for a total of K snapshots is given as

$$\hat{\boldsymbol{R}} = \frac{1}{K} \sum_{k=1}^{K} \boldsymbol{x}(k)\boldsymbol{x}(k)^H \tag{3.2.5}$$

For $\boldsymbol{w}$ weight vector the response of the beamformer at $k^{(th)}$ instant, is given as

$$\boldsymbol{y}(k) = \boldsymbol{w}^H \boldsymbol{x}(k) \tag{3.2.6}$$

The total output power of the received signal $\boldsymbol{x}(k)$ is calculated by utilizing expectation operator.

$$\mathrm{E}\{|\boldsymbol{w}^H \boldsymbol{x}(k)|^2\} = \boldsymbol{w}^H \boldsymbol{R} \boldsymbol{w} \tag{3.2.7}$$

The optimization problem of SCB is computed by reducing the total output power while restricting the output towards SOI to unity. It is mathematically represented as

$$\min_{\boldsymbol{w}} \ \boldsymbol{w}^H \hat{\boldsymbol{R}} \boldsymbol{w}, \quad s.t.\ \boldsymbol{w}^H \boldsymbol{a}(\theta_o) = 1 \tag{3.2.8}$$

The equation 3.2.8 is solved by Lagrange multiplier [97,98] and the weight vector can be computed as

$$\boldsymbol{w} = \frac{\hat{\boldsymbol{R}}^{-1}\boldsymbol{a}(\hat{\theta_o})}{\boldsymbol{a}(\hat{\theta_o})^H\hat{\boldsymbol{R}}^{-1}\boldsymbol{a}(\hat{\theta_o})} \tag{3.2.9}$$

3.3 Proposed robust beamformer

A taper matrix is utilized in the interference steering matrix to handle interferences in motion. The taper matrix is computed by inserting fake interferences in close proximity to the real interferences

3.3.1 Taper matrix for null broadening

The $P-1$ interference signals arriving at the antenna array from $\theta_1, \theta_2 ... \theta_{P-1}$ directions. The steering matrix for i^{th} interference is given by

$$\boldsymbol{A}(\theta_i) = \boldsymbol{a}(\theta_i)\boldsymbol{a}^H(\theta_i) \tag{3.3.1}$$

Let F be the fictitious interferences inserted around the actual ones, and W_f is the null width. For i^{th} original interference, the fictitious interferences are placed at the following positions:

$$\theta_{fi} = \theta_i + q\Delta \tag{3.3.2}$$

where q should lie in the range $\frac{-(F-1)}{2} \leq q \leq \frac{(F-1)}{2}$, and $\Delta = \frac{W_f}{F-1}$. The new steering vector and matrix are given as

$$\boldsymbol{a}_{new}(\phi_i) = [1, ..., e^{j(M-1)\sin(\theta_i+q\Delta)}]^T \tag{3.3.3}$$

$$\boldsymbol{A}_{new}(\theta_i) = \boldsymbol{a}_{new}(\theta_i)\boldsymbol{a}^H_{new}(\theta_i) \tag{3.3.4}$$

Elucidate the equation 3.3.4 by using equation 3.3.1-equation 3.3.3, yields

$$[\boldsymbol{A}_{new}(\theta_i)]_{m,f} = \frac{\sin(F\Phi/2)}{\sin(\Phi/2)}[\boldsymbol{A}(\theta_i)]_{m,f}; \quad 1 \leq m, \quad f \leq M \tag{3.3.5}$$

$$\Phi = \pi\Delta(remainder(f-1, M) - remainder(f-1, M)) \tag{3.3.6}$$

In the equation 3.3.6, $remainder(x, y)$ refers to the remaining amount after dividing x with y. Finally, the taper matrix is given as

$$[\boldsymbol{T}]_{m,f} = \frac{\sin(F\Phi/2)}{\sin(\Phi 2)}; \quad 1 \leq m, \quad f \leq M \tag{3.3.7}$$

Now, the $\boldsymbol{A}_{new}(\theta_i)$ can be rewritten in the form of taper matrix and Hadamard product $\odot$.

$$\boldsymbol{A}_{new}(\theta_i) = \boldsymbol{A}(\theta_i) \odot \boldsymbol{T} \tag{3.3.8}$$

3.3.2 Robustness against DOA mismatch along with null expansion

To create a beamformer that is resilient against DOA mismatch, the strength of the ROI is maintained at a constant level of unity. The semidefinite approach [99,100] is used to resolve the proposed beamformer, and the final solution is obtained by the CVX toolbox [101] of Matlab. When there is precise knowledge of SOI's steering vector $\boldsymbol{a}(\theta_o)$ and the INCM $\boldsymbol{R}_{i+n}$ then the weight vector can be computed by maximizing the SINR, which is given as

$$\max_{\boldsymbol{w}} \; SINR = \frac{\sigma_o^2 |\boldsymbol{w}^H \boldsymbol{a}(\theta_o)|^2}{\boldsymbol{w}^H \boldsymbol{R}_{i+n} \boldsymbol{w}} \tag{3.3.9}$$

The equation 3.3.9 can be expressed as

$$\begin{aligned} \max_{\boldsymbol{w}} \; SINR &= \frac{\sigma_o^2 |\boldsymbol{w}^H \boldsymbol{a}(\theta_o)|^2}{\sum_{i=1}^{P-1} \sigma_i^2 \boldsymbol{w}^H \boldsymbol{a}(\theta_i) \boldsymbol{a}^H(\theta_i) \boldsymbol{w} + \sigma_n^2 \boldsymbol{w}^H \boldsymbol{w}} \\ &= \frac{\sigma_o^2 |\boldsymbol{w}^H \boldsymbol{a}(\theta_o)|^2}{\sum_{i=1}^{P-1} \sigma_i^2 |\boldsymbol{w}^H \boldsymbol{a}(\theta_i)|^2 + \sigma_n^2 \boldsymbol{w}^H \boldsymbol{w}} \end{aligned} \tag{3.3.10}$$

Now, consider a ROI in which SOI has a high probability and the magnitude response of the ROI is set to unity. Let the ROI be denoted as $\Omega_s = \{\theta_1, ..., \theta_S\}$ and the SOI

should lie in the ROI $\theta_0 \in \Omega_s$. The magnitude response condition is represented as

$$|\boldsymbol{w}^H \boldsymbol{a}(\theta_s)|^2 = 1; \quad \theta_s \in \Omega_S \tag{3.3.11}$$

To fulfill the objectives of null broadening and DOA mismatch simultaneously, the optimization is expressed as

$$\begin{aligned} \max_{\boldsymbol{w}} \; SINR &= \frac{\sigma_o^2 |\boldsymbol{w}^H \boldsymbol{a}(\theta_o)|^2}{\sum_{i=1}^{P-1} \sigma_i^2 |\boldsymbol{w}^H \boldsymbol{a}(\theta_i)|^2 + \sigma_n^2 \boldsymbol{w}^H \boldsymbol{w}} \\ subject\ to \quad & |\boldsymbol{w}^H \boldsymbol{a}(\theta_s)|^2 = 1; \quad \theta_s \in \Omega_s \\ & |\boldsymbol{w}^H \boldsymbol{a}_{new}(\theta_i)|^2 = \mu_i \end{aligned} \tag{3.3.12}$$

In the above equation, μ_i is the null level and calculated via SCB using the weight vector of equation 3.2.9 $|\boldsymbol{w}^H \boldsymbol{a}(\theta_i)|^2 = \mu_i$. The SINR in equation 3.3.12 can be expressed as

$$SINR = \frac{\sigma_o^2}{\sum_{i=1}^{P-1} \sigma_i^2 \mu_i + \sigma_n^2 \boldsymbol{w}^H \boldsymbol{w}} \tag{3.3.13}$$

There is a need to deal with only one part of the denominator $\boldsymbol{w}^H \boldsymbol{w}$ to optimize the SINR. Consequently, the optimization problem of equation 3.3.12 can be rewritten as

$$\min_{\boldsymbol{w}} \quad \boldsymbol{w}^H \boldsymbol{w} = ||\boldsymbol{w}||_2^2$$

$$\begin{aligned} s.t. \quad & |\boldsymbol{w}^H \boldsymbol{a}(\theta_s)|^2 = 1; \quad \theta_s \in \Omega_s \\ & |\boldsymbol{w}^H \boldsymbol{a}_{new}(\theta_i)|^2 = \mu_i \end{aligned} \tag{3.3.14}$$

In the equation 3.3.14, $||.||$ represents the l_2 norm. The optimization problem of equation 3.3.14 is non-convex, which needs to be converted into convex. So, the convex form is presented as

$$\min_{\boldsymbol{W}} \quad trace\{\boldsymbol{W}\}$$

$$\begin{aligned} s.t. \quad & trace\{\boldsymbol{A}(\theta_s)\boldsymbol{W}\} = 1; \quad \theta_s \in \Omega_s \\ & trace\{\boldsymbol{A}_{new}(\theta_i)\boldsymbol{W}\} = \mu_i \end{aligned} \tag{3.3.15}$$

$$\boldsymbol{W} \succeq 0$$

where $\boldsymbol{W} = \boldsymbol{w}\boldsymbol{w}^H$ and $\boldsymbol{A}(\theta_i) = \boldsymbol{a}(\theta_i)\boldsymbol{a}(\theta_i)^H$. For converting non-convex problems into convex problems, various formulas have been used, which are given as

$$||\boldsymbol{w}||_2^2 = trace\{\boldsymbol{w}^H\boldsymbol{w}\} = trace\{\boldsymbol{w}\boldsymbol{w}^H\} \tag{3.3.16}$$

$$|\boldsymbol{w}^H\boldsymbol{a}(\theta)|^2 = trace\{\boldsymbol{w}^H\boldsymbol{a}(\theta)\boldsymbol{a}^H(\theta)\boldsymbol{w}\} = trace\{\boldsymbol{a}(\theta)\boldsymbol{a}^H(\theta)\boldsymbol{w}\boldsymbol{w}^H\} \tag{3.3.17}$$

Now, the optimization problem is solved to get the weight vector $\boldsymbol{W}$ in the CVX toolbox of Matlab. Then eigen decomposition is applied to $\boldsymbol{W}$ to get the largest eigenvalue λ_{max} and corresponding eigenvector $\boldsymbol{v}_{max}$. The optimal weight vector $\boldsymbol{w}^*$ is calculated as

$$\boldsymbol{w}^* = \sqrt{\lambda_{max}}\boldsymbol{v}_{max} \tag{3.3.18}$$

3.4 Simulation results and discussions

The proposed beamformer is tested under diverse situations, and its effectiveness is measured against SCB, RCB [12] and RSLC [92]. A half wavelength $d = \lambda/2$ spaced ULA of $M = 10$ antenna elements is considered for all the considered beamformers except for [92]. In RSLC, $M = 21$ primary antenna elements assumed at $d = \lambda/2$ and $L = 8$ auxiliary antenna elements located at non-uniform positions at both ends of the primary array. For RCB, the uncertainty level is assumed to be $\epsilon = 6$ and for other considered beamformers, the uncertainty range is $[-3^o, 3^o]$. The performance of the considered beamformers under different scenarios is described as follows:

3.4.1 Null expansion and no mismatch

The SOI is assumed to arrive at 0^o while the two interferences incident on the array from -25^o and 40^o directions. It is assumed that the interferences are in motion and the SOI is perfectly known. For suppressing the moving interferences $N = 5$ virtual interferences are considered around each actual interference to widen the null. The width of each null is considered $W_n = 0.04$. The number of snapshots for simulations is taken as $K = 100$. The input SNR and INR are 10 dB and 30 dB respectively.

To observe the null widening, an illustration of the radiation patterns obtained through the use of considered approaches, is presented in Figure 3.1. While both

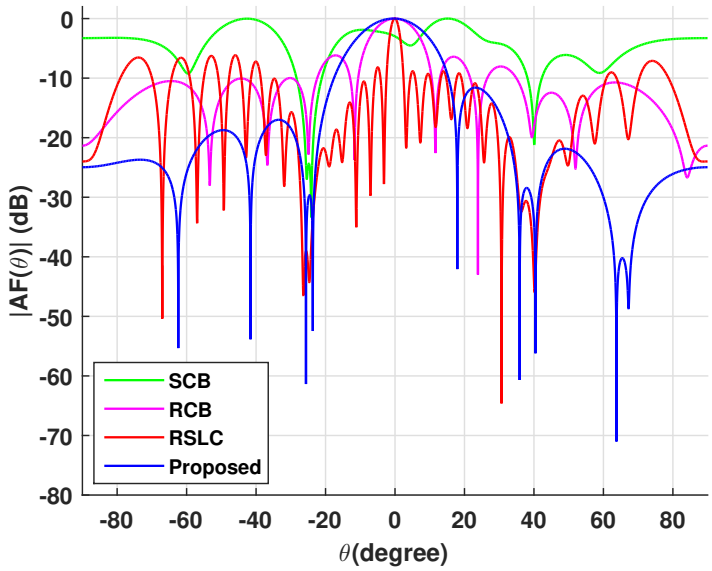

Figure 3.1: Radiation patterns for null widening at -25^o and 40^o

SCB and RCB create distinct nulls in relation to the two interferences, these nulls are unable to eliminate the interferences that are in motion. Therefore, moving interferences cannot be controlled by SCB or RCB. Conversely, broad nulls are observed in the case of the proposed beamformer and RSLC that can control the moving interferences. Apart from broad nulls, the proposed algorithm produces lower sidelobes as compared to the other tested approaches.

The output SINR is assessed for the examined beamformers by altering the input signal-to-noise ratio (SNR) and the number of snapshots, and the corresponding results are shown in Figures 3.2 and 3.3, respectively. To determine SINR, the INR and snapshot number are held constant while altering the SNR. Conversely, when seeking to find the SINR by adjusting the snapshot number, both the SNR and INR remain unchanged.To acquire the average results for each SINR calculation, 500 distinct simulation runs are carried out. According to Figures 3.2 and 3.3, the proposed beamformer clearly outperforms the other beamformers tested since it generates an output SINR that closely matches that of the optimal beamformer, regardless of the SNR and snapshot number. Contrastingly, the effectiveness of the other examined algorithms deteriorates as SNR increases, and a small number of snapshots result in a significantly low SINR.

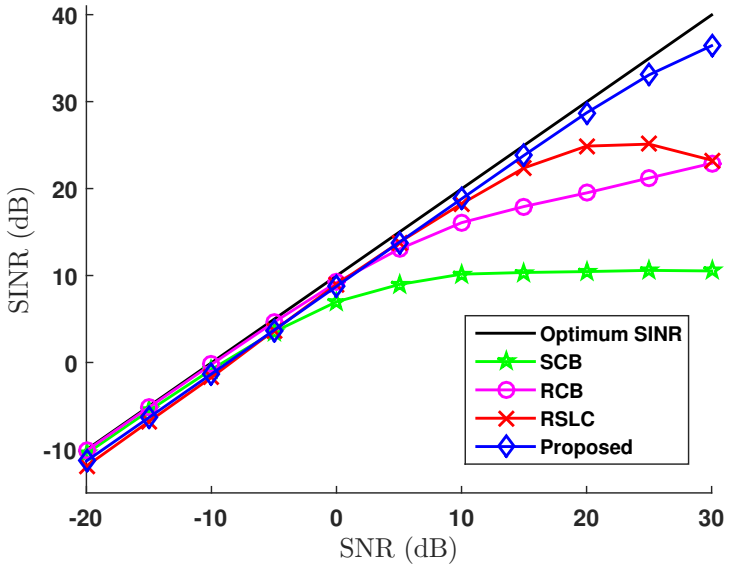

Figure 3.2: Output SINR performance with varying SNR at $K = 100$

3.4.2 Null expansion and mismatch in SOI's direction

In the current section, the performance of the considered beamformers is investigated under SOI mismatch conditions along with moving interferences. In the previous section, it was presumed that SOI strikes the array from 0^o however, it is incident

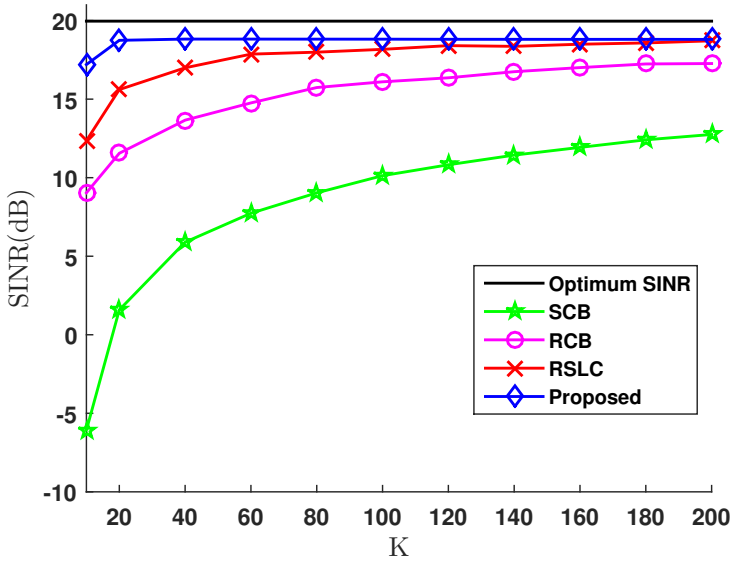

Figure 3.3: Output SINR performance with varying snapshot number K

from 2^o. So, the mismatch of 2^o is considered in the simulations. The directions, quantity of fictitious interferences, and null width remain intact from the previous section of this chapter.

The effect of varying input SNR and snapshot number on the output SINR is

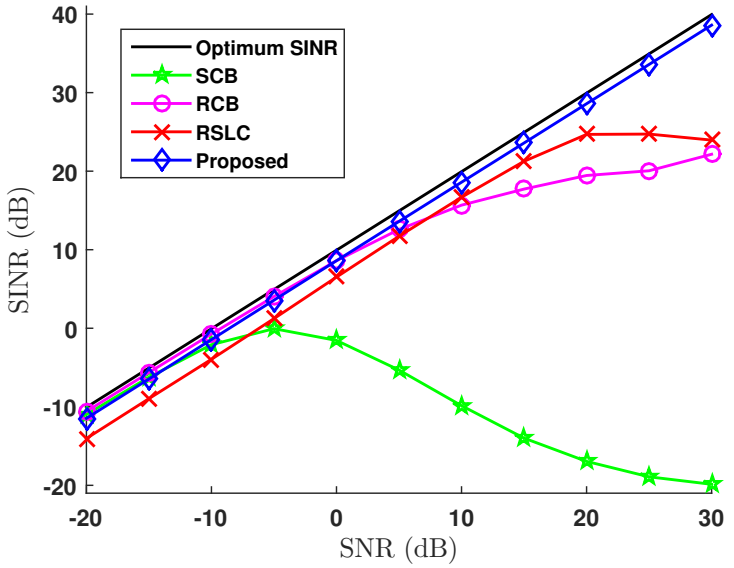

Figure 3.4: Output SINR performance with varying SNR at $K = 100$ in the presence of mismatch in SOI

investigated for the tested algorithms, and the corresponding results are depicted in Figures 3.4 and 3.5, respectively. The performance of null broadening along with DOA mismatch of the tested beamformers in the case of SNR variation is given in Figure 3.4. From there, it can be seen that the output SINR of the proposed technique tracks the optimum beamformer accurately, indicating that as SNR rises, the output SINR goes up linearly. However, the output SINR of RCB and RSLC failed to follow the optimal SINR for higher range of input SNR. The output SINR of the proposed beamformer is unaffected by the number of snapshots, as seen in Figure 3.5. Additionally, the suggested beamformer keeps the output SINR close to the

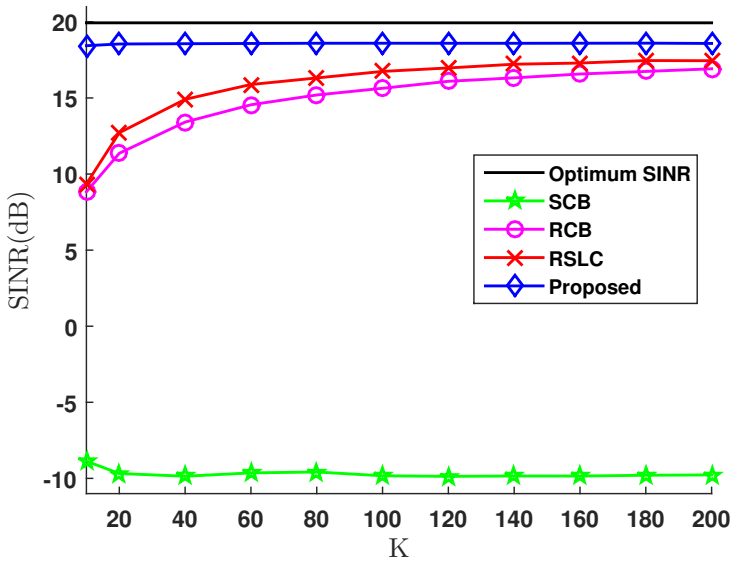

Figure 3.5: Output SINR performance with varying snapshot number K in the presence of mismatch in SOI

ideal curve. Consequently, it could be stated that the suggested beamformer is more reliable and offers greater resistance to DOA mismatch with broad nulls to cope with non-stationary interferences. Whereas, SCB is not suited for moving interferences and DOA mismatch, which is visible from its performance.

3.4.3 Minimization of moving interferences

In the present section, the impact of variation in the directions of interferences on the considered beamformers in two distinct situations is discussed in subsections 3.4.3.1 and 3.4.3.2.

3.4.3.1 Minimization of moving random interferences random with random SOI direction

In the current scenario, the directions of SOI as well as each interference are varied for each simulation run, while they are kept the same for every snapshot. The SOI is varied in the range of $[-2^o, 2^o]$ whereas the two interferences are uniformly distributed in $[-28^o, -22^o]$ and $[37^o, 43^o]$. The output SINR performance of the tested beamformers is shown in Figures 3.6 and 3.7, respectively. When attempting to identify SINR by varying SNR, the number of snapshots remains constant at $K = 100$, whereas when attempting to acquire SINR by changing the number of snapshots, the input SNR remains the same at 20 dB.

Figure 3.6 illustrates the performance of the tested beamformers in terms of SINR across varying SNR levels. It is evident that the proposed beamformer is better than the existing ones, especially when the SNR is high. The performance of the available methods declines for these higher levels of SNR. The impact of variation in snapshot number on the output SINR is depicted in Figure 3.7 which indicates that the suggested beamformer achieved satisfactory results when compared to the other beamformers that are taken into account.

3.4.3.2 Minimization of moving interferences with mismatches in SOI direction

It is considered that the DOA of SOI suffers from a mismatch of 2^o and the two interference signals also show deviation in the range of $[-3^o, 3^o]$ around -25^o, 40^o respectively. It is also assumed that the angles of interferences are altered within

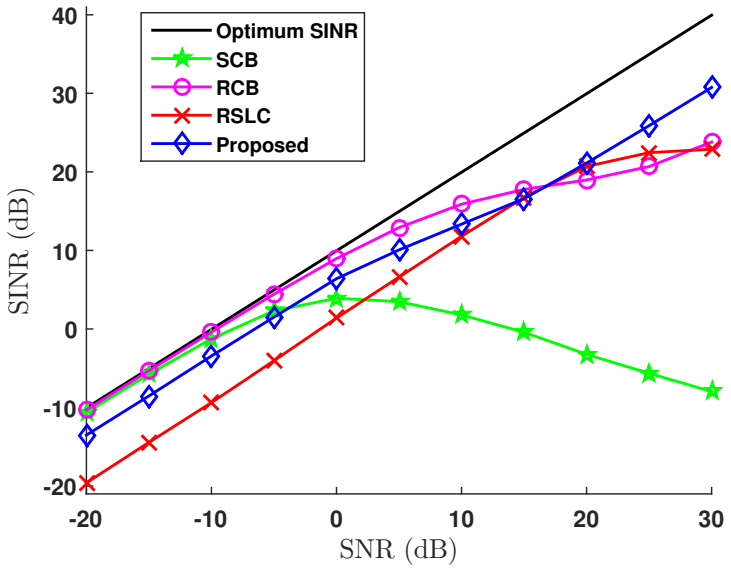

Figure 3.6: Output SINR performance comparison with varying SNR at $K = 100$ for minimization of quickly moving random interferences and random SOI direction

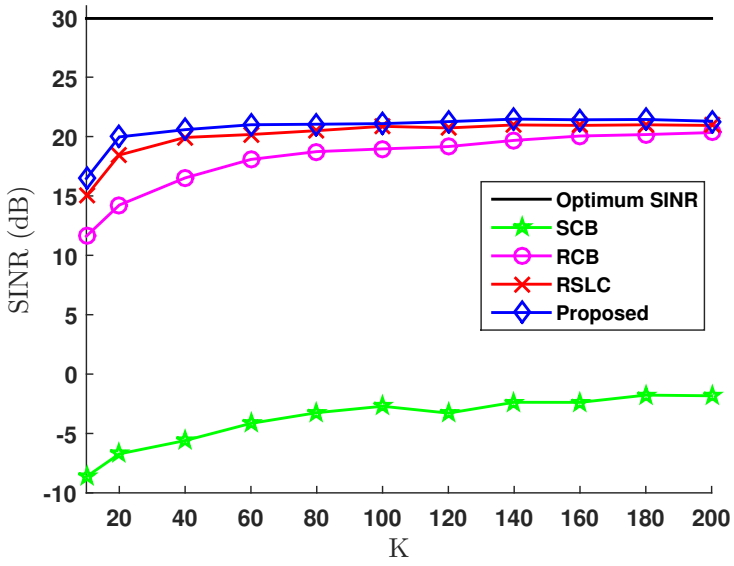

Figure 3.7: Output SINR performance comparison with varying snapshot number K at $SNR = 20$ dB for minimization of quickly moving random interference sources and random SOI direction

the considered deviation range for each snapshot while remaining the same for every simulation run.

As illustrated in Figure 3.8, the output SINR of the suggested approach precisely

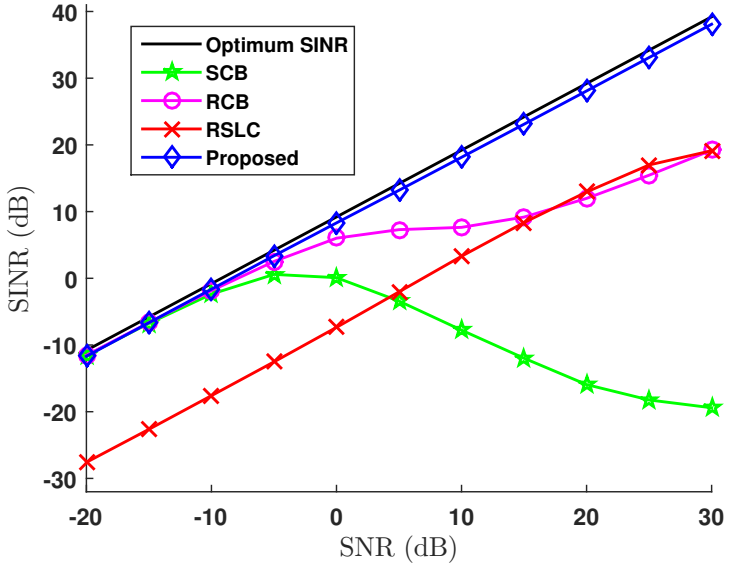

Figure 3.8: Output SINR performance comparison with varying SNR at $K = 100$ for minimization of quickly moving random interferences and mismatches in SOI

mirrors the optimal beamformer, meaning that, when SNR increases, the SINR output rises in a proportional manner. As the SNR increases, the effectiveness of SCB and RCB decreases, while the SINR of RSLC increases linearly, but there is a gap of approximately 20 as compared to an optimal beamformer. So, it can be said that in the mismatch scenario, the proposed beamformer outperforms the other considered beamformers. Now, snapshots number is also varied, and the effect is depicted in Figure 3.9. The figure highlights the superior performance of the proposed beamforming method compared to other tested beamformers. While the SINR remains nearly constant across all considered approaches for every snapshot number, a substantial difference in the actual output SINR values is observed. The SINR difference of approximately 1.5 dB, 10 dB, 13.5 dB and 25 dB is observed in the proposed, RSLC, RCB, and SCB, respectively, as compared to optimal SINR.

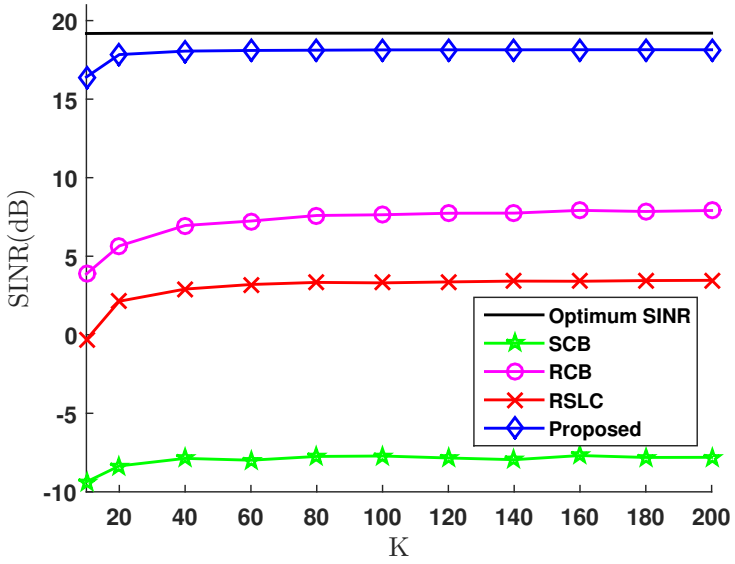

Figure 3.9: Output SINR performance comparison with varying snapshot number K at $SNR = 10$ dB for minimization of quickly moving random interferences and mismatches in SOI

3.5 Conclusion

This chapter introduces an adaptive beamformer capable of suppressing the interference from moving sources and being robust against errors in the DOA estimation of the SOI. The computation of the optimal weight vector involves the use of the reformulated interference matrix and imposing magnitude regulations on the Region of Interest (ROI). The performance of the proposed beamformer is examined by comparing its simulation results with those of conventional and recent methods. Simulation results reveal that the proposed beamformer is able to widen the nulls and, consequently, offer a higher output SINR compared to the other methods tested.

Chapter 4

Dual Beam Adaptive Beamforming with SLL Control

4.1 Introduction

In recent years, a lot of work has been done in array signal processing to address the issues of adaptive beamforming, which is incredibly essential for radar, navigation, wireless communication, remote sensing, etc. [67, 102–104]. Adaptive beamforming is a significant technique utilized to amplify the SOI while minimizing the effect of interferences and background noise through dynamic alterations made to the array components' weights [2].

There are many adaptive beamforming algorithms in the literature, and the most widely used beamformer is MVDR [69] that is also called SCB. Despite being the renowned beamformer, it does have some limitations. It can only deal with a single SOI at a particular moment, and in numerous fields of wireless communications such as satellite communications [105–108], mobile communications [109], etc., it is necessary to process several SOIs at the same time while also handling interfering signals [110–112]. Therefore, the adaptive beamforming algorithms must be able to create multiple beams so they can efficiently receive multiple signals from different desired directions while blocking out interfering signals at the same time. Moreover,

the SCB does not take into account the SLL, which is a critical attribute of the beampattern. In an adaptive antenna array environment, it is possible for sudden or unexpected interferences to disrupt the array, resulting in reduced performance since the beamformer is unable to minimize these unexpected interferences. Hence, an efficient method to take care of this issue is by controlling the SLL so that the unintentional interferences can be suppressed.

Various techniques for controlling the SLL have been described in the literature [113–116, 118–124]. For reducing the SLL, several quadratic constraints have been applied on the complete beampattern area except the main lobe region. The quadratic constraints in the considered region keep the SLL level below a certain value, but employing excessive constraints may overconstrain the optimization problem, which can lead to an infeasible solution. A subspace based approach is presented in [123] to minimize the SLL. The subspace comprises the entire sidelobe region, and sampling is performed on several angles of the subspace region. The powers of sampled angles in the subspace region are minimized to reduce the SLL. Nevertheless, the number of angles in the subspace region is not specified to ensure SLL control. Evolutionary computing has also been utilized for regulating the SLL and described in [114–117], but their iterative behavior sometimes makes them impractical because of their large convergence times. Another method based on gravitational search to minimize the SLL is presented in [119]. However, the search procedure is quite ad hoc and also not restricted to a global search.

This chapter presents an adaptive beamforming technique that is capable of directing dual beams towards two distinct desired directions while simultaneously diminishing interferences and managing the SLL. The optimization problem of SCB for obtaining dual beams only involves only one additional constraint. Essentially, this involves generating a fresh steering vector for the second SOI, and the response towards that direction is limited to a value of one. For managing the SLL, four regions of interest (ROIs) are chosen in the vicinity of the two beams, and the strengths that correspond to these regions are limited to a particular value. Beamwidth between first minimas (BWFM) is employed for calculating the ROIs widths, and to address the issue of overconstraints, a practical formula has been devised to determine the appropriate

constraint number. The optimization of dual beams is altered by incorporating inequality constraint on ROIs for reducing SLL. consequently, the suggested algorithm is able to receive dual SOIs from two different sources at the same time. In addition to this, the devised algorithm is capable of regulating the sidelobe level at a predefined value, thus, the algorithm becomes less susceptible to unanticipated interferences around dual lobes.

The organization of this chapter is as follows. The basic mathematical modeling of received signals on the antenna array and SCB's optimization problem are deduced in section 4.2. The mathematical modeling of the suggested algorithm is given in sections 4.3 and 4.4. Simulation results for various scenarios are detailed in section 4.5, followed by the concluding section.

4.2 Signal model

Consider a ULA consisting of M number of elements with an inter-element spacing of half wavelength. For multiple desired signal environments, it is considered that N number of desired signals with J interference signals in the presence of noise are incident on the M antenna elements. It is assumed that the total K number of snapshots are received on the array. The mathematical representation of the received signal vector for the k^{th} snapshot is as follows:

$$\boldsymbol{x}(k) = \boldsymbol{A}_o\boldsymbol{s}_o(k) + \boldsymbol{A}_i\boldsymbol{s}_i(k) + \boldsymbol{n}(k), \quad k = 1, 2, ..., K \tag{4.2.1}$$

The dimensions of the received signal vector are $M \times 1$. $\boldsymbol{s}_o$ and $\boldsymbol{s}_i$ represent the vectors of SOIs and interference signals, respectively.

$$\boldsymbol{s}_o = [s_{o_1}, s_{o_2}, ..., s_{o_N}]_{N\times 1} \tag{4.2.2}$$

$$\boldsymbol{s}_i = [s_{i_1}, s_{i_2}, ..., s_{i_J}]_{J\times 1} \tag{4.2.3}$$

In the equation (4.2.1), the matrices that represent the steering vectors of SOIs and interferences are indicated by $\boldsymbol{A}_o$ and $\boldsymbol{A}_i$.

$$\boldsymbol{A}_o = [\boldsymbol{a}(\theta_{o_1}), \boldsymbol{a}(\theta_{o_2}), ..., \boldsymbol{a}(\theta_{o_N})]_{M\times N} \tag{4.2.4}$$

$$\boldsymbol{A}_i = [\boldsymbol{a}(\theta_{i_1}), \boldsymbol{a}(\theta_{i_2}), ..., \boldsymbol{a}(\theta_{i_J})]_{M\times J} \tag{4.2.5}$$

For n^{th} desired signal, the steering vector is represented by $\boldsymbol{a}(\theta_{o_n})$, n=1,2,..,N with DOA θ_{o_n} and $\boldsymbol{a}(\theta_{o_j})$, j=1,2,..J is the steering vector for j^{th} interference with the DOA of θ_{i_j}. For M antenna elements in the array the vector $\boldsymbol{a}(\theta)$ for angle θ is represented as

$$\boldsymbol{a}(\theta) = [1, e^{j\pi \sin(\theta)}, ..., e^{j\pi(M-1)\sin(\theta)}]^T \tag{4.2.6}$$

where $(.)^T$ represent the transpose.

From the received K snapshots on the antenna array, the covariance matrix is estimated, which is written as

$$\hat{\boldsymbol{R}} = \frac{1}{K}\sum_{k=1}^{K} \boldsymbol{x}(k)\boldsymbol{x}(k)^H \tag{4.2.7}$$

The formulation SCB is determined by reducing the output power and constraining the unity response to the DOA of the single SOI. For the weight vector $\boldsymbol{w}$ and DOA of the desired signal θ_{o_1}, the formulation of SCB is given as

$$\min_{\boldsymbol{w}} \ \boldsymbol{w}^H \hat{\boldsymbol{R}} \boldsymbol{w}, \quad s.t.\ \boldsymbol{w}^H \boldsymbol{a}(\theta_{o_1}) = 1 \tag{4.2.8}$$

The SCB is limited to single SOI situations and therefore cannot be used in scenarios where multiple desired signals are present. In scenarios with multiple desired signals at the same time, a beamformer should have distinct main beams pointing towards every desired signal for its efficient reception [125, 126]. Thus, there is a need to modify the SCB for receiving multiple desired signals simultaneously. In the current chapter, the SCB is adjusted to effectively receive a couple of SOIs simultaneously, even when there are interferences and noise present.

4.3 Proposed dual beam beamformer

To enhance the performance of SCB, an additional constraint is added to its optimization problem. The additional constraint restricts the response to unity in the DOA of the second desired signal θ_{o_2}. Thus, a modified SCB facilitates the reception of the second desired signal by forming an independent beam towards its direction.

The modified optimization problem for dual beams is described as

$$\begin{aligned} &\min_{\boldsymbol{w}_d} \ \boldsymbol{w}_d^H \hat{\boldsymbol{R}} \boldsymbol{w}_d \\ &subject \quad to \\ &\boldsymbol{w}_d^H \boldsymbol{a}(\theta_{o_1}) = 1 \\ &\boldsymbol{w}_d^H \boldsymbol{a}(\theta_{o_2}) = 1 \end{aligned} \tag{4.3.1}$$

where $\boldsymbol{w}_d$ is the optimal weight vector for SCB-dual beam (SCB-DB) and it is calculated by solving the equation (4.3.1) in convex optimization solvers CVX [101].

4.4 Sidelobe level management with dual beam

The SCB pays attention to the SOI and interferences and put less emphasis on the SLL. Since the sidelobes are more prevalent close to the main lobe, these should be decreased. If interferences strike the antenna array from the dominant sidelobe directions, then the performance of the beamformer is adversely affected as the interfering signals are amplified instead of being blocked. In these scenarios, reducing the level of the sidelobes located close to the main beam can ameliorate the performance of the beamformer since it can withstand unexpected interferences [122]. Thus, a beamformer is developed for dual beams and SLL minimization and explained as follows:

1. Initial parameters: (i). Define antenna number (M)
   (ii) Number of received samples (K)
   (iii) DOAs of SOIs θ_{o_1}, θ_{o_2} and interferences θ_{i_1}, θ_{i_2}.

2. Determine the sample covariance matrix using the received K snapshots as per the formula provided in equation (4.2.7).

3. To acquire dual beams towards the two SOIs, modify the SCB beamformer according to equation (4.3.1).

4. Determine the weight vector $\boldsymbol{w}_d$ and array factor (AF1) utilizing equation (4.3.1).

5. From the AF1 of the radiation pattern, compute the BWFM for the dual beams. The BWFM for the two beams are denoted as Δ_{m_1} and Δ_{m_2}.

6. Four ROIs are chosen that are located near to the main lobes.

   - The sizes of ROIs are chosen based on the DOAs and BWFM of the dual beams. The ROIs' widths are chosen based on the DOAs and BWFM of both main lobes. The sizes of four ROIs are represented as u_1, u_2, u_3, and u_4, which are computed as follows:

$$\begin{aligned} \boldsymbol{u_1} &= [\theta_{o1} - \alpha_1, \theta_{o1} - \alpha_2] \\ \boldsymbol{u_2} &= [\theta_{o1} + \alpha_1, \theta_{o1} + \alpha_2] \\ \boldsymbol{u_3} &= [\theta_{o2} - \alpha_3, \theta_{o2} - \alpha_4] \\ \boldsymbol{u_4} &= [\theta_{o2} + \alpha_3, \theta_{o2} + \alpha_4] \end{aligned} \tag{4.4.1}$$

   where, $\alpha_1 = \frac{3\Delta_{m1}}{4}$, $\alpha_2 = \frac{\Delta_{m1}}{2}$,$\alpha_3 = \frac{3\Delta_{m2}}{4}$ and $\alpha_4 = \frac{\Delta_{m2}}{2}$.

7. The same number of constraints are imposed on every ROI, and the amount of constraints put into place for each ROI is decided by an experimentally derived formula, which is illustrated as

$$\frac{\log_2 N}{2} \tag{4.4.2}$$

8. The outputs of all the ROIs are computed and restricted to a particular value δ. Then the computed conditions are included in equation (4.3.1) and the reformulated problem is given as

$$\begin{aligned} &\min_{\boldsymbol{w}_o} \ \boldsymbol{w}_o^H \hat{\boldsymbol{R}} \boldsymbol{w}_o \\ &subject \quad to \\ &\boldsymbol{w}_o^H \boldsymbol{a}(\theta_{o_1}) = 1 \\ &\boldsymbol{w}_o^H \boldsymbol{a}(\theta_{o_2}) = 1 \\ &|\boldsymbol{w}_o^H \boldsymbol{a}(\theta_{SLL})| <= \delta; \quad \theta_{SLL} \in (u_1 ... u_4) \end{aligned} \tag{4.4.3}$$

9. The optimum weight vector for minimizing SLL and obtaining dual beams is calculated by solving the equation (4.4.3) using the CVX toolbox of Matlab.

4.5 Simulation results and discussions

To examine the efficiency of the suggested beamformer, simulations are performed for two distinct conditions that are symmetric SOIs and the asymmetric SOIs. For both scenarios, an array of $M = 32$ antenna elements equi-spaced at distances $\lambda/2$ is assumed. λ is the wavelength. To compute the sample covariance matrix, $K = 500$ snapshots are utilized.

4.5.1 Symmetric SOIs

In the current scenario, it is assumed that the two SOIs θ_{o_1} and θ_{o_2} are incident on the antenna array from symmetric directions, so if the DOA of the first SOI is θ_{o_1} then the second SOI will impinge the array from $\theta_{o_2} = -\theta_{o_1}$. For carefully analyzing the proposed algorithm, the directions of the SOIs are changed in the range of $\text{SOI}_1 = [-60^o, -10^o]$ and $\text{SOI}_2 = [10^o, 60^o]$ with a step size of 1^o. It is considered that two interference signals also impinge on the array from directions $\theta_{i_1} = -30^o$ and $\theta_{i_2} = 25^o$ along with the two SOIs. The SNRs of both the SOIs are 20 dB and 10 dB, while the INRs of the interference signals are 15 dB and 20 dB for this scenario. Angles ranging from $[\theta_i - 8^o, \theta_i + 8^o]$ are left out because the proposed algorithm finds it challenging to effectively block out the interferences inside the main beam area.
The simulations are carried out for all the angles of the considered range $[-60^o, 60^o]$ with a step size of 1^o. However, it is impractical to display all the beam patterns that have been produced for the specified range. As a result, three diverse angles have been selected that situate in the farthest left, farthest right, and amid the considered range.
The radiation patterns for these three angles are illustrated in Figures 4.1, 4.2 and 4.3. The beampatterns indicate that the proposed algorithm minimizes the SLL for the entire considered range and also correctly places the main lobes to the two SOIs. Further, it can be easily noticed from the obtained radiation patterns that the SCB-DB beamformer has increased sidelobes, and these sidelobes are more prominent close to the main lobes. These prominent sidelobes can enhance unexpected interferences

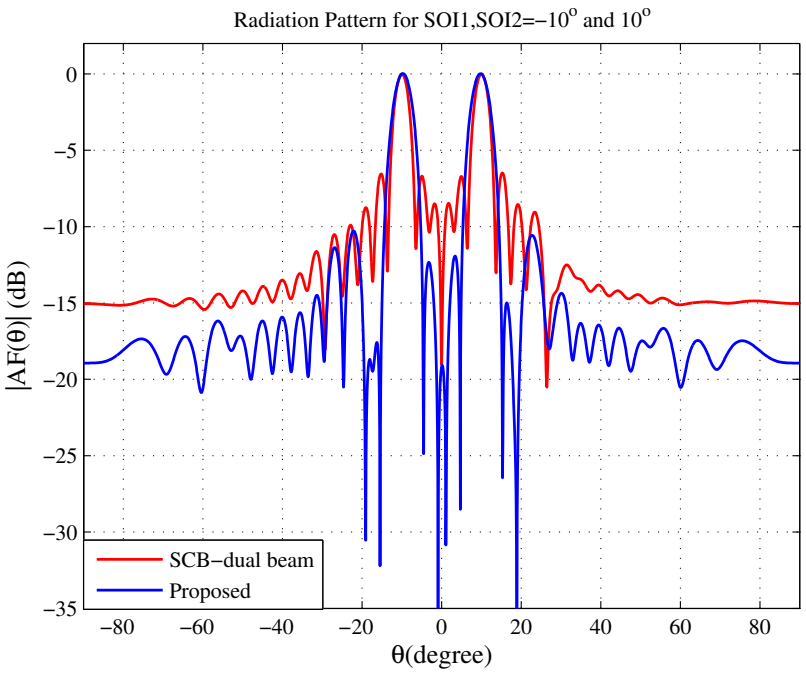

Figure 4.1: Radiation patterns produced for $\theta_{o_1} = -10^o$, $\theta_{o_2} = 10^o$.

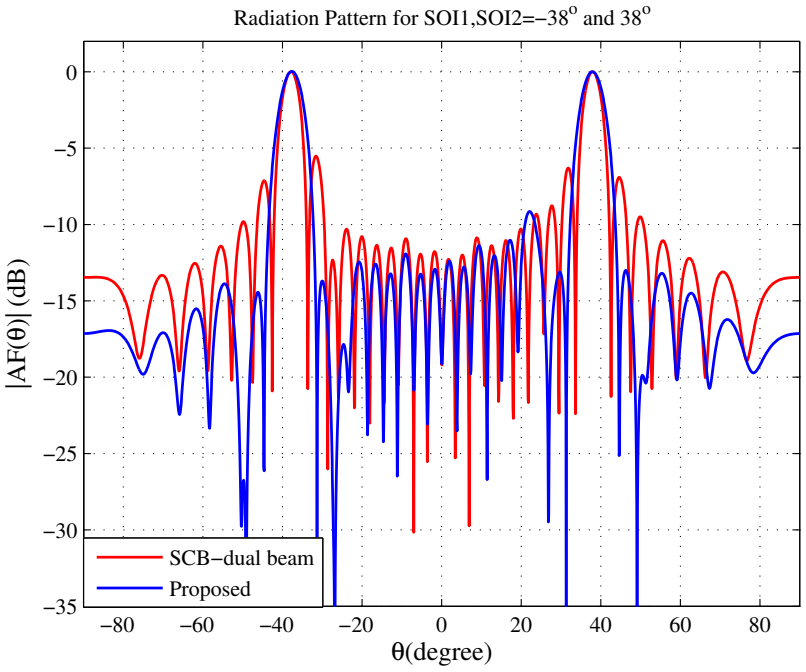

Figure 4.2: Radiation patterns obtained for $\theta_{o_1} = -38^o$, $\theta_{o_2} = 38^o$.

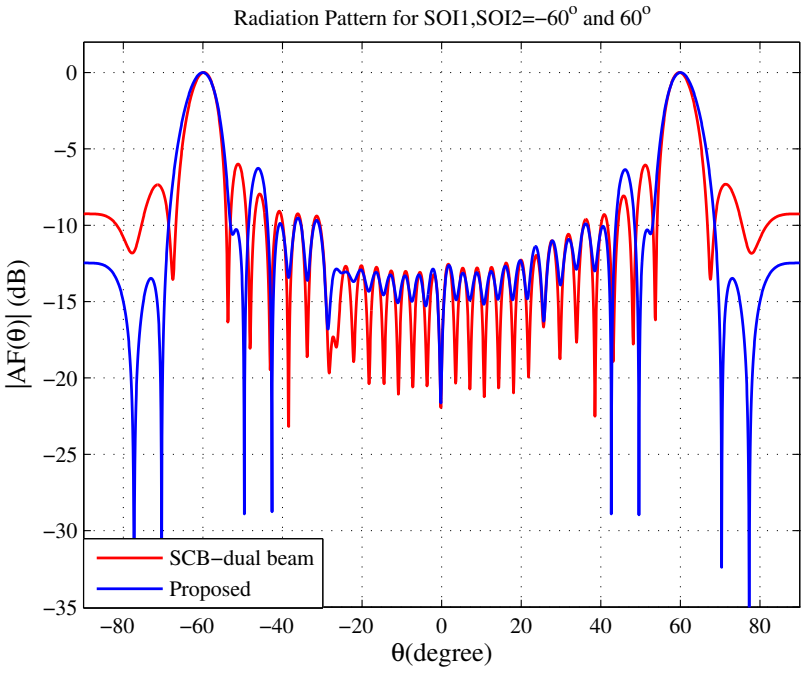

Figure 4.3: Radiation patterns obtained for $\theta_{o_1} = -60^o$, $\theta_{o_2} = 60^o$.

which leads to performance deterioration.

Due to the practical limitation of not showing each obtained beam patterns for the considered range of DOAs of SOIs $[-60^o, 60^o]$, the proposed algorithm is investigated by computing characteristic parameters.These parameter measurements are derived from the radiation patterns across the specified range. The characteristic parameters include relative SLL, maximum SLL, 3-dB beamwidth (BW), BWFM, and the angular disparity in the main lobe's position from the corresponding angle of SOI.

The angular disparity between main lobe's position and the SOI's direction as well as relative SLL for the SCB-DB and the suggested algorithm is depicted in Figure 4.4. From there, it is evident that the suggested approach minimizes the SLL in the ROI. The proposed algorithm attains the greatest and least improvement of around 20 dB and 2 dB, respectively, in comparison to the SCB-DB beamformer in terms of relative SLL. Now, the main lobe deviation w.r.t. the actual DOA of SOI is computed, and the results are shown in the third and fourth graphs of Figure 4.4. It is observed from the graphs that the mean deviation for the considered range is less than 1% which can be considered negligible and can be neglected.

The performances of BWFM and 3-dB BW for the considered algorithms are shown

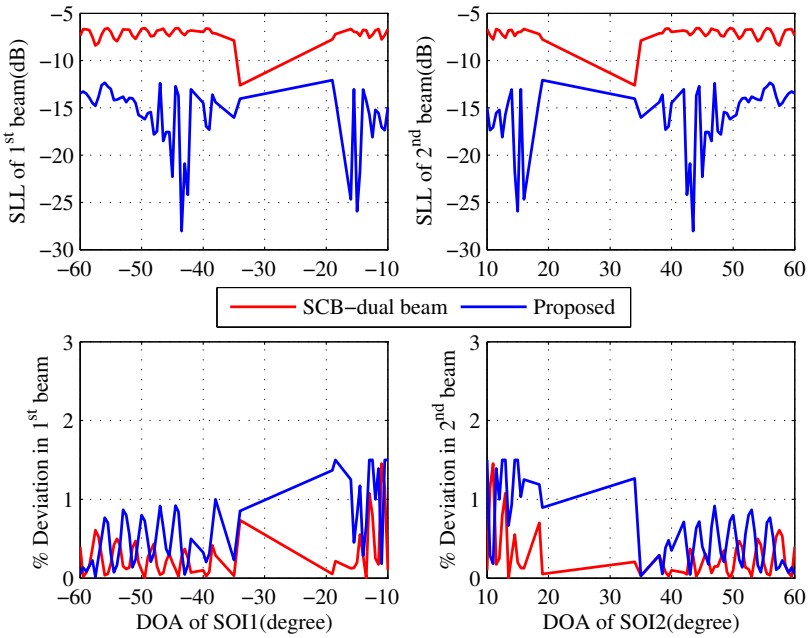

Figure 4.4: Relative SLL and deviation in main lobes in SCB-DB and the proposed method

in Figure 4.5.From there, it is noticeable that a slight expansion of the main lobes is seen, which is likely a consequence of minimizing the sidelobes. The proposed algorithm widens the BWFM and 3-dB BW by approximately 4^o and 1.5^o respectively, as compared to the SCB-DB. It is already anticipated that reducing the strength of the sidelobes can result in the concentration of energy towards the main lobes and causes beam broadening.

The evaluated performance of the beamformers under consideration is analyzed concerning SLL across the entire beam pattern area. The outcomes are illustrated in Figure 4.6. The proposed method potentially reduces the SLL even for non-ROIs, which makes the method less vulnerable to unanticipated interferences in the non-ROIs. The proposed algorithm demonstrates a notable improvement, with a maximum increase of 4 dB observed in the side lobe level (SLL) in comparison to the SCB-DB.

To achieve a more precise comprehension, the average of the distinctive parameters

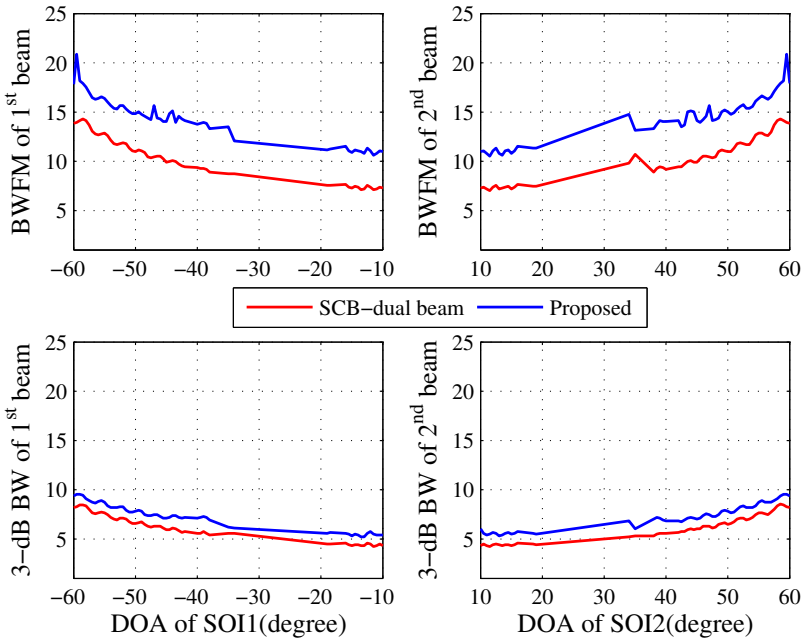

Figure 4.5: BWFM and 3-dB BW of the SCB-DB and the suggested method

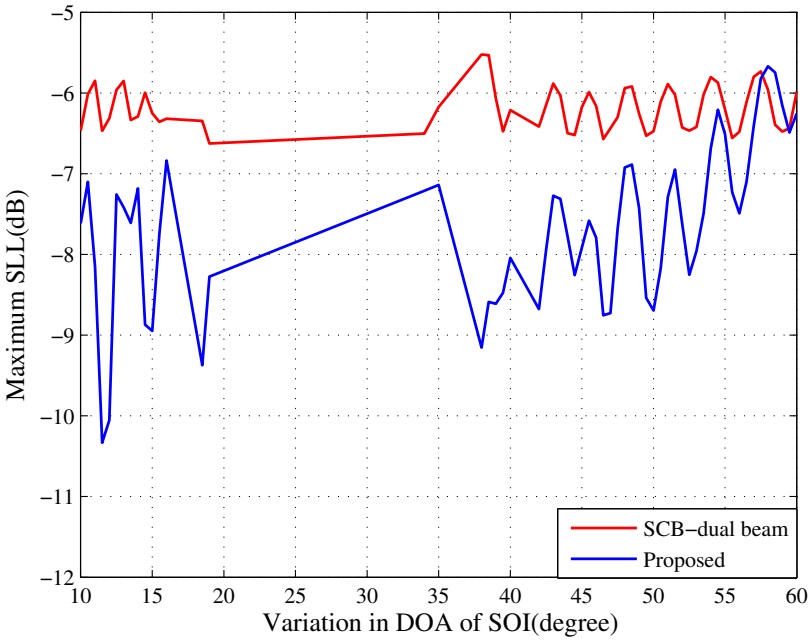

Figure 4.6: Maximum SLL obtained of the SCB-DB and the suggested method

are computed for the all the angles of SOIs and shown in Table 4.1. The improvement of 8 dB in the SLL of the ROIs is observed in the proposed algorithm. Additionally, the maximum SLL is also minimized by 1.4 dB as compared to the SCB-DB. However, the enhancement comes with the drawback of beam widening. The beam widening is evaluated by 3-dB BW and BWFM, which are increased by 1.1^o and 4^o, respectively. The angular disparities between the actual main lobes' directions and the assigned desired directions, as well as the nulls' positions and the interference directions, are also determined, and insignificant discrepancies are produced by the proposed approach.

Table 4.1: Characteristic parameters for symmetric SOIs scenario

Characteristic Parameters	SCB-DB	Proposed Algorithm
SLL of first lobe (dB)	-7.1792	-15.8140
SLL of second lobe (dB)	-7.1792	-15.814
Maximum SLL (dB)	-6.1934	-7.678
3-dB BW first lobe (^{o})	6.1307	7.2717
3-dB BW second lobe (^{o})	6.1017	7.2427
BWFM first lobe (^{o})	10.2371	14.1925
BWFM second lobe (^{o})	10.2737	14.2383
Angular deviation in first lobe (^{o})	0.1008	0.1015
Angular deviation in second lobe (^{o})	0.0939	0.1001
Angular deviation in first null (^{o})	0.0032	0.0021
Angular deviation in second null (^{o})	0.0018	0.0034

4.5.2 Asymmetric SOIs

For this scenario, it is assumed that SOIs impinge on the antenna array from asymmetric directions. Therefore, the first desired signal is taken at $\theta_{o_1} = 0^o$, and the DOA of the second signal is changed in a step size of 1^o for the range of

$[40^o, 60^o]$. The remaining parameters such as SNR, number of interferences, directions of interferences, and INR, are kept the same as that of the symmetric SOIs scenario. The beam patterns are produced for all the angles in the range $[40^o, 60^o]$ but all the obtained radiation patterns can not be shown here. Consequently, three individual angles are selected that are located at the most left end, the most right end, and amid the specified range. The results for the chosen angles are shown in Figures 4.7, 4.8 and 4.9. From the figures of the radiation patterns, it is observed that the proposed approach fulfill its objectives of dual beams along with SLL minimization as the main lobes are pointed towards the two SOIs and sidelobes are also minimized in the ROIs.

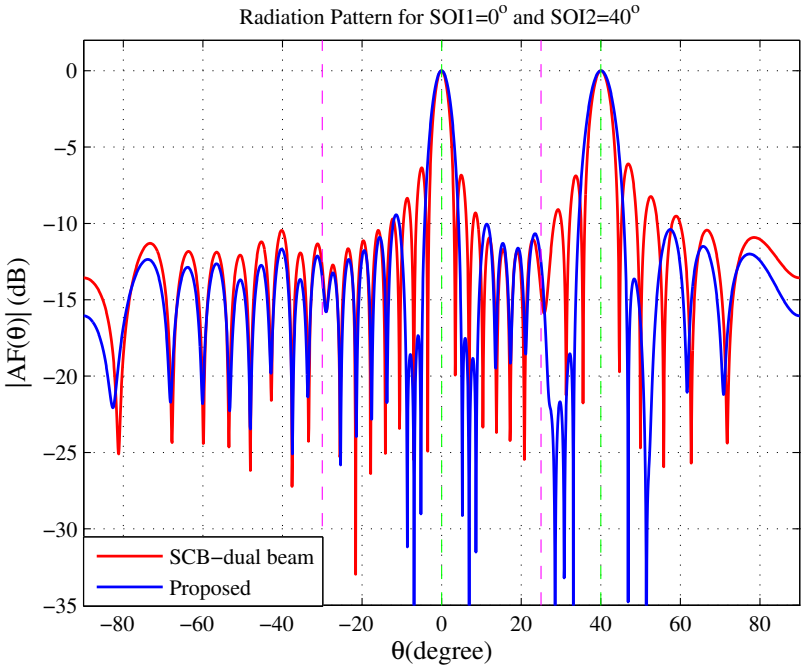

Figure 4.7: Radiation patterns for $\theta_{o_1} = 0^o$, $\theta_{o_2} = 40^o$

For an asymmetric scenario, radiation patterns are obtained for the entire considered range, and characteristic parameters are computed from the radiation patterns. The determined parameters are illustrated in Figures 4.10 and 4.11. From the first and second graphs of Figure 4.10, it is observed that the SLL is greatly reduced and preserved below -16 dB for the whole set of angles. The proposed algorithm improves the relative SLL by as much as 16 dB, when compared to the

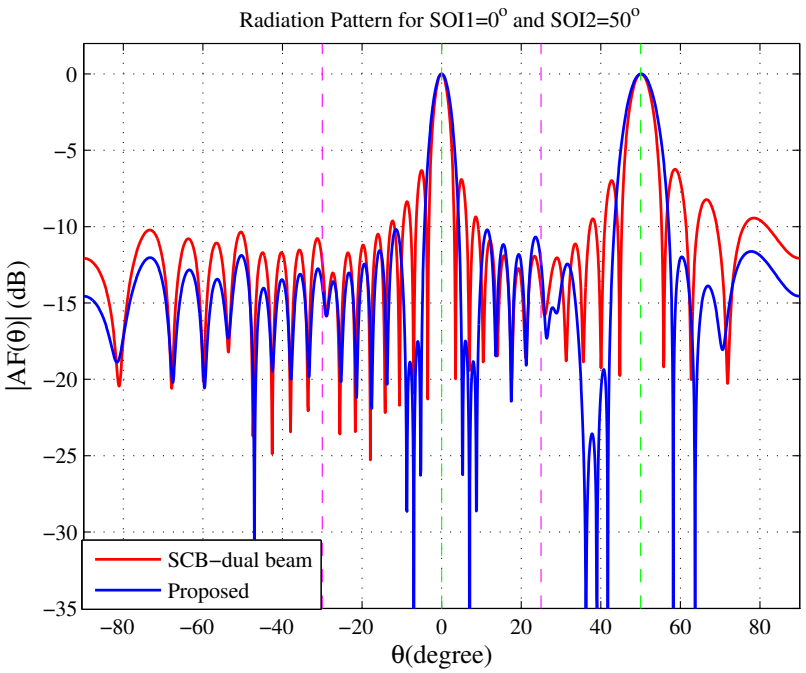

Figure 4.8: Radiation patterns for $\theta_{o_1} = 0^o$, $\theta_{o_2} = 50^o$

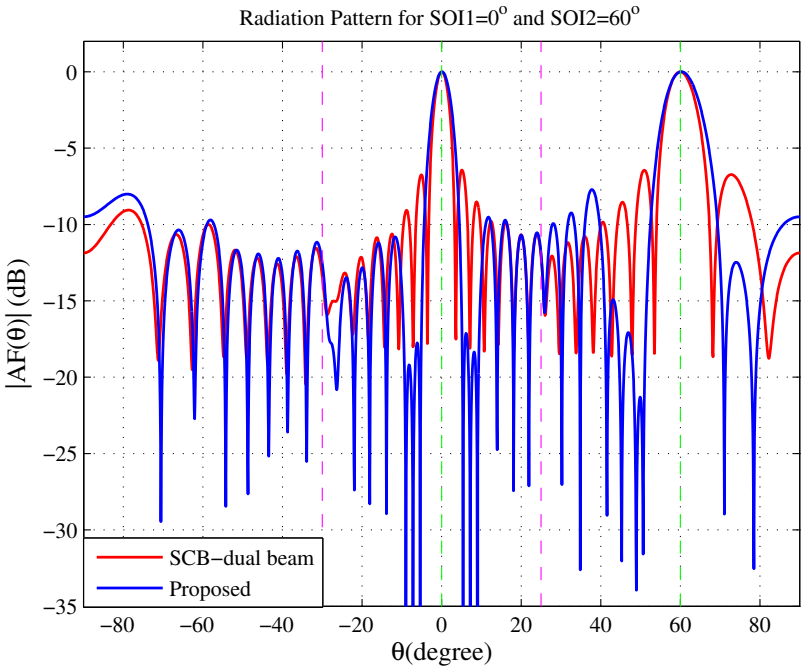

Figure 4.9: Radiation patterns for $\theta_{o_1} = 0^o$, $\theta_{o_2} = 40^o$

SCB-DB beamformer. The SLL in non-ROI is indicated in the third graph of Figure 4.10, from there it is evident that the suggested beamformer effectively reduces the SLL even outside the desired area, which can be seen as an added benefit. For the entire specified range, the SLL is maintained below the SCB-DB beamformer. Now, the difference between the direction of the main beam in the obtained radiation patterns and its actual DOA is computed and shown in the fourth trace of Figure 4.10. The deviation of 0.6% is observed in the main beam, which is very insignificant. So, it can efficiently point main lobes to its DOAs.

The BWFM and 3-dB BW are also evaluated from the obtained radiation patterns

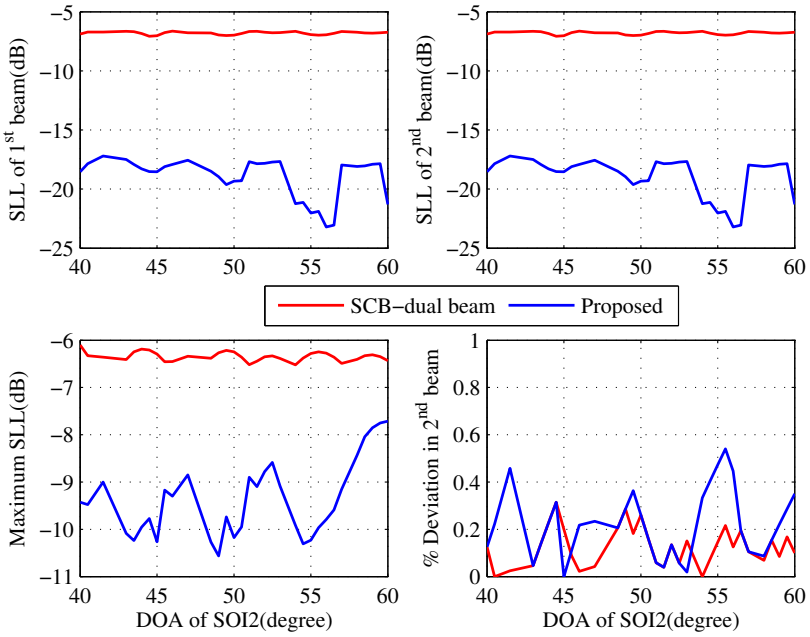

Figure 4.10: Relative SLL and deviation in dual beams obtained for asymmetric case

and illustrated in Figure 4.11. Both the beamwidths BWFM and 3-dB BW of the proposed beamformer are increased in comparison to the SCB-DB beamformer. The increase in beamwidths causes the widening of beams that can be expected because when the power of the sidelobes is decreased, it can be accumulated towards the main lobes.

Table 4.2 illustrates the important characteristic parameters produced by the tested beamformers. It is clear that the suggested algorithm provides a significant

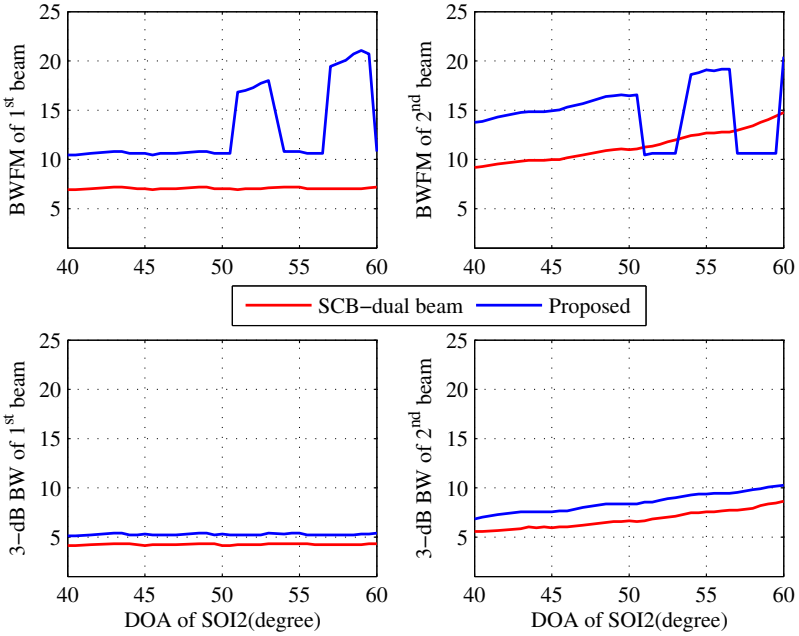

Figure 4.11: BWFM and 3-dB BW for asymmetric case

Table 4.2: Characteristic parameters for asymmetric SOIs scenario

Characteristic Parameters	SCB-DB	Proposed Algorithm
SLL of first lobe (dB)	-6.8052	-18.9746
SLL of second lobe (dB)	-6.8053	-18.9749
Maximum SLL (dB)	-6.3410	-9.3766
3-dB BW first lobe (^{o})	4.2518	5.2718
3-dB BW second lobe (^{o})	6.8809	8.6073
BWFM first lobe (^{o})	7.0609	13.1509
BWFM second lobe (^{o})	11.52	14.6945
Angular deviation in first lobe (^{o})	0.0200	0.0300
Angular deviation in second lobe (^{o})	0.0645	0.0730
Angular deviation in first null (^{o})	0.0141	0.0160
Angular deviation in second null (^{o})	0.0023	0.0041

enhancement of 12 dB in the SLL surrounding the main lobes. Furthermore, a 3 dB improvement is offered by the proposed method in the maximum SLL outside the ROI as compared to the SCB-DB.The notable enhancement in SLL has a slight repercussion, which is manifested in the 3-dB BW and BWFM values, which indicate a little expansion of the main beam. The stable main beams and sharp nulls are directed toward the DOA of SOIs and interferences, respectively, as the suggested algorithm exhibits a negligible angular disparity in the main lobes and nulls directions.

4.5.2.1 Output SINR performance

To evaluate the output SINR for the considered beamformers, a formula is utilized, which is given in equation (4.5.1).

$$\begin{aligned} output\ SINR &= \frac{output\ signal\ power}{output\ interference\ plus\ noise\ power} \\ &= \frac{\boldsymbol{w}_o^H \boldsymbol{R}_{ss} \boldsymbol{w}_o}{\boldsymbol{w}_o^H \boldsymbol{R}_{i+n} \boldsymbol{w}_o} \end{aligned} \tag{4.5.1}$$

Where $\boldsymbol{w}_o$, $\boldsymbol{R}_{ss}$ and $\boldsymbol{R}_{i+n}$ represent the weight vector, signal covariance matrix, and interference plus noise covariance matrix. The covariance matrices are determined as

$$\boldsymbol{R_{ss}} = \sum_{n=1}^{N} \sigma_{o_n}^2 \boldsymbol{a}(\theta_{o_n}) \boldsymbol{a}(\theta_{o_n})^H \tag{4.5.2}$$

$$\boldsymbol{R_{i+n}} = \sum_{j=1}^{J} \sigma_{i_j}^2 \boldsymbol{a}(\theta_{i_j}) \boldsymbol{a}(\theta_{i_j})^H + \sigma_p^2 \boldsymbol{I} \tag{4.5.3}$$

where, $\sigma_{o_n}^2$ represent the power of n^{th} desired signal, $\sigma_{i_j}^2$ is the power of j^{th} interfering signal and σ_p^2 is the noise power.

In both symmetric and asymmetric scenarios, the output SINR for the first SOI is computed by considering the second desired signal as interference. The output SINR is computed by varying the input signal-to-noise ratio (SNR). The comparison of output SINR for SCB-one beam, SCB-DB, and the suggested beamformer for both symmetric and asymmetric scenarios is depicted in Figures 4.12 and 4.13 respectively. From there, it can be seen that the proposed algorithm does not result in an adverse effect on output SINR even with two main lobes and sidelobes minimization. The

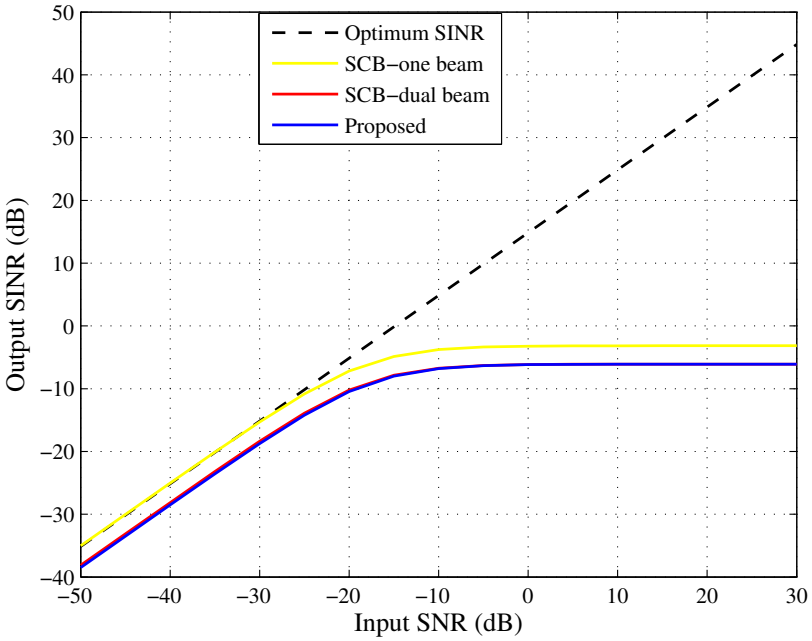

Figure 4.12: Output SINR performance with input SNR in symmetric SOIs

suggested beamformer performs at a comparable level to the SCB-DB in terms of SINR. Additionally, there is only a small disparity in SINR between the SCB-one beam and the suggested beamformer.

Table 4.3 illustrates a comparison of different methodologies with the proposed work. The authors in [112] employed a planar array consisting of 16×10 antenna elements, capable of resolving two SOIs separated by an angle of 40^o.The SLL of -10 dB may be insufficient to effectively reduce undesired signals within the sidelobe region.In [122] and [123], a single desired signal is addressed using 30 and 32 antenna elements, respectively. The authors of [122] reduced the SLL to -20 dB, while the authors of [123] achieved a reduction to -30 dB. The proposed approach can simultaneously address two desired signals that are merely 20^o apart using an array of 32 antenna elements. Additionally, the SLL has been diminished to -19 dB.

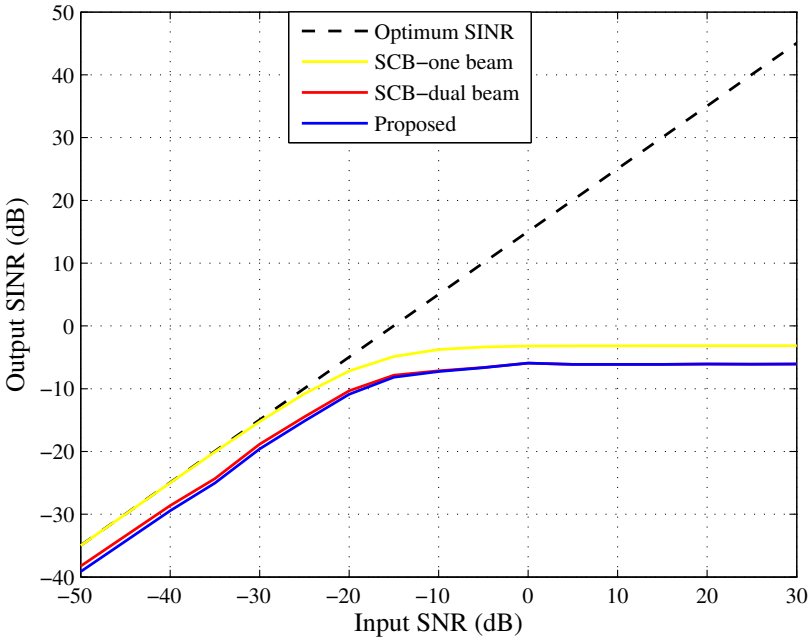

Figure 4.13: Output SINR performance with input SNR in asymmetric SOIs

Table 4.3: Comparative analysis of various methods.

Methods ↓	**Antenna Elements**	**No. of SOIs**	**SLL**
H. Singh et al. [112]	16×10 Planar	Two SOIs 40^o apart	-10 dB
I.P. Gravas et al. [122]	30 ULA	Single SOI	-20 dB
M. Zhou et al. [123]	32 ULA	Single SOI	-30 dB
Proposed work	32 ULA	Two SOIs 20^o apart	-19 dB

4.6 Conclusion

A new method is devised to minimize the SLL when two desired signals are present along with interferences. For achieving the aim, the optimization of the traditional SCB is reformulated for two SOIs and by introducing appropriate number of constraints for SLL reduction. By doing so, the algorithm is less likely to be affected by any unexpected interruptions, and at the same time, it can create two

lobes in the two preferred directions. The findings from the suggested algorithm demonstrate that it can realize its objectives even when the SOIs are situated near one another. Furthermore, stable main beams and nulls are steered to the desired signals and interferences, respectively.

Chapter 5

Improvements in sparse array via additional constraints

Antenna array configuration has a substantial influence on the performance of a beamformer. The majority of beamforming algorithms are limited to ULA only. Sparse array [127, 128] configurations can be utilized for beamforming as they offer numerous advantages, such as minimizing mutual coupling between antenna elements, reducing antenna system complexity, etc., over ULAs [129–131]. A few examples of well-known SAs are coprime arrays, nested arrays, minimum holes arrays, and minimum redundancy arrays [132]. Apart from these, SAs are formed by selecting a subset of antenna elements from the entire antenna array, and only the selected elements are utilized for subsequent calculations such as DOA estimation, weight vector estimation, etc. A simple illustration of SA is depicted in Figure 5.1.

SAs are designed to meet certain criteria that include output SINR (OSINR)

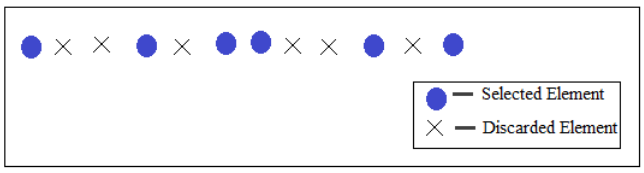

Figure 5.1: Sparse Array

maximization, BW management, SLL minimization, and MC reduction, to name

a few [133–139]. The OSINR plays a crucial role in assessing the effectiveness of a beamformer, and its value is influenced by the arrangement of the array. The correlation between OSINR and the quantity of antennas in the array is directly correlated. In certain environments, the OSINR for an ULA does not follow a linear pattern in relation to the number of antenna elements. This observation serves as motivation to enhance the linearity of sparse arrays.

The authors of [138,139] designed a sparse array with the objective of SINR maximization. The designed SA cannot be used in unpredictable interference environments because the obtained beam patterns have high sidelobes. Numerous techniques have been utilized for SLL management [119–123] but they are applied to ULAs only. In [140], a method for designing SAs is discussed that effectively reduces sidelobes. However, the proposed configuration utilizes 70% of the elements found in a full array. The researchers have not placed much emphasis on controlling sidelobes in sparse arrays until now. This chapter introduces an enhanced approach to beamforming, taking into account additional constraints.

The chapter involves designing a sparsely populated array to maximize the OSINR. The design process involves deriving the relation between the OSINR and the number of antenna elements. Subsequently, an optimal weight vector is computed, taking into account additional constraints to regulate the level of sidelobes. Then an analysis is performed to prevent the grating lobes and reduce the MC by varying the separation between the antenna elements of the designed SA.

The sequential process of the work done is as follows:

1. Derive the relationship between the OSINR and the number of antenna elements in an antenna array.
2. Find the optimal positions of antenna elements, i.e., SA based on the OSINR maximization criteria.
3. Apply additional constraints to the optimization problem for SLL regulation.
4. Perform distance analysis to circumvent the grating lobes and mutual coupling.

The remainder of this chapter is structured as follows:
The basic algorithm for beamforming is described in section 5.1. The relationship between N and OSINR is formulated in section 5.1.1 which is followed by motivation presented in section 5.2. The mathematical formulations of the SA configurations, SLL control, and distance analysis with their respective simulations are illustrated in sections 5.3, 5.4 and 5.5, respectively. A summary of the chapter is outlined in section 5.6 .

5.1 Signal model

The mathematical representation of a beamformer's output for a received signals vector $\boldsymbol{x}(k)$ at k^{th} instant and the weight vector $\boldsymbol{w}$ [17] is as follows:

$$\boldsymbol{y}(k) = \boldsymbol{w}^H \boldsymbol{x}(k) \tag{5.1.1}$$

The optimization problem for the MVDR is stated in equation 5.1.2 and the weight vector is determined from the optimization problem via Lagrange multiplier and illustrated in equation 5.1.3.

$$min\ \boldsymbol{w}^H \boldsymbol{R} \boldsymbol{w} \qquad s.t. \quad \boldsymbol{w}^H \boldsymbol{a}(\theta_0) = 1 \tag{5.1.2}$$

In the equation 5.1.2, $\boldsymbol{R}$ is the practical covariance matrix, and $\boldsymbol{a}(\theta_0)$ denotes the steering vector for SOI with direction θ_0.

$$\boldsymbol{w} = \frac{\boldsymbol{R}^{-1}\boldsymbol{a}(\theta_0)}{\boldsymbol{a}(\theta_0)^H \boldsymbol{R}^{-1}\boldsymbol{a}(\theta_0)} \tag{5.1.3}$$

The practical covariance matrix is computed for K number of snapshots from the received signals vector $\boldsymbol{x}(k)$ and is given as:

$$\boldsymbol{R} = \frac{1}{K}\sum_{k=1}^{K} \boldsymbol{x}(k)\boldsymbol{x}^H(k) \tag{5.1.4}$$

The crucial parameter for examining the performance of a beamformer is OSINR, which is determined by dividing the output signal power by the summation of the

output interference power and output noise power. Mathematically, OSINR is written as:

$$OSINR = \frac{\sigma_0^2 |\boldsymbol{w}^H \boldsymbol{a}(\theta_0)|^2}{\boldsymbol{w}^H \boldsymbol{R}_{i+n} \boldsymbol{w}} \tag{5.1.5}$$

In the equation 5.1.5, $\boldsymbol{R}_{i+n}$ is the interference plus noise covariance matrix which can be deduced from the theoretical covariance matrix $\hat{\boldsymbol{R}}$.

$$\hat{\boldsymbol{R}} = \boldsymbol{R}_s + \boldsymbol{R}_{i+n} = \sigma_0^2 \boldsymbol{a}(\theta_0) \boldsymbol{a}(\theta_0)^H + \sum_{i=1}^{P} \sigma_i^2 \boldsymbol{a}(\phi_i) \boldsymbol{a}(\phi_i)^H + \sigma_n^2 \boldsymbol{I} \tag{5.1.6}$$

In equation 5.1.6, $\boldsymbol{R}_s$ is the SOI's covariance matrix, and the power of SOI is denoted by σ_0^2. P denotes the number of interferences incident on the array from the directions $[\phi_1, ..., \phi_P]$ with powers $\sigma_1^2, ..., \sigma_P^2$, respectively. It is presumed that along with the SOI and interferences, noise is also present in the received data, which is Gaussian in nature with a zero mean. The power of noise is noted as σ_n^2.

5.1.1 Relationship between number of antenna elements and the OSINR

The weight vector stated in equation 5.1.3 is utilized in the expression of equation 5.1.5 and the OSINR is expressed as

$$OSINR = ISNR\, \boldsymbol{a}(\theta_0)^H \boldsymbol{R}_a^{-1} \boldsymbol{a}(\theta_0) \tag{5.1.7}$$

The input SNR (ISNR) is the ratio of input signal power and input noise power that is written as:

$$ISNR = \frac{\sigma_o^2}{\sigma_n^2} \tag{5.1.8}$$

The expression for $\boldsymbol{R}_a$ is given as

$$\boldsymbol{R}_a = \frac{\boldsymbol{R}_{i+n}}{\sigma_n^2} = I + \sigma_n^{-2} \boldsymbol{T} \boldsymbol{R}_i \boldsymbol{T}^H \tag{5.1.9}$$

The covariance matrix of interferences is denoted as $\boldsymbol{R}_i$ stated in equation 5.1.6 and $\boldsymbol{T}$ denotes the matrix of interference signals received on the antenna array.
The inverse of $\boldsymbol{R}_a$ is evaluated as

$$\boldsymbol{R}_a^{-1} = I - \boldsymbol{T}(\boldsymbol{R}_j + \boldsymbol{T}^H \boldsymbol{T})^{-1} \boldsymbol{T}^H \tag{5.1.10}$$

$$\boldsymbol{R}_j = \frac{\sigma_n^2}{\boldsymbol{R}_i} \tag{5.1.11}$$

Now, the expression of $\boldsymbol{R}_a$ is utilized in equation 5.1.7 for simplifying the OSINR

$$OSINR = ISNR[M - \boldsymbol{a}(\theta_0)\boldsymbol{T}(\boldsymbol{R}_j + \boldsymbol{T}^H\boldsymbol{T})^{-1}\boldsymbol{T}^H\boldsymbol{a}(\theta_0)] \tag{5.1.12}$$

From the equation 5.1.12, it is evident that there is a direct relationship between OSINR and the number of antenna elements (M) in an antenna array.

5.2 Analysis of number of antenna elements in an ULA

The practical implementation of the linear relationship is carried out by evaluating the OSINR against the number of antenna elements in an ULA. For simulations, it is presumed that a SOI and three interferences impinge the array from $\theta_o = 90^o$ and $\phi_1 = 76^o$, $\phi_2 = 83^o$, $\phi_3 = 101^o$ respective directions. The frequencies of the three interferences are $f_{i1} = 2.9$ GHz, $f_{i2} = 3.1$ GHz, and $f_{i3} = 3.2$ GHz, with the frequency of SOI being $f_{SOI} = 3.0$ GHz. The powers of interferences are assumed to be 20 dB, 20 dB, and 30 dB, respectively.

The OSINR examination is done by varying $M = 2$ to $M = 40$ and the results are illustrated in Figures 5.2 and 5.3. From the figures, it can be observed that there is a discrepancy between the actual and expected OSINR. The OSINR of an ULA does not exhibit a linear correlation with the number of antenna elements. It can also be seen that the deviation is greater for lower range of antenna elements. There is a 3 dB disparity between the obtained and expected OSINR at M=12.

Now, radiation patterns are also obtained for ULA with lower antenna elements in the considered range that are M=8 and M=16. The obtained radiation pattern is shown in Figure 5.4. It is found out from the radiation pattern for ULA that for M=8 the sidelobes become very dominant and the main lobe is deviated by 1.26^o from the actual SOI's direction.

From the results, it can be said that the ULAs are unable to give a decent radiation

pattern as the sidelobes are very dominant and there is a deviation between the direction of SOI and the main lobe position in the obtained pattern. Moreover, the obtained OSINR does not follow the expected values. This observation provides motivation to improve the performance of a beamformer with fewer antenna elements in the array. Therefore, sparse arrays are explored, in which only some elements are selected from the whole array.

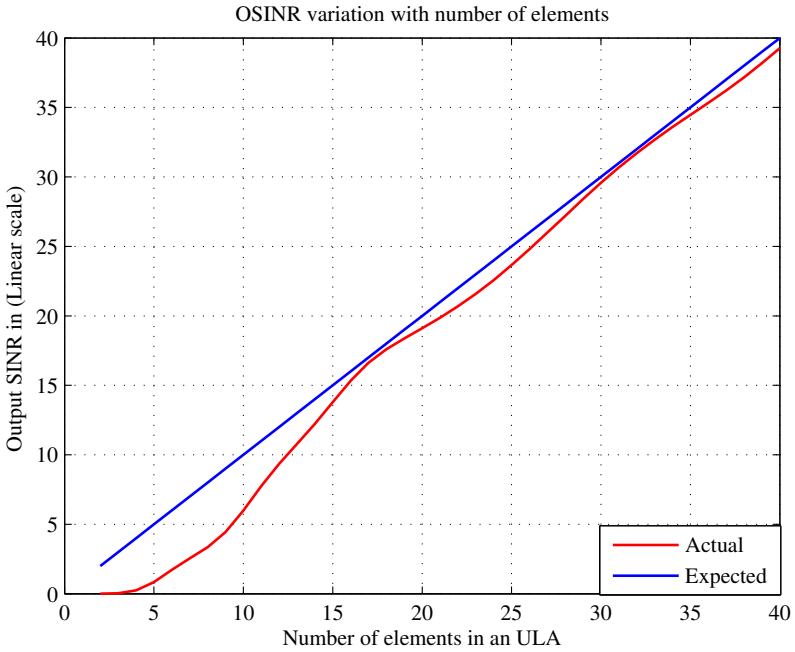

Figure 5.2: OSINR versus antenna elements number in linear scale.

5.3 Analysis and design of sparse array

The optimal array configuration is determined based on the OSINR maximization criteria. The entire process has illustrated in a step-by-step process.

1. Choose a specific number of antenna elements (V) from the overall number of antennas in the array (M).

2. Explore all potential combinations of C(V,M) and compute the OSINR using equation 5.1.12 for each combination.

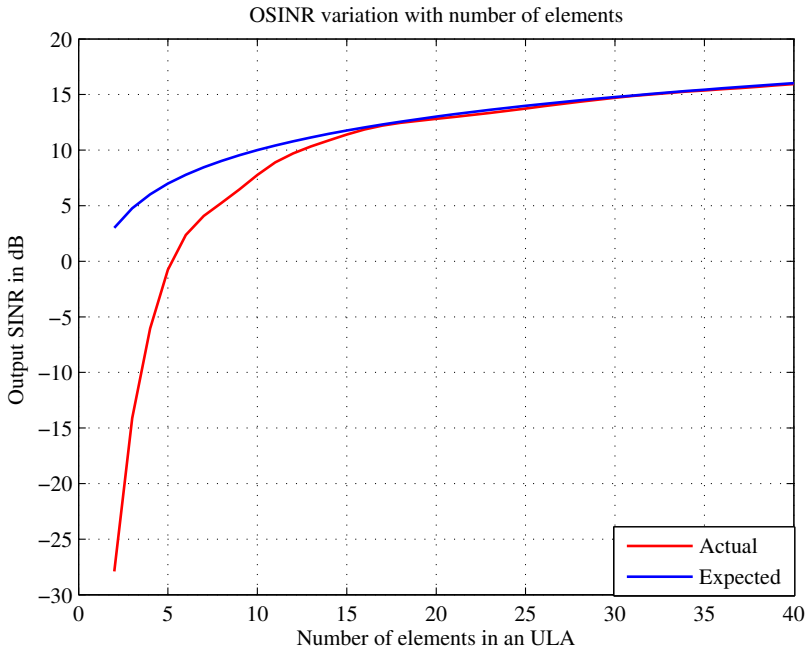

Figure 5.3: OSINR versus antenna elements number in dB scale.

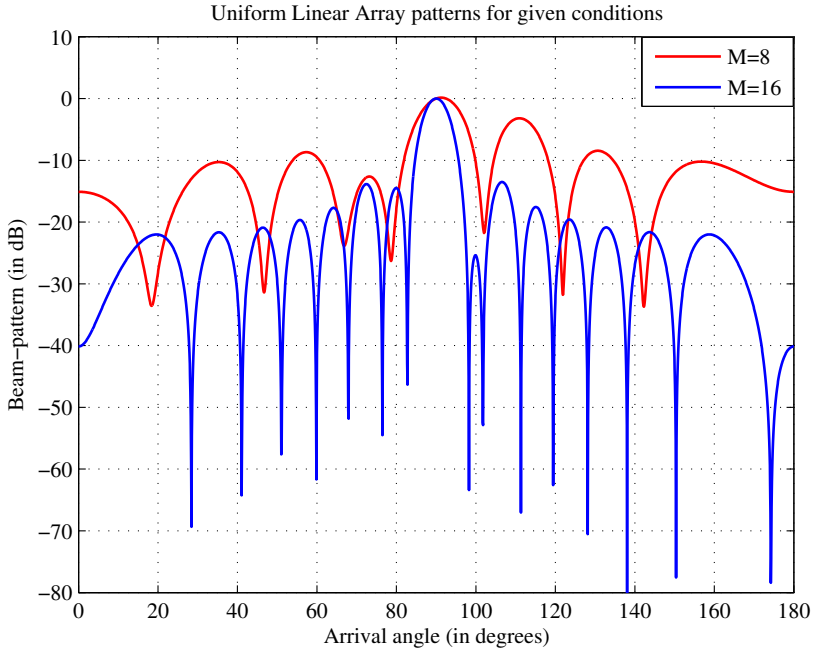

Figure 5.4: Radiation pattern obtained for ULA with M=8 and 16.

3. After careful consideration, the configuration that offers the highest OSINR is chosen and referred to as the optimal configuration.

In this work, it is considered that the total number of antenna elements in the array is $M = 16$. The sparsity of 50% and 56% is considered by choosing $V = 8$ and $V = 9$, respectively. The OSINR is computed for every combination of $C(16, 8)$ and $C(16, 9)$ and illustrated in Figure 5.5. From there, it can be noted that the OSINR of the best and worst array structures differ by around 9 dB.

The optimal antenna locations for $V = 8$ and $V = 9$ are given in equations 5.3.1 and

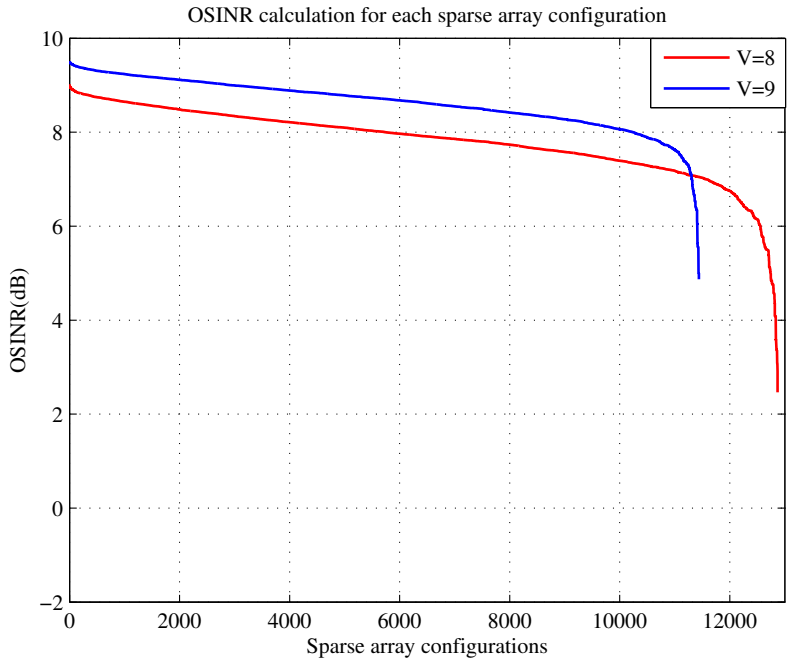

Figure 5.5: OSINR performance for all combinations of $C(16, 8)$ and $C(16, 9)$

5.3.2, respectively.

$$[1 \quad 3 \quad 6 \quad 7 \quad 9 \quad 11 \quad 13 \quad 16] \qquad V = 8 \tag{5.3.1}$$

$$[1 \quad 4 \quad 5 \quad 7 \quad 9 \quad 10 \quad 11 \quad 14 \quad 16] \qquad V = 9 \tag{5.3.2}$$

In both optimal SA configurations, the array aperture remains the same as the elements at both end positions are active.

5.3.1 Simulation results of OSINR and beampattern with sparse array

To examine the performance of SA, OSINR is determined by changing the antenna elements from 8 to 16. The OSINR performance for SA and ULA is compared in Figure 5.6. The figure clearly indicates that the OSINR of the sparse array meets the expected OSINR, while the ULA fails to achieve the desired OSINR, especially for a smaller number of antenna elements. The beam patterns are also obtained for

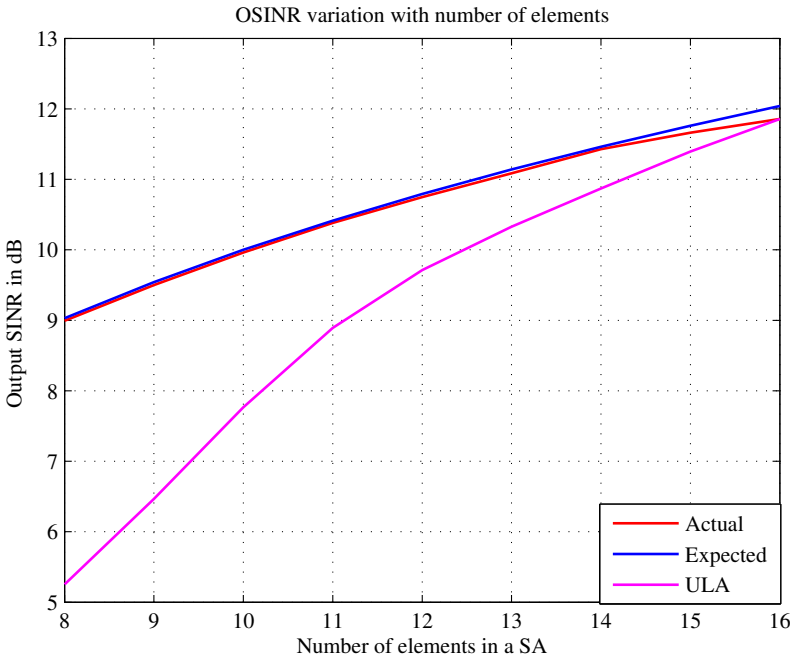

Figure 5.6: Comparison of OSINR of sparse arrays and ULA

the optimal SAs with $V = 8$ and $V = 9$. The results are portrayed in Figure 5.7. It is observed from the beam patterns that the SA for $V = 8$ have greater sidelobes as compared with the $V = 9$. The highly SA is producing higher sidelobe levels near the outer region of the beampattern. In some environments, it is necessary to minimize the SLL. Therefore, improvements should be made to enhance the performance of SAs.

In a uniform linear array, gain is directly proportional to the number of antenna elements. High gain implies more focused energy, which improves signal strength in

the desired direction. The proposed algorithm aims to design a sparse antenna array to maximize the OSINR. A higher OSINR indicates that the desired signal strength is significantly higher compared to the combined levels of interference and noise. However, implementing a sparse array configuration introduces trade-offs, primarily between gain and sidelobe levels. While the designed sparse array can maintain high gain, directing maximum energy towards the desired signal despite interferences and noise (as illustrated in Figure 5.7), it also results in the presence of prominent sidelobes in the radiation pattern. These sidelobes can potentially capture and amplify unwanted signals or noise, thereby degrading overall system performance. To address this issue, the algorithm incorporates SLL constraints into the optimization problem, as detailed in Section 5.4. These constraints help mitigate the impact of sidelobes by reducing their levels, thereby improving the array's ability to reject interference from directions other than the main beam. The proposed sparse array configuration balances the trade-off between gain and sidelobe levels by maximizing output SINR while applying SLL constraints to manage sidelobe performance.

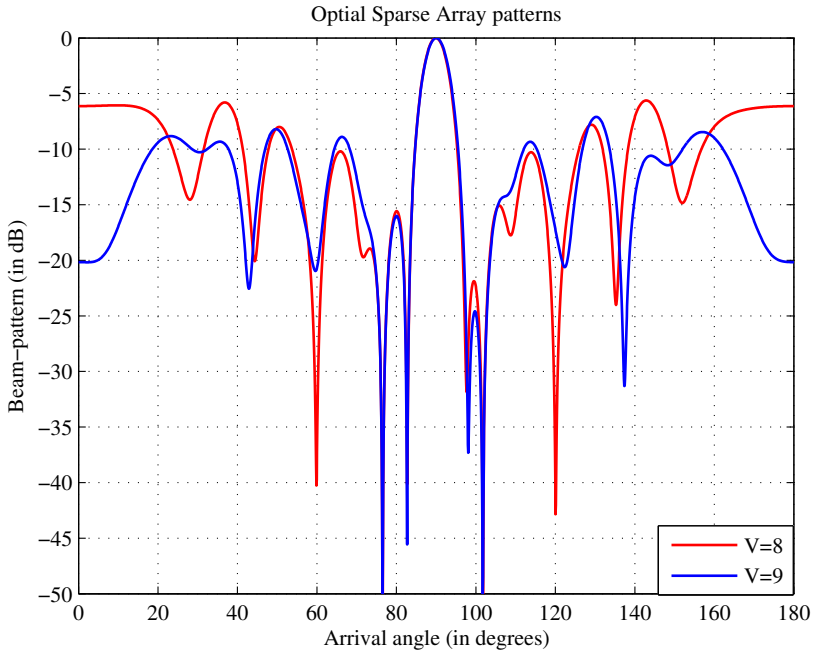

Figure 5.7: Radiation pattern for optimal SA configurations

5.4 SLL control for sparse array

For managing the SLL, constraints are applied to the entire radiation pattern area except the main beam region. The response of the considered region, or ROI, for SLL control is maintained below a certain value. The optimization problem given in equation 5.1.2 is modified by introducing SLL constraints. The modified problem is given in equation 5.4.1

$$\begin{aligned} \min_{w} \quad & \boldsymbol{w}^H \boldsymbol{R} \boldsymbol{w} \\ & subject\ to \\ & \boldsymbol{w}^H \boldsymbol{a}(\theta_0) = 1 \\ & \left| \boldsymbol{w}^{\mathbf{H}} \mathbf{A}_{\mathbf{ROI}} \right| <= \epsilon \end{aligned} \tag{5.4.1}$$

It is considered that the ROI contains the angles $[\psi_1....\psi_2] \cup [\psi_3....\psi_4]$. The steering vectors are determined for all the angles in the considered range, and the matrix $\boldsymbol{A}_{ROI}$ is formed from all the determined steering vectors. The response towards the ROI is constrained to a certain level ϵ.

In the simulations the ROI includes $[30^o\ 70^o] \cup [110^o\ 150^o\ ]$. The step size in the considered ROI is 5^o. The angles of ROI are computed in such a way that they do not take into account SOIs or interferences. The radiation patterns for the optimal SAs are obtained by utilizing the equation 5.4.1 and the results are shown in Figure 5.8. Based on the figure, it is apparent that when $V = 8$, the SLL remains at -10 dB in the region proximate to the main lobe. However, the beam pattern becomes more prominent at angles far away from the main beam. This occurrence can be viewed as the manifestation of the grating lobe. Therefore, to further improve the performance of the beamformer, another degree of flexibility as the distance between the antennas is taken into account.

5.5 Analysis of sparse array with variable distance

To avoid the grating lobe appearing in the beam pattern, distance analysis has been performed. Generally, the separation between the antenna elements 'd' is

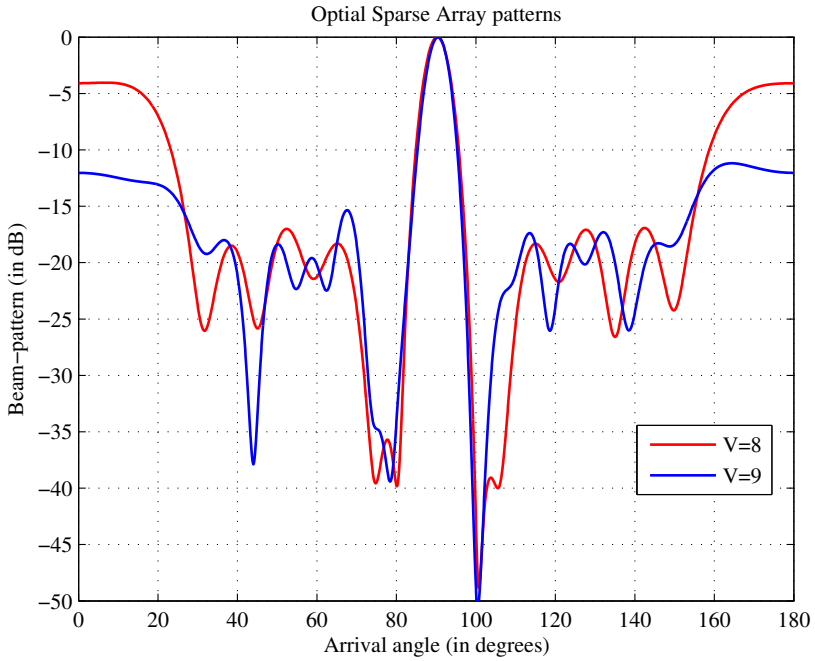

Figure 5.8: Radiation pattern for SLL control in SA

considered $d = \lambda/2 = 0.5\lambda$. Now, the variation of 'd' is achieved by incorporating an additional condition in the optimization problem outlined in equation 5.4.1. The modified optimization is stated as:

$$\begin{aligned} \min_{w} \quad & \boldsymbol{w}^H \boldsymbol{R} \boldsymbol{w} \\ & subject\ to \\ & \boldsymbol{w}^H \boldsymbol{a}(\theta_0) = 1 \\ & |\boldsymbol{w}^H \boldsymbol{A}_{ROI}| <= \epsilon \\ & d \in \left\{0.5\lambda \pm n\tfrac{\lambda}{16}, n = 0\ to\ 4\right\} \end{aligned} \tag{5.5.1}$$

In the modified optimization, a new parameter $'n'$ is defined in the span of [0 4] with a step size of 0.5. Therefore, the distance varies in the range of 0.25λ to 0.75λ. This range is chosen to ensure that the spacing between the elements is both practical and manageable. It is important to strike a balance between the distance that is too small, which is not feasible, and a distance that is too large, which would result in an excessively long array.

The radiation patterns obtained for the distance variations are shown in Figure 5.9. In the figure, the patterns are only shown for three different distances, as the other

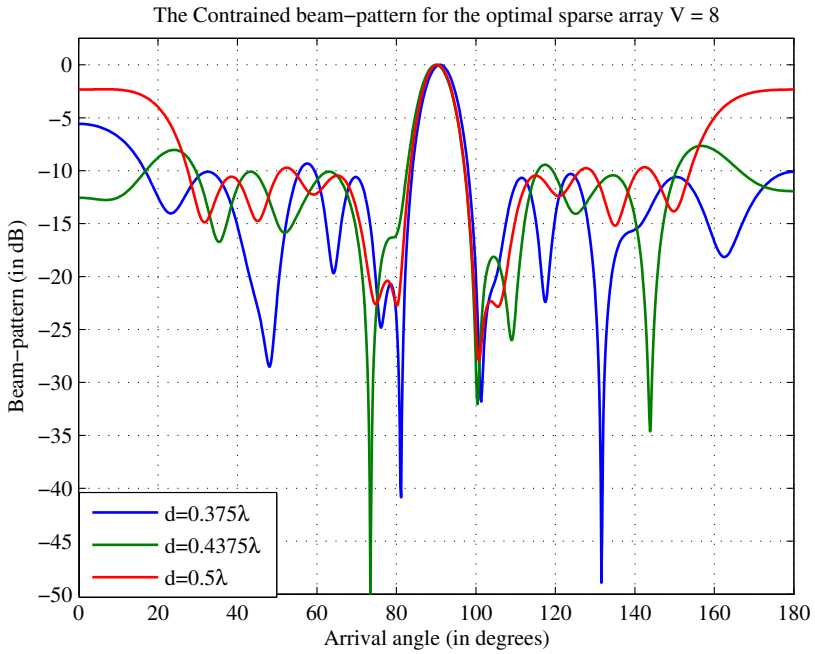

Figure 5.9: Radiation pattern for SA (V=8) with distance variation.

patterns obtained with the remaining distances are infeasible. It is noted that, with the exception of the primary beam, the pattern is remarkably uniform at a distance of 0.4375λ. The grating lobes obtained in Figure 5.8 also disappear with the suggested distance based modification. The radiation pattern for SA with 56% sparsity is shown in Figure 5.10. From the figure, it can be noticed that when comparing $V = 8$, the SLL outside the region of interest is effectively reduced by approximately 1 dB across all distances.

The effect of distance variation on the OSINR is also studied. The results obtained for OSINR with different distances are shown in Figures 5.11 and 5.12. To analyze how the distance between antenna elements impacts the OSINR, the distance is altered for different situations. In Figure 5.11, the distances $d \leq 0.5\lambda$ are shown, and from there it can be seen that as the distance between antenna elements shrinks, the OSINR also reduces. The OSINR is reduced by about 3 dB as the 'd' shrinks from $d = 0.5\lambda$ to $d = 0.25\lambda$. The results obtained for the other situation of $d \geq 0.5\lambda$ are illustrated in Figure 5.12. For this scenario, the OSINR shows a negative correlation,

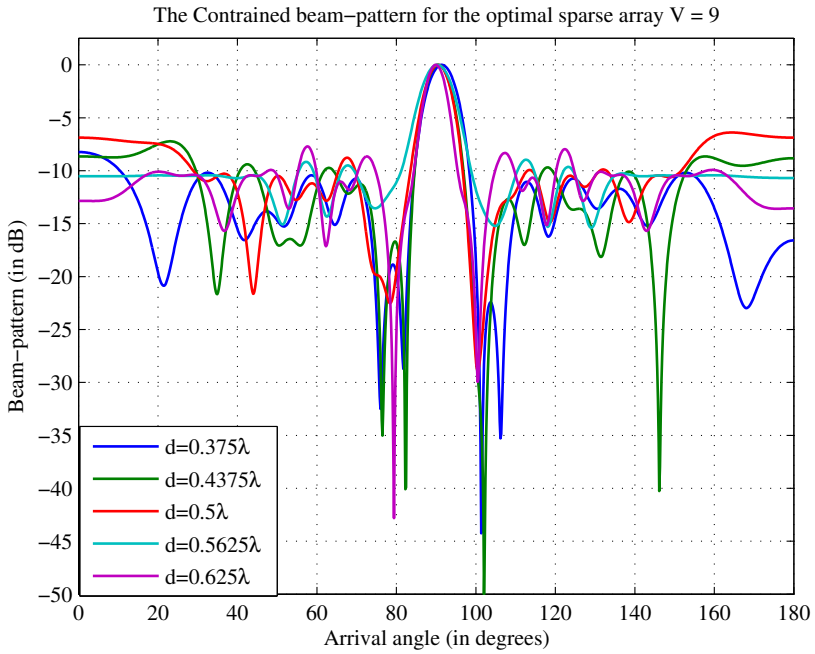

Figure 5.10: Radiation pattern for SA (V=9) with distance variation.

as with the increase in distance, the OSINR decreases. For the $d \geq 0.5\lambda$ situation, the decrease in OSINR is very small in comparison to $d \leq 0.5\lambda$. From the distance variations, it is clear that the appropriate spacing is $d = 0.5\lambda$ because the OSINR is maintained near optimal.

Results from several methodologies are presented in Table 5.1 and are contrasted with the suggested approach. The number of antenna elements chosen V from the full array, the level of sidelobes, and OSINR are the parameters on which the proposed work is compared with various methods in the literature. From the comparison table, it is observed that the 57% and 70% antenna elements are used in the designed SAs of [139] and [140], respectively. On the other hand, the proposed work utilized only 50% elements from the full array. In [138], 50% sparsity is achieved but at the cost of OSINR. The proposed work improves the OSINR in comparison to the considered methods, which in turn enhance the system performance in SAs. The proposed work produces a level of sidelobes below -10 dB, with which unwanted sidelobes can be minimized.

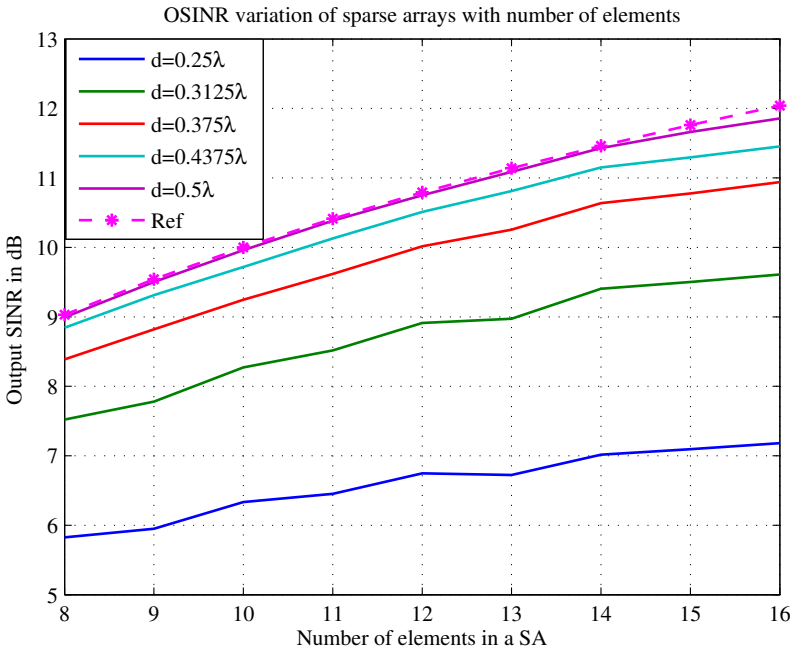

Figure 5.11: Effect on OSINR for SA with variable distance (for $d \leq 0.5\lambda$)

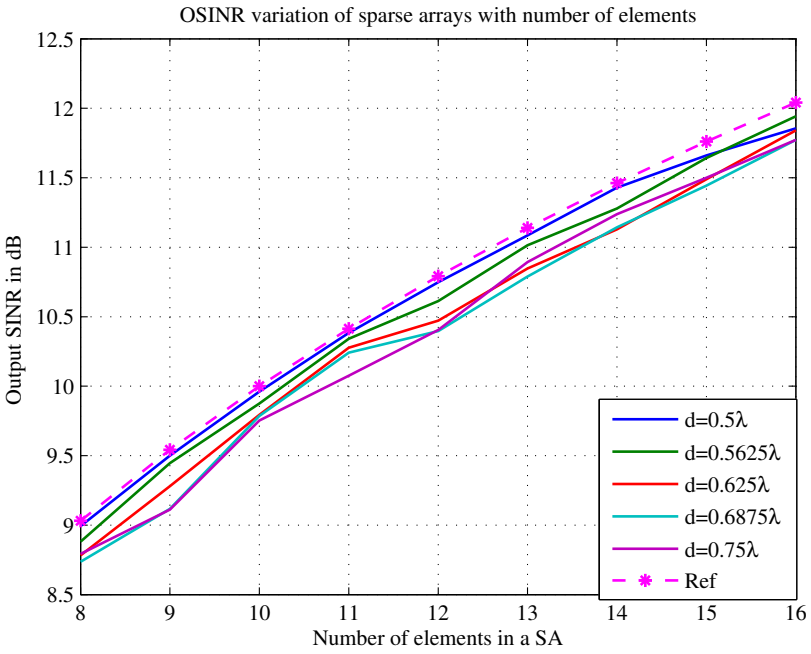

Figure 5.12: Effect on OSINR for SA with variable distance (for $d \geq 0.5\lambda$)

Table 5.1: Comparison of the suggested work with the existing techniques

Parameter	X.Wang et al. [138]	X.Wang et al. [139]	Z.Zheng et al. [140]	Suggested work
V(%)	50	57	70	50
SLL (dB)	-15	above -10	above -10	below -10
OSINR (dB)	7.5	10.68	NA	11.98

5.6 Conclusion

To improve the performance of a beamformer with sparse arrays, an analysis is carried out by appropriately defining the additional constraints. The optimal positions of the antenna elements for sparse arrays are determined via SINR maximization criteria. The additional constraints are introduced for SLL minimization, avoiding grating lobes, and reducing mutual coupling between the antenna elements. Analysis results show that by properly defining the additional constraints in sparse arrays, the stringent requirements of the beamformer can be fulfilled.

Chapter 6

Wideband Beamforming using Evolutionary Algorithms

6.1 Introduction

Array signal processing has been thoroughly researched because of its importance in numerous areas such as communications, medical, microphone arrays, etc. The array of antennas is utilized to receive signals from different directions, and these signals are further processed to achieve beamforming. Beamforming can be divided into two categories, namely narrowband beamforming and wideband beamforming, based on the bandwidth of the signals received [67].

Fractional bandwidth is utilized to classify the signals as wideband or narrowband. Signals with a fractional bandwidth of less than 1% are categorized as narrowband, while those with a bandwidth between 1% and 20% are known as wideband. To deal with wideband signals, wideband beamformers are required, as the efficacy of narrowband beamformers deteriorates as the bandwidth of received signals increases [141,142]. To deal with wideband beamforming, a tapped delay line (TDL) is incorporated with every antenna element of the receiving array to counterpoise the phase shift for different frequencies.

The most renowned method for wideband beamforming is the Frost algorithm [143].

It is also known as the linearly constrained minimum variance (LCMV) algorithm and is used for beamforming in a given frequency range. In the literature, multiple techniques have been devised to enhance the effectiveness of the Frost algorithm. The subsequent discourse offers a discussion on some of these strategies. In [144], the LCMV beamformer is improved by adding a response variation factor to its optimization problem so that the algorithm becomes robust against DOA mismatch. The output obtained may have different responses that correspond to different frequencies, which distort the array pattern. Therefore, its performance is further enhanced in [145] by incorporating norm bound along with response variation factor that provide frequency response consistency. To reduce the computational complexity of [144] and [145], derivative constraints are used in place of worst case criteria in the optimization problem [146]. Now, to deal with quickly moving interferences in wideband beamforming, null widening is recommended in [91]. The optimization problem of the Frost algorithm is reformulated by adding a taper matrix of virtual interferences around the original ones.

Evolutionary optimizations have several benefits over traditional optimization methods, making them a suitable choice for developing wideband beamforming [147]. Therefore, evolutionary optimizations can be employed for this purpose. The most popular evolutionary method utilized in the literature is PSO [148]. In [149,150], beamforming examples for different scenarios are carried out via PSO. The major drawback of the presented method is the deviation in the direction of the null as the frequency changes, and for suppression of interference, nulls should be placed in the exact interference direction. Therefore, OPSO and PSO with new objective functions are discussed to enhance the effectiveness of wideband beamforming. An identical objective function is used for both OPSO as well as PSO.

PSO is a bio-inspired optimization technique in which the optimal solution to a particular problem is obtained by the continuous interaction of swarm particles [151]. It is motivated by the social behavior of swarms in nature, such as fish schools, bird flocks, and bee swarms. The entire search space is explored by continuously updating the velocity and position of each particle. This update is done by continuously evaluating particle's best fitness P_{best} and swarm's best fitness g_{best} . PSO is developed

based on two equations that are velocity update and position update, which are given in equations 6.1.1 and 6.1.2, respectively.

$$v_i(k+1) = w_i v_i(k) + c_1 r_1(x_p(k) - x_i(k)) + c_2 r_2(x_g(k) - x_i(k)) \tag{6.1.1}$$

$$x_i(k+1) = x_i(k) + v_i(k+1) \tag{6.1.2}$$

The velocity and position of i^k particle for k^{th} iteration are denoted as $v_i(k)$ and $x_i(k)$ respectively. The inertia weight w exhibits the effect of the previous velocity vector on the new vector, and it also prohibits the particle from moving very fast from one area to another in the search space. c_1, c_2 are the positive acceleration coefficients, and r_1, r_2 are random numbers with a uniform distribution between 0 and 1. $x_p(k)$ and $x_g(k)$ are individual best and global best values. The complete procedure of PSO is depicted in Figure 6.1. In PSO algorithm, every individual particle adjusts both its velocity and position based on the most optimal values obtained from its personal experience and that of its neighboring particles. The particles become disoriented as they struggle to ascertain the path of their motion, resulting in the occurrence of an oscillation phenomenon [152]. Therefore, this phenomenon impairs the algorithm's search ability and delays convergence. To enhance the searching ability of PSO, orthogonality is introduced in conventional PSO. Orthogonality is employed to distribute the points of a starting population throughout the potential solution space. This ensures that the algorithm can uniformly explore the solution space and identify suitable points for further investigation in subsequent iterations.

In OPSO [153], only some particles are selected from the swarm that have possible solutions. This selection is carried out via the process of OD [154] in which orthogonal vectors are produced from current position vectors. The orthogonal vectors undergo updates during each iteration, guiding the chosen particles towards the global solution. To derive the mathematical equations of OPSO, a swarm with n number of particles is considered, and each i^{th} particle consists of a position vector $\boldsymbol{X}_i$ and a velocity vector $\boldsymbol{V}_i$. These vectors are illustrated in equations 6.1.3 and 6.1.4, respectively.

$$\boldsymbol{X}_i = [x_{i1}, x_{i2}, x_{i3}.....x_{in}] \tag{6.1.3}$$

$$\boldsymbol{V}_i = [v_{i1}, v_{i2}, v_{i3}.....v_{in}] \tag{6.1.4}$$

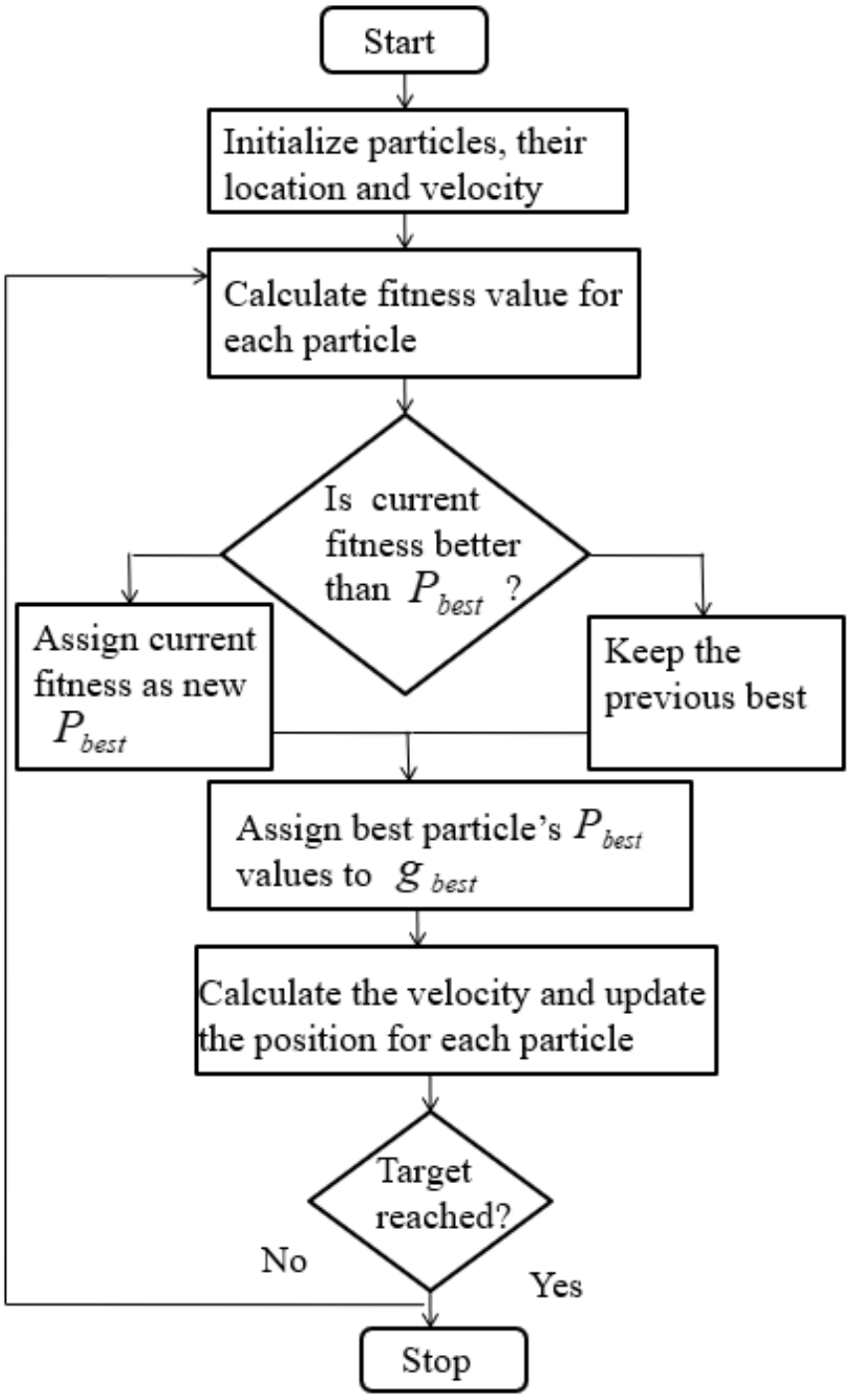

Figure 6.1: Flowchart of PSO

In the OPSO algorithm, the particles' position and velocity undergo updates during each iteration through a set of specific steps, which are as follows:

1. The fitness of each swarm's particle is evaluated via fitness function, and the particles are sorted in ascending order of their fitness function value.

2. A matrix $\boldsymbol{K}$ from the best particle positions according to their fitness values is formed, having dimensions $n \times m$. A symmetric matrix $\boldsymbol{L}_{m\times m}$ is formed from the $\boldsymbol{K}$ utilizing the method mentioned in [155].

3. By utilizing the Gram–Schmidt orthogonalization method [154], the orthogonal matrix $\boldsymbol{M}$ is created from the symmetric matrix $\boldsymbol{L}$.

4. Then, the orthogonal diagonalization (OD) process is utilized to create an orthogonal diagonal matrix $\boldsymbol{N}$ having dimensions $m \times m$.

$$\boldsymbol{N} = \boldsymbol{M}\boldsymbol{L}\boldsymbol{M}^T \tag{6.1.5}$$

Now, the orthogonal diagonal matrix $\boldsymbol{N}_{m\times m}$ is utilized to evaluate the best position and velocity from the equations 6.1.6 and 6.1.7, respectively.

$$v_i(k+1) = w_i v_i(k) + cr(\boldsymbol{N}_i(k) - x_i(k)) \tag{6.1.6}$$

$$x_i(k+1) = x_i(k) + v_i(k+1) \tag{6.1.7}$$

In the equation 6.1.6, $\boldsymbol{N}_i$ is the i^{th} row of $\boldsymbol{N}$ and here i varies from $1, 2...m$. The inertia weight and acceleration constant are denoted as w and c, respectively. The r represents the random number whose values are uniformly distributed between $[0, 1]$. Once the velocity parameters are determined, the position is then modified according to equation 6.1.7.In OPSO, the velocity equation has only one guide, which causes particles to move toward the target rather than getting stuck in oscillation. The entire process of the OPSO is presented in the flowchart given in Figure 6.2.

The chapter is organized as follows. The problem formulation and novel objective functions are illustrated in section 6.2. Several examples of wideband beamforming and diverse characteristic parameters of array patterns are deliberated in section 6.4,

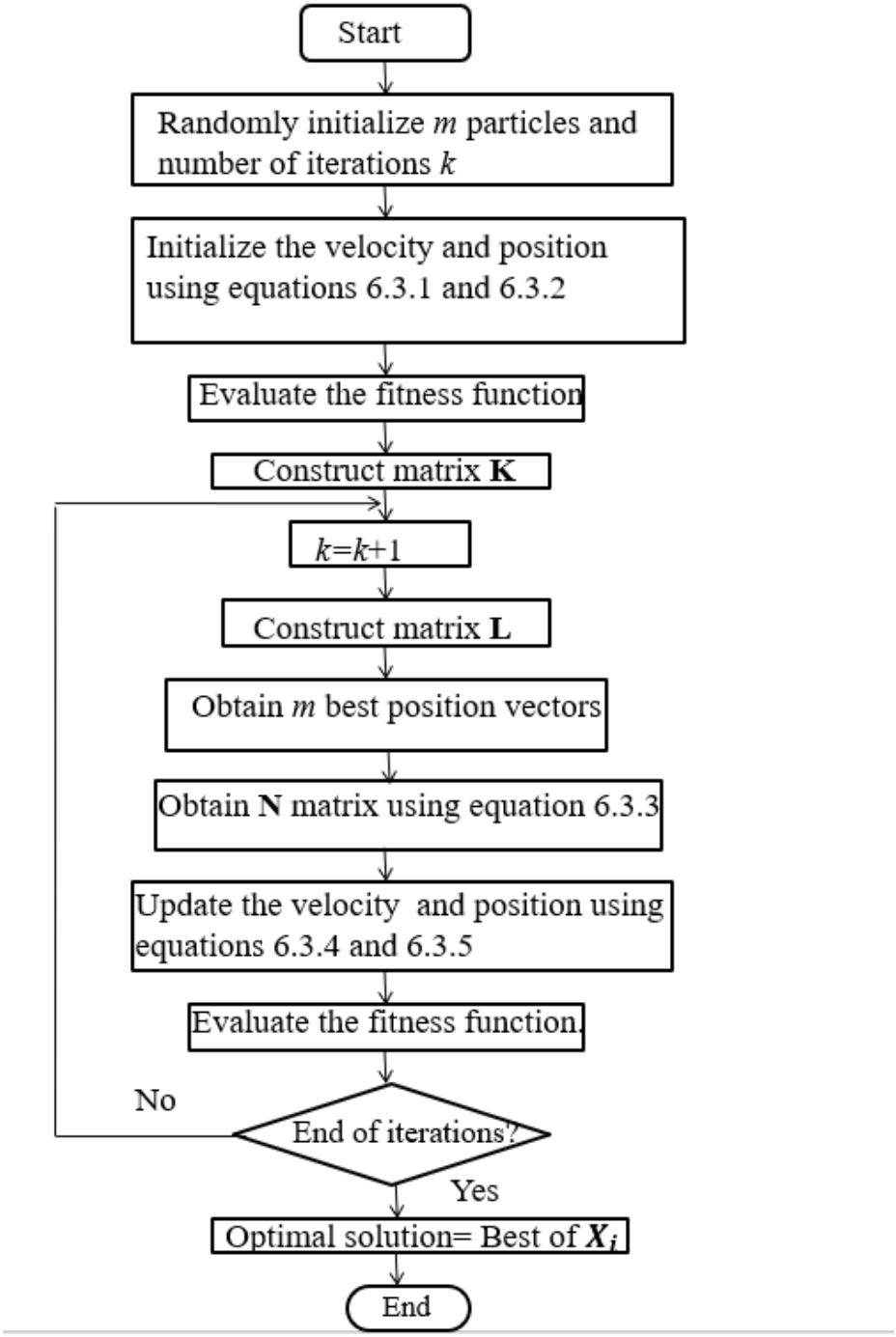

Figure 6.2: Flowchart of OPSO

subsequently followed by a conclusion.

6.2 Signal model

Wideband beamformers with H number of taps are utilized to process the wideband signals received on the array of M antenna elements. At a particular time instant k, the response at the output of the wideband beamformer is given in equation 6.2.1.

$$\boldsymbol{y}(k) = \sum_{m=0}^{M-1} \sum_{h=0}^{H-1} w_{m,h} x_m(k - (\tau_m + hT_s)) \tag{6.2.1}$$

where x_m denotes the received signal at the m^{th} antenna element and w is the weight vector element. τ and T_s represent the propagation delay between the antenna elements and the delay between adjacent taps. If it is considered that the signals received on the array are sinusoidal then the array response based on the angular frequency ω and the angle of arrival θ, is expressed as:

$$\boldsymbol{y}(\omega, \theta) = \sum_{m=0}^{M-1} \sum_{h=0}^{H-1} w_{m,h} exp^{-j\omega(\tau_m + hT_s)} \tag{6.2.2}$$

The vector representation of equation 6.2.2 is presented as

$$\boldsymbol{Y}(\omega, \theta) = \boldsymbol{w}^T \boldsymbol{S}(\omega, \theta) \tag{6.2.3}$$

The weight vector and steering vector are illustrated in equation 6.2.4 and 6.2.5, respectively.

$$\boldsymbol{w} = [w_{0,0}...w_{M-1,0}...w_{0,H-1}...w_{M-1,H-1}]^T \tag{6.2.4}$$

$$\boldsymbol{S}(\omega, \theta) = [e^{-j\omega\tau_o}, ..e^{-j\omega\tau_{M-1}}, ..e^{-j\omega(\tau_o + (H-1)T_s)}, ..e^{-j\omega(\tau_{M-1} + (H-1)T_s)}]^T \tag{6.2.5}$$

$$\boldsymbol{S}(\omega, \theta) = \boldsymbol{x}_{T_s}(\omega) \odot \boldsymbol{x}_{\tau_m}(\omega, \theta) \tag{6.2.6}$$

In the equation 6.2.6, $\boldsymbol{x}_{T_s}(\omega)$ is the received signal on antenna elements. The received signal is then sampled using H number of taps, and the sampled signal is denoted

as $\boldsymbol{x}_{\tau_m}(\omega,\theta)$. The $\boldsymbol{x}_{T_s}(\omega)$ and $\boldsymbol{x}_{\tau_m}(\omega,\theta)$ are given in equations 6.2.7 and 6.2.8, respectively.

$$\boldsymbol{x}_{T_s}(\omega) = [1, ...e^{-j\omega(H-1)T_s}]^T \tag{6.2.7}$$

$$\boldsymbol{x}_{\tau_m}(\omega,\theta) = [1, ...e^{-j\omega(M-1)d\sin(\theta)/c}]^T \tag{6.2.8}$$

In the equation 6.2.7, d denotes the separation in antenna elements and c indicate the speed of light. The output of a beamformer depends mainly on the weight vector, which is now calculated via PSO and OPSO. MSE serves as a measure of fitness.

6.3 Modeling of novel objective function for PSO and OPSO

The MSE is determined by comparing the beam pattern generated from uniform unity weights (where the weight vector is set to 1) and the beam pattern generated from OPSO/PSO. This comparison is done in such a way that the nulls' position remains fixed in the specified direction for each frequency. The PSO/OPSO updates the calculated weights with each iteration, ensuring that the MSE is minimized during the calculation process. The vector with the minimum MSE is chosen for obtaining the wideband beamformer's output and is termed as optimum weight vector. The formulation of the fitness function is presented as follows:

$$\boldsymbol{Y}_{best}(\omega,\theta) = MSE[\boldsymbol{Y}_{OPSO/PSO}(\omega,\theta) - \boldsymbol{Y}_{uniform}(\omega,\theta)] \tag{6.3.1}$$

The responses obtained from references pattern and PSO/OPSO are given in equation 6.3.2 and 6.3.3, respectively.

$$\boldsymbol{Y}_{uniform}(\omega,\theta) = \boldsymbol{X}(\omega,\theta)\boldsymbol{W}_{uniform} \qquad \forall \;\; \omega,\theta \;\; except \;\; \theta_j \tag{6.3.2}$$

where, θ_j represent the nulls locations. The response obtained from OPSO/PSO is given as

$$\boldsymbol{Y}_{OPSO/PSO}(\omega,\theta) = \boldsymbol{X}(\omega,\theta)\boldsymbol{W}_{OPSO/PSO} \tag{6.3.3}$$

6.4 Simulation results and discussions

The array consists of 10 antenna elements, each having 5 taps. is considered for the simulations. A bandwidth of 200MHz is assumed to have a frequency range of 1.2GHz to 1.4GHz. The desired signal strikes the array from 0^o and two interferences are at -40^o and 30^o. The values of constants for both PSO and OPSO are kept the same at $c_1 = c_2 = 1.042$ and the inertia weight w_i decays linearly with every iteration from 0.8 to 0.4. 500 iterations are taken for the simulations, which are enough for the convergence of the considered algorithms.

The comparison of convergence plots obtained from PSO and OPSO is depicted in

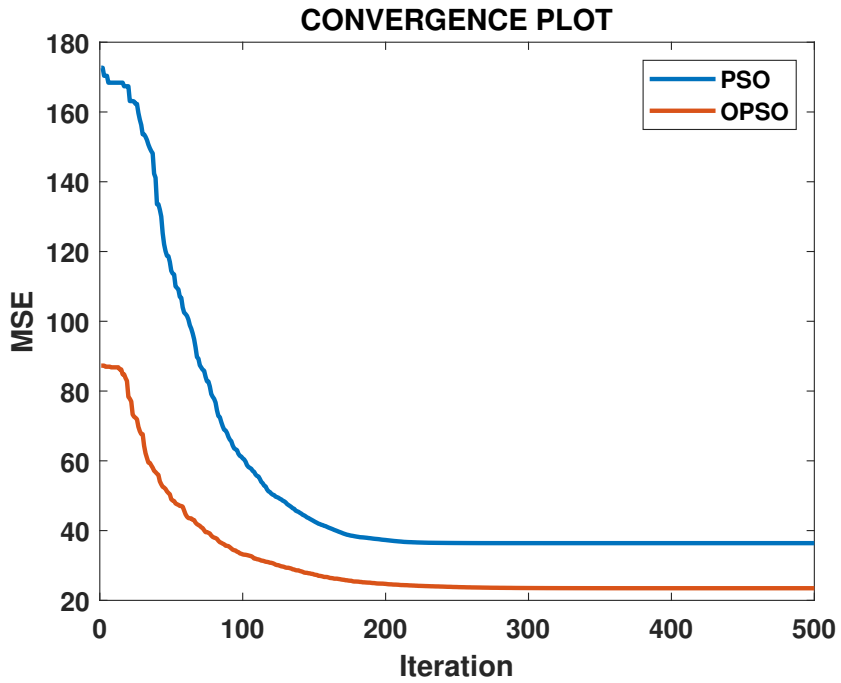

Figure 6.3: Comparison of convergence curves obtained from PSO and OPSO.

Figure 6.3. From there, it can be noticed that OPSO offers a lower MSE than PSO. The beampatterns obtained from the considered algorithms Frost, PSO, and OPSO for three distinct frequencies are illustrated in Figures 6.4, 6.5 and 6.6 respectively. From the figures, it can be said that all three algorithms considered achieve wideband beamforming by placing main beams in the intended directions and nulls towards the interference directions for each of the three distinct frequencies.

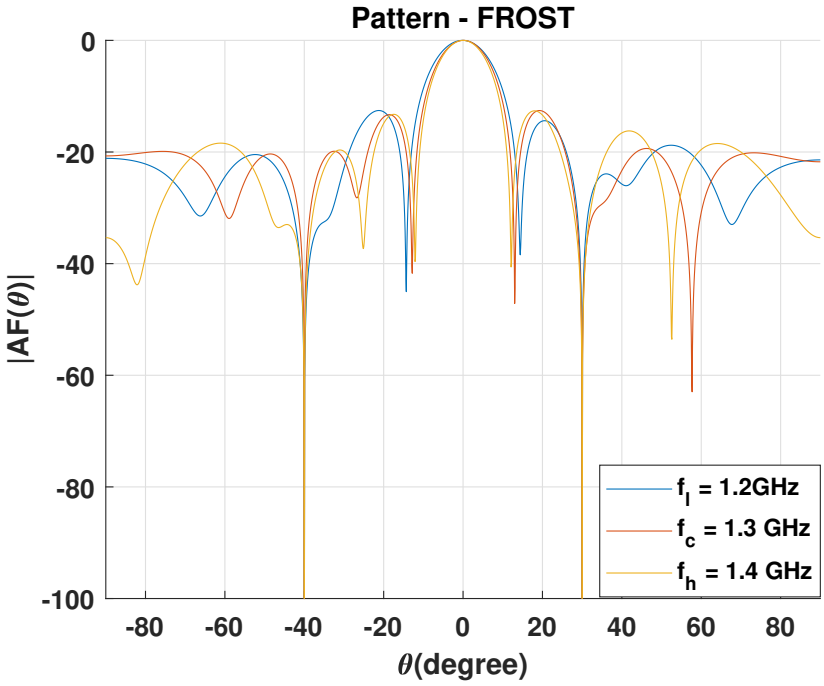

Figure 6.4: Radiation pattern obtained from the Frost algorithm.

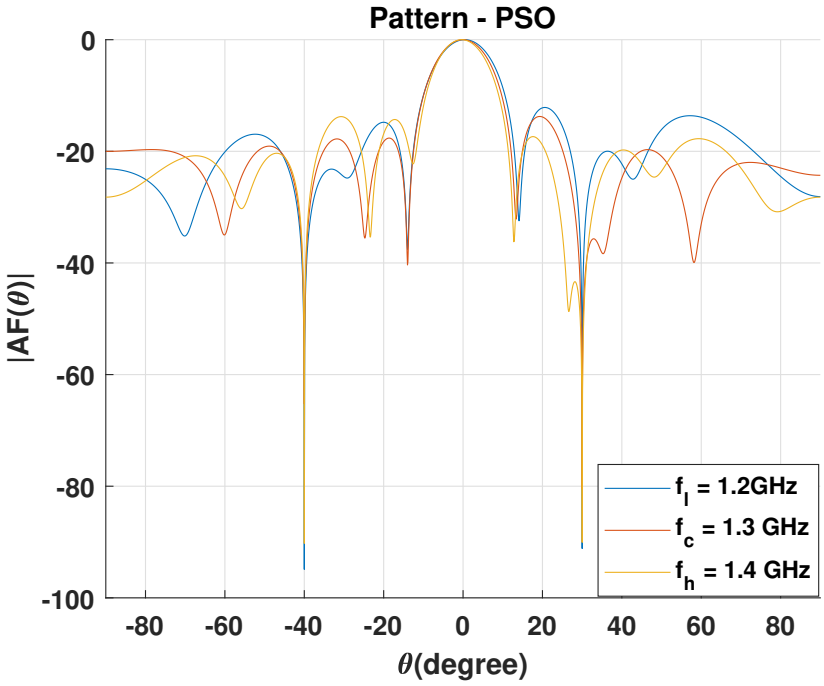

Figure 6.5: Radiation pattern produced from PSO algorithm.

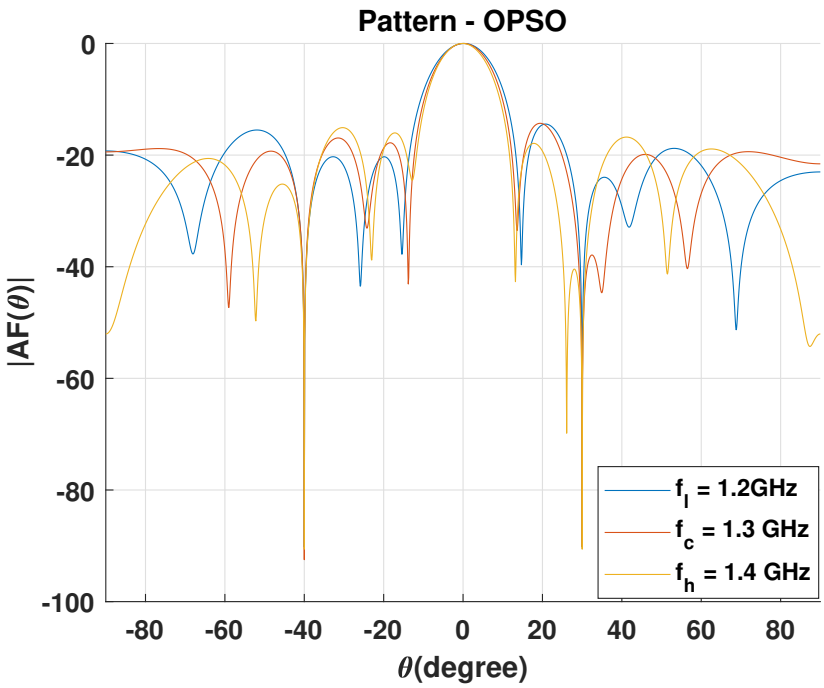

Figure 6.6: Radiation pattern produced from OPSO algorithm.

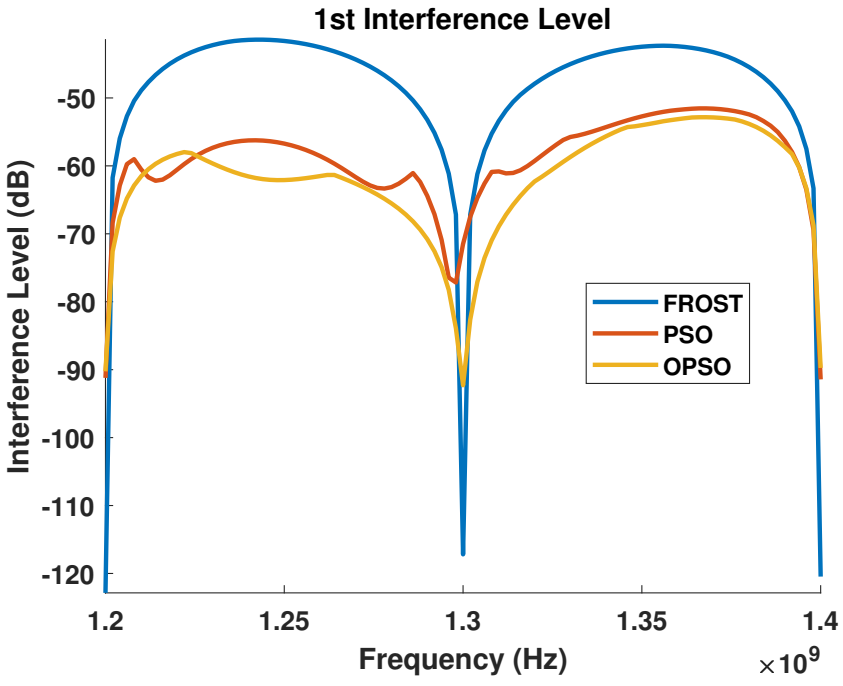

Figure 6.7: First interference level acquired through Frost, PSO and OPSO.

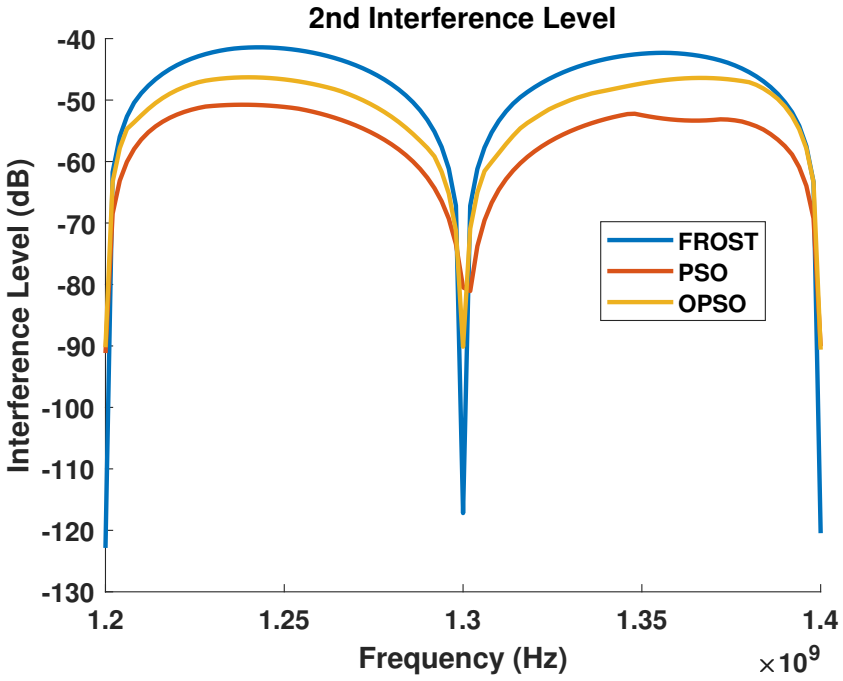

Figure 6.8: Second interference level acquired through Frost, PSO and OPSO.

The considered algorithms are compared in terms of performance parameters such as peak SLL, interference level, and discrepancy in the respective interference direction and null position. These parameters are plotted separately for a more clear comparison of the considered algorithms.

The levels of both interferences for the algorithms are shown in Figures 6.7 and 6.8. The figures illustrate the depth of nulls for the considered frequency range of $1.2GHz$ to $1.4GHz$. It is evident that both PSO and OPSO yield lower interference levels compared to the conventional Frost algorithm across all the considered frequencies.The training of the evolutionary algorithms is limited to just three frequencies ($1.2GHz$, $1.2GHz$, and $1.3GHz$) but they also reduce null depth for the other frequencies in the considered range.

The deviation in null's direction w.r.t. interference direction is evaluated and shown in Figures 6.9 and 6.10. The interferences can be effectively canceled out by minimizing the deviation in the null's position w.r.t. the angle of interference, and it is evident from the figures that OPSO provides no deviation. PSO also reduces the deviation in the null position as compared to the Frost algorithm. The comparison

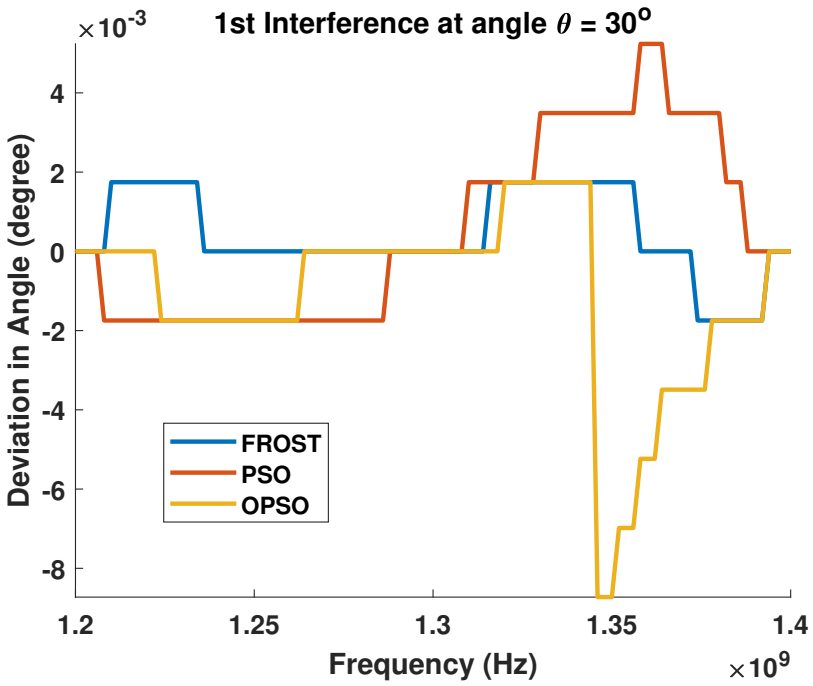

Figure 6.9: Deviation in null position and first interference direction for Frost, PSO and OPSO algorithms.

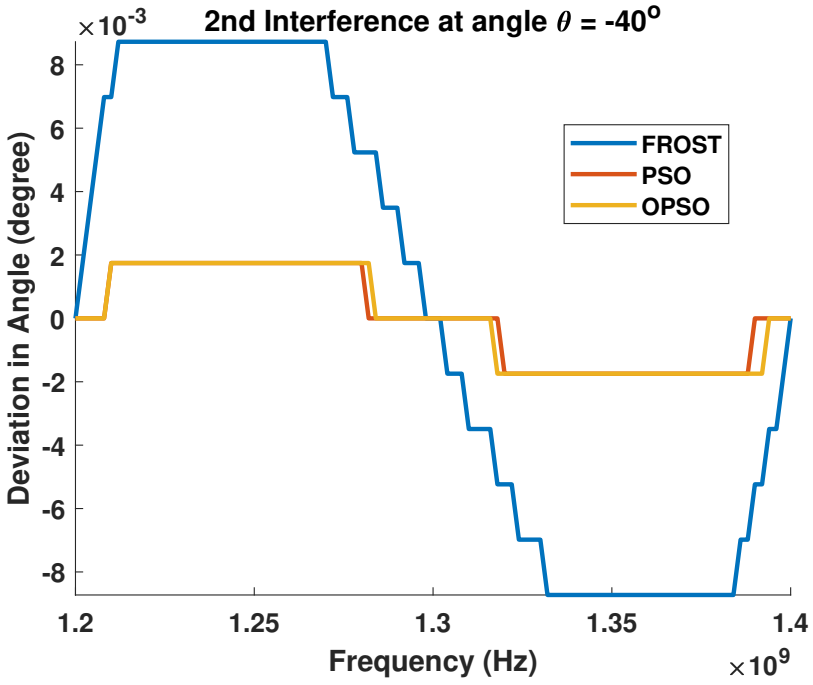

Figure 6.10: Deviation in null position and second interference direction for Frost, PSO and OPSO algorithms.

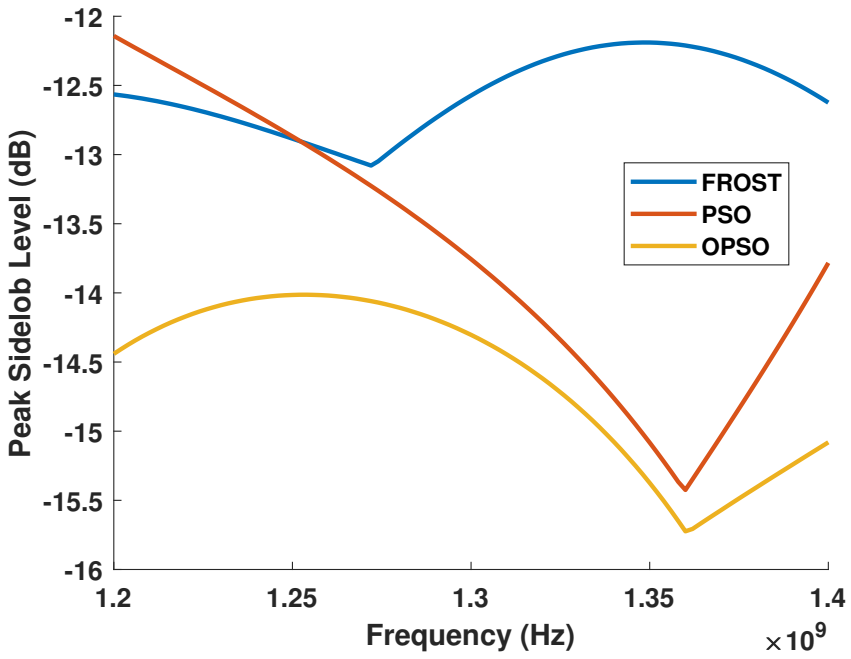

Figure 6.11: Comparison of peak SLL acquired through Frost, PSO and OPSO algorithms.

of SLL determined from Frost, PSO, and OPSO is depicted in Figure 6.11 and it has been discovered that OPSO displays a lower SLL in comparison to PSO as well as the classical Frost algorithm.

6.5 Conclusion

In this chapter, wideband beamforming is achieved through the evolutionary algorithms PSO and OPSO. A novel objective function based on MSE is devised, which is utilized by the evolutionary algorithms to produce frequency invariant beampatterns over the $200MHz$ bandwidth. The results achieved by utilizing the formulated objective function are evaluated against the Frost method for both PSO and OPSO. The simulations clearly show that OPSO excels over the other algorithms under consideration concerning peak SLL, interference levels, and deviation in null position relative to the interference angle.

Chapter 7

Conclusion and Future Scope

7.1 Conclusion

This thesis presents a range of algorithms aimed at achieving robust adaptive beamforming. The factors affecting the performance of beamforming algorithms such as mismatch in DOA of SOI, moving interferences, multiple SOIs, SLL control etc. are thoroughly investigated. Robustness against these factors is achieved via developing novel beamforming techniques and the simulation results are obtained as well as compared with state-of-the-art methods. The significant observations and results obtained in this work are outlined as follows.

First and foremost, the PGRCB provides robustness against large DOA mismatch by estimating the actual DOA of SOI.The PGRCB enhances the output SINR in the presence of significant DOA mismatch. Additionally, it demonstrates accurate estimation of the power of the SOI, as validated through simulations.

A novel algorithm is developed in chapter 3 to offer a comprehensive solution addressing both moving interferences and DOA mismatch. Magnitude constraints are imposed on the ROI to handle DOA mismatch, while the Taper matrix is employed for null widening to address moving interferences efficiently. The proposed beamformer's output SINR accurately matches the optimal beamformer's SINR which make the developed algorithm more reliable in non-stationary interferences and resistant to

DOA mismatch in SOI.

Efficiently monitoring multiple SOIs simultaneously is crucial for various applications. To address this need, an algorithm is devised for dual beam adaptive beamforming algorithm with SLL control. This algorithm generates dual beams towards the two distinct SOIs with effective management of interferences and noise. Additionally, the proposed algorithm ensures precise control over the SLL.

To streamline system complexity and optimize performance of adaptive beamforming algorithm, Chapter 5 employs sparse arrays. An analysis with sparse arrays is conducted by appropriately incorporating additional constraints into the optimization problem of the SCB. The analysis results illustrate the fulfillment of the beamformer's stringent requirements in terms of output SINR and SLL.

Further, wideband beamforming is implemented via evolutionary algorithms PSO and OPSO in chapter 6. A novel MSE-based objective function is designed for these algorithms. Computer simulations proves that with the proposed objective function both PSO and OPSO provides better peak SLL, interference rejection capability as well no deviation in null's position w.r.t their directions for all the frequencies in the 200MHz range.

It is evident that all the proposed robust beamforming techniques have effectively fulfilled their objectives and outperformed current state-of-the-art algorithms. Consequently, the novel proposed algorithms can be applied in their respective domains of application.

7.2 Future Scope

Array signal processing remains a pressing issue, with numerous unresolved challenges awaiting solutions from researchers in the field. Possible future work for the current thesis could include the following:

1. The array geometries such as circular or planar arrays can be utilized in the signal model of adaptive beamforming algorithms. Circularly-polarized antennas

radiate electromagnetic waves with electric fields rotating in a circular manner, either left-hand circular polarization (LHCP) or right-hand circular polarization (RHCP) [156, 157]. The adaptive beamforming algorithms must account for the polarization properties while adjusting the amplitude and phase weights. Adapting beamforming algorithms for circularly-polarized antenna arrays involves incorporating polarization states throughout the entire algorithm design. This includes the mathematical modeling of circularly polarized antenna elements in the signal model and calculating complex weights for dual polarization.

2. The physical constraints such as mutual coupling between the adjacent antenna elements can also be taken into account for more realistic simulation environment.

3. The optimal sparse array configuration can be identified through an efficient search algorithm rather than relying on enumeration.

List of Publications

Journals

1. D. Thakur, V. Baghel and S.R. Talluri,"Proximal gradient method based robust Capon beamforming against large DOA mismatch", *Frequenz*, vol. 75, no. 7–8, pp. 259–266, 2021.

2. D. Thakur, V. Baghel and S.R. Talluri,"A dual beam adaptive beamforming algorithm with sidelobe suppression", *Measurement: Sensors*, vol. 24, pp. 100514, 2023.

3. D. Thakur, V. Baghel and S.R. Talluri,"Improvements in sparse array based beamformer via additional constraints", *International Journal of Computing and Digital Systems*, vol. 13, no. 1, 2023.

4. D. Thakur, V. Baghel and S.R. Talluri,"Design of an Efficient Wideband Beamformer using OPSO", *International Journal of Innovative Technology and Exploring Engineering*, vol. 8, no. 11, pp. 2144–2152, 2019.

Conference

1. D. Thakur, V. Baghel and S.R. Talluri,"Robust beamforming against mismatched signal steering vector using ellipsoidal constraints", in 2020 *Sixth International Conference on Parallel, Distributed and Grid Computing (PDGC)*, pp. 303–307.

2. D. Thakur, V. Baghel and S.R. Talluri,"Robust beamforming against DOA mismatch with null broadening for moving interferences", in 2020 *International symposium on signal processing and intelligent recognition systems*, pp.290–301.

Communicated

1. D. Thakur, V. Baghel, S.R. Talluri, “Analysis of SCB-DB algorithm for various characteristic parameters”, *Recent Patents on Engineering*, June 2024.

Bibliography

[1] M. Chryssomallis, “Smart antennas,” *IEEE Antennas and Propagation magazine*, vol. 42, no. 3, 129-–136, 2000.

[2] F. Gross, *Smart antennas for wireless communications*, McGraw-Hill Professional, 2005.

[3] C. Balanis, *Antenna theory analysis and design*, A John Wiley and Sons, 2005.

[4] K. Vasudevan, *Digital communications and signal processing*, Universities Press, 2010.

[5] K. Vasudevan, "Optimum predictive iterative decoding of turbo codes in coloured Gaussian noise," in 2004 *Proceedings of the Fourth IASTED International Multi Conference on Wireless and Optical Communication, Banff, Canada*, 306–311.

[6] L. C. Godara, *Smart antennas*, CRC press, 2004.

[7] S.A. Vorobyov, "Adaptive and robust beamforming," *Academic Press Library in Signal Processing*, vol. 3, 503–552, 2014.

[8] M.A. Azam, A.K. Dutta and A. Mukharjee, "Performance analysis of dipole antenna based planar arrays with mutual coupling and antenna position error in mmWave hybrid system," *IEEE Transactions on Vehicular Technology*, vol. 70, no.10, 10209–10221, 2021.

[9] B.D. Carlson, "Covariance matrix estimation errors and diagonal loading in adaptive arrays," *IEEE Transactions on Aerospace and Electronic systems*, vol.24, no.4, 397–401, 1988.

[10] H. Cox, R.M. Zeskind and M. M. Owen, "Robust adaptive beamforming," *IEEE Transactions on Acoustics, Speech, and Signal Processing*, vol.35, no.10, 1365–1376, 1987.

[11] M.H. Er and A. Cantoni,"An alternative formulation for an optimum beamformer with robustness capability," in 1985 *IEEE Proceedings (Communications, Radar and Signal Processing)*, vol.132, no.6, 447–460.

[12] J. Li, P. Stocia and Z. Wang," On robust Capon beamforming and diagonal loading," *IEEE transactions on signal processing*, vol.51, no.7, 1702–1715, 2003.

[13] S. Shahbazpanahi *et al.*,"Robust adaptive beamforming for general-rank signal models," *IEEE Transactions on Signal Processing*, vol.51, no.9, 2257–2269, 2003.

[14] A. Elnashar, S.M. Elnoubi and H.M. El-mikati, "Further study on robust adaptive beamforming with optimum diagonal loading," *IEEE Transactions on Antennas and Propagation*, vol.54, no.12, 3467–3658, 2006.

[15] A. Thakre, M. Haardt and K. Giridhar, "Single snapshot spatial smoothing with improved effective array aperture," *IEEE Signal Processing Letters*, vol.16, no.6, 505–508, 2009.

[16] V.V. Krishna, J.V. Avadhanulu, K. Giridhar and A. Paulraj,"Eigenstructure methods for direction-of-arrival estimation of frequency hop (FH) emitters," in 1990 *IEEE Conference on Military Communications*, vol.1, 1133–1137.

[17] W. Liu and S. Ding, "An efficient method to determine the diagonal loading factor using the constant modulus feature," *IEEE Transactions on Signal Processing*, vol.56, no.12, 6102–6106, 2008.

[18] L. DU, J. Li and P. Stocia, "Fully automatic computation of diagonal loading levels for robust adaptive beamforming," *IEEE Transactions on Aerospace and Electronic Systems*, vol.46, no.1, 449–458, 2010.

[19] X. Gou, Z. Liu and Y. Xu, "Fully automatic robust adaptive beamforming using the constant modulus feature," *IET Signal Processing*, vol.8, no.8, 823–830, 2014.

[20] J. Zhuang, Q. Ye, Q. Tan and A.H. Ali,"Low-complexity variable loading for robust adaptive beamforming," *Electronics Letters*, vol.52, no.5, 338–340, 2016.

[21] X. Li *et al.*,, "Robust adaptive beamforming using iterative variable loaded sample matrix inverse," *Electronics Letters*, vol.54, no.9, 546–548, 2018.

[22] J. Huang, H. Su and Y. Yang, "Robust adaptive beamforming for MIMO radar in the presence of covariance matrix estimation error and desired signal steering vector mismatch," *IET Radar, Sonar & Navigation*, vol.14, no.1, 118–126, 2020.

[23] P.R. Muduli and A. Mukherjee , "A subspace projection-based joint sparse recovery method for structured biomedical signals," *IEEE Transactions on Instrumentation and Measurement*, vol.66, no.2, 234–242, 2016.

[24] L. Chang and C.C. Yeh, "Performance of DMI and eigenspace-based beamformers," *IEEE Transactions on Antennas and Propagation*, vol.40, no. 11, 1336–1347, 1992.

[25] J.W. Kim and C.K. Un,"A robust adaptive array based on signal subspace approach," *IEEE transactions on signal processing*, vol.41, no.11, 3166–3171, 1993.

[26] L. Chang and C.C.Yeh,"Effect of pointing errors on the performance of the projection beamformer," *IEEE transactions on antennas and propagation*, vol.41, no.8, 1045–1056, 1993.

[27] D.D. Fedman and L.J. Griffiths, "A projection approach for robust adaptive beamforming," *IEEE Transactions on signal processing*, vol.42, no.4, 867–876, 1994.

[28] W.S. Youn and C.K. Un, "Robust adaptive beamforming based on the eigenstructure method,"*IEEE transactions on signal processing*, vol.42, no.6, 1543–1547, 1994.

[29] C.C. Lee and J.H. Lee,"Eigenspace-based adaptive array beamforming with robust capabilities," *IEEE Transactions on Antennas and Propagation*,vol.45, no. 12, 1711–1716, 1997.

[30] Z. Yongbo and Z. Shouhng,"A modified eigenspace-based algorithm for adaptive beamforming," in 2000 *5th International Conference on Signal Processing Proceedings*, vol.1, 468–471.

[31] A.C. Chang, C.T. Chiang and Y.H. Chen, "A generalized eigenspace-based beamformer with robust capabilities," in Proceedings 2000 *IEEE International Conference on Phased Array Systems and Technology*, 553–556.

[32] F. Huang, W. Sheng and X. Ma, "Modified projection approach for robust adaptive array beamforming," *Signal Processing*, vol.92, no.7, 1758–1763, 2012.

[33] J. Zhuang and A. Manikas, "Interference cancellation beamforming robust to pointing errors," *IET Signal Processing*, vol.7, no.2, 120–127, 2013.

[34] W. Jia et al., "Robust adaptive beamforming based on a new steering vector estimation algorithm," *Signal processing*, vol.93, no.9, 2539–2542, 2013.

[35] S.Mohammadzadeh and O. Kukrer,"Modified robust capon beamforming with approximate orthogonal projection onto the signal-plus-interference subspace," *Circuits, Systems, and Signal Processing*, vol.37, no.12, 5351–5368, 2018.

[36] S.A. Vorobyov, A.B. Gershman and Z.Q. luo, "Robust adaptive beamforming using worst-case performance optimization: A solution to the signal mismatch problem," *IEEE transactions on signal processing*, vol.51, no.2, 313–324, 2003.

[37] S.A. Vorobyov, A.B. Gershman and Z.Q. luo, "Robust adaptive beamforming using worst-case performance optimization via second-order cone programming," in 2002 *IEEE International Conference on Acoustics, Speech, and Signal Processing*, vol.3, III–2901.

[38] S.A. Vorobyov et al., "Adaptive beamforming with joint robustness against mismatched signal steering vector and interference nonstationarity," *IEEE Signal Processing Letters*, vol.11, no.2, 108–111, 2004.

[39] J. Li, P.Stoica and Z. Wang,"Doubly constrained robust Capon beamformer",*IEEE Transactions on Signal Processing*, vol.52, no.9, 2407–2423, 2004.

[40] R.G. Lorenz and S.P. Boyd,"Robust minimum variance beamforming," *IEEE transactions on signal processing*, vol.53, no.5, 1684–1696, 2005.

[41] A.beck and Y.C. Eldar,"Doubly constrained robust Capon beamformer with ellipsoidal uncertainty sets," *IEEE Transactions on signal processing*, vol.55, no.2, 753–758, 2007.

[42] S.A. Vorobyov, H. Chen and A.B. Gershman,"On the relationship between robust minimum variance beamformers with probabilistic and worst-case distortionless response constraints," *IEEE Transactions on Signal Processing*, vol.56, no.11, 5719–5724, 2008.

[43] A. Hassanien,S.A. Vorobyov and K.M. Wong,"Robust adaptive beamforming using sequential quadratic programming: An iterative solution to the mismatch problem,"*IEEE Signal Processing Letters*,vol.15, 733–736, 2008.

[44] Z.L. Yu et al., "A robust adaptive beamformer based on worst-case semi-definite programming," *IEEE Transactions on Signal Processing*, vol.58, no.11, 5914–5919, 2010.

[45] Z.L. Yu, M.H. Er and W. Ser,"A novel adaptive beamformer based on semidefinite programming (SDP) with magnitude response constraints,"*IEEE Transactions on Antennas and Propagation*, vol.56, no.5, 1297–1307, 2008.

[46] Y. Gu and A. Leshem,"Robust adaptive beamforming based on jointly estimating covariance matrix and steering vector," in 2011 *IEEE International Conference on Acoustics, Speech and Signal Processing (ICASSP)*, 2640–2643.

[47] J.P. Lie, W. Ser and C.M.S. See,"Adaptive uncertainty based iterative robust Capon beamformer using steering vector mismatch estimation," *IEEE Transactions on Signal Processing*, vol.59, no.9, 4483–4488, 2011.

[48] S.E. Nai et al., "Iterative robust minimum variance beamforming," *IEEE transactions on signal processing*, vol.59, no.4, 1601–1611, 2011.

[49] B. Liao, K.M. Tsui and S.C. Chan,"Robust beamforming with magnitude response constraints using iterative second-order cone programming," *IEEE Transactions on Antennas and Propagation*, vol.59, no.9, 3477–3482, 2011.

[50] A. Khabbazibasmenj, A.S. Vorobyov and A. Hassanien,"Robust adaptive beamforming based on steering vector estimation with as little as possible prior information," *IEEE Transactions on signal processing*, vol.60, no.6, 2974–2987, 2012.

[51] B. Liao, S.C. Chan and K.M. Tsui, "Recursive steering vector estimation and adaptive beamforming under uncertainties," *IEEE Transactions on Aerospace and Electronic Systems*, vol.49, no.1, 489–501, 2013.

[52] A.P. Guimaraes et al., "A (very) brief survey on optimization methods for wireless communication systems," in 2010 *International Telecommunications Symposium*, vol.7, 1–8.

[53] S. Yi, Y. Wu and Y. Wang, "Projection-based robust adaptive beamforming with quadratic constraint," *Signal Processing*, vol.122, 65–74, 2016.

[54] J. Zhuang et al., "Robust adaptive beamforming with minimum sensitivity to correlated random errors," *Signal Processing*, vol.131, 92–98, 2017.

[55] B. Liao,"Robust adaptive beamforming with precise main beam control," *IEEE Transactions on Aerospace and Electronic Systems*, vol.53, no.1, 2017.

[56] Y. Gu and A. Leshem,"Robust adaptive beamforming based on interference covariance matrix reconstruction and steering vector estimation," *IEEE Transactions on Signal Processing*, vol.60, no.7, 3881–3885, 2012.

[57] Z. lu et al., "Interference covariance matrix reconstruction via steering vectors estimation for robust adaptive beamforming," *Electronics Letters*, vol.49, no.22, 1373–1374, 2013.

[58] H. Ruan R.C.De Lamare, "Robust adaptive beamforming using a low-complexity shrinkage-based mismatch estimation algorithm," *IEEE Signal Processing Letters*, vol.21, no.1, 60–64, 2013.

[59] Y. Gu et al., "Robust adaptive beamforming based on interference covariance matrix sparse reconstruction," *Signal Processing*, vol.96, 375–381, 2014.

[60] F. Shen, F. chen and J. Song,"Robust adaptive beamforming based on steering vector estimation and covariance matrix reconstruction," *IEEE Communications Letters*, vol.19, no.9, 1636–1639, 2015.

[61] L. Huang et al., "Robust adaptive beamforming with a novel interference-plus-noise covariance matrix reconstruction method ," *IEEE Transactions on Signal Processing*, vol.63, no.7, 1643–1650, 2015.

[62] Z. ZHang et al., "Interference-plus-noise covariance matrix reconstruction via spatial power spectrum sampling for robust adaptive beamforming," *IEEE Signal Processing Letters*, vol.23, no.1, 121–125, 2015.

[63] Y. Zhang, Y. Li and M. Gao, "Robust adaptive beamforming based on the effectiveness of reconstruction," *Signal Processing*, vol.120, 572–579, 2016.

[64] X. Yuan and L. Gan,"Robust adaptive beamforming via a novel subspace method for interference covariance matrix reconstruction," *Signal Processing*, vol.130, 233–242, 2017.

[65] C. Zhou et al., "A robust and efficient algorithm for coprime array adaptive beamforming," *IEEE Transactions on Vehicular Technology*, vol.67, no.2, 1099–1112, 2018.

[66] Z. Zhang et al., "Robust adaptive beamforming via simplified interference power estimation," *IEEE Transactions on Aerospace and Electronic Systems*, vol.55, no.6, 3139–3152, 2019.

[67] W. Liu and S. Weiss, *Wideband beamforming: concepts and techniques*, John Wiley & Sons, vol.17, 2010.

[68] H.L. Van Trees, *Optimum array processing: Part IV of Detection, estimation, and modulation theory*, New York, Wiley 2002.

[69] J. Capon, "High-resolution frequency-wavenumber spectrum analysis", in 1969 *Proc.of IEEE*, vol.57, no.8, 1408–1418.

[70] Y. Selen, R. Abrahamsson and P. Stocia,"Automatic robust adaptive beamforming via ridge regression,", *Signal Processing*, vol.88, 33-49, 2007.

[71] A. Elnashar, S. Elnoubi and H. Elmikati, "A robust quadratically constrained adaptive blind multiuser receiver for cellular DS/CDMA systems," in 2004 *Eighth IEEE International Symposium on Spread Spectrum Techniques and Applications-Programme and Book of Abstracts (IEEE Cat. No. 04TH8738)*, 164–168.

[72] K.L. Bell, Y. Ephraim and H.L. Van Trees, "A Bayesian approach to robust adaptive beamforming," *IEEE Transactions on Signal Processing*, vol.48, no.2, 386–398, 2000.

[73] W. Zhang, S. Wu and J. Wang, "Robust Capon beamforming in presence of large DOA mismatch," *Electronics Letters*, vol.49, no.1, 75–76, 2013.

[74] Y. Huang, M. Zhou and S.A. Vorobyov,"New designs on MVDR robust adaptive beamforming based on optimal steering vector estimation," *IEEE Transactions on Signal Processing*, vol.67, no.14, 3624–3638, 2019.

[75] S. Mohammadzadeh and O. Kukrer, "Adaptive beamforming based on theoretical interference-plus-noise covariance and direction-of-arrival estimation", *IET Signal Processing*, vol.12, no.7, 819–825, 2018.

[76] S. Barratt and S. Boyd, "Least squares auto-tuning", *Engineering Optimization*, vol.53, no.5, 789–810, 2021.

[77] J. Li and P. Stoica, *Robust Adaptive Beamforming*, Hoboken,Wiley Online Library, 2006.

[78] L. Du et al., "Review of user parameter-free robust adaptive beamforming algorithms," *Digital Signal Processing*, vol.19, no.4, 567–582, 2009.

[79] S.A. Vorobyov, "Principles of minimum variance robust adaptive beamforming design," *Signal Processing*, vol.93, 3264–3277, 2013.

[80] H. Wan et al., "Robust beamforming against direction-of-arrival mismatch via signal-to-interference-plus-noise ratio maximization", in 2017 *9th International Conference on Wireless Communications and Signal Processing (WCSP)*, 1–5.

[81] R. Wu, Z. Wao and Y. Ma,"Control of peak sidelobe level in adaptive arrays," *IEEE Transactions on Antennas and Propagation*, vol.44, no.10, 1341–1347, 1966.

[82] W. Wang, R. Wu and J. Liang, "A novel diagonal loading method for robust adaptive beamforming" *Progress In Electromagnetics Research*, vol.18, 245–255, 2011.

[83] P. Stoica , Z. Wang and J. Li, "Robust Capon beamforming," *IEEE signal processing Letters*, vol.10, no.6, 172–175, 2003.

[84] B. Liao et al., "A robust beamformer with main beam control" in 2016 *IEEE Sensor Array and Multichannel Signal Processing Workshop (SAM)*, 1–5.

[85] F.L. Liu et al., "Robust MVDR beamformer for nulling level control via multi-parametric quadratic programming," *Progress In Electromagnetics Research*, vol.20, 239–254, 2011.

[86] J.R. Guerci, "Theory and application of covariance matrix tapers for robust adaptive beamforming" *IEEE Transactions on Signal Processing*, vol.47, no.4, 977–985, 1999.

[87] R. Li, Y. Wang and S. Wan,"Research on adaptive pattern null widening techniques" *Modern Radar*, vol.25, no.2, 42–45, 2003.

[88] S. Wu, J. Zhang, and S. Zhang,"Research on beamforming of wide nulling algorithm," *Journal of Harbin Engineering University*, vol.25, no.5, 658–661, 2004.

[89] Z.Q. Xing, "Transmitting beamforming technique with widen null based on zero space," *Communications Technology*, vol.40, no.11, 22–24, 2007.

[90] F. Liu et al., "A robust adaptive control method for widening interference nulls' in 2009 " *IET International Radar conference*, 1–4.

[91] X. Yang et al.,"Adaptive null broadening method in wideband beamforming for rapidly moving interference suppression," *Electronics Letters*, vol.54, no.16, 1003–1005, 2018.

[92] Z. Liu et al.,"Robust adaptive beamforming for sidelobe canceller with null widening," *IEEE Sensors Journal*, vol.19, no.23, 11213–11220, 2019.

[93] Z. Liu, H. Su and Q. Hu, "Robust sidelobes cancellation algorithm with null broadening" *Journal of Electronics and Information Technology*, vol.38, no.3, 565–569, 2016.

[94] R.J. Mailloux, "Covariance matrix augmentation to produce adaptive array pattern troughs," *Electronics Letters*, vol.31, no.10, 771–772, 1995.

[95] M. Zatman, "Production of adaptive array troughs by dispersion synthesis," *Electronics Letters*, vol.31, no.25, 2141–2142, 1995.

[96] G. Ram et al., "Optimal design of timed antenna arrays for SLL reduction, dual and multiple broad nulls in the radiation pattern," *IETE Technical Review*, vol.37, no.6, 622–631, 2020.

[97] R.T. Rockafellar,"Lagrange multiplies and optimality," *SIAM review*, vol.35, no.35, 183-238, 1993.

[98] D.P. Bertsekas,"Constrained optimization and lagrange multiplier methods," *Academic press*, New York, 2014.

[99] L. Vandenberghe and S. Boyd, "Semidefinite programming," *SIAM review*, vol.38, no.1, 49–95, 1996.

[100] Z.Q. Luo, "Semidefinite relaxation of quadratic optimization problems and applications," *IEEE Signal Processing Magazine*, vol.1053, no.5888, 2010.

[101] *CVX: Matlab software for disciplined convex programming version 2.1.*(2014). Available:http://cvxr.com/cvx

[102] K. Kim et al., "A fast minimum variance beamforming method using principal component analysis," *IEEE transactions on ultrasonics, ferroelectrics, and frequency control*, vol.61, no.6, 930–945, 2014.

[103] A.C. Jensen and A. Austeng, "An approach to multibeam covariance matrices for adaptive beamforming in ultrasonography," *IEEE transactions on ultrasonics, ferroelectrics, and frequency control*, vol.59, no.6, 1139–1148, 2012.

[104] F. Vignon and M. R. Burcher, "Capon beamforming in medical ultrasound imaging with focused beams," *IEEE transactions on ultrasonics, ferroelectrics, and frequency control*, vol.55, no.3, 619–628, 2008.

[105] B. Patnaik and P.K. Sahu, "Inter-satellite optical wireless communication system design and simulation," *IET Communications*, vol.6, no.16, 2561–2567, 2012.

[106] P. Somanath, P.K. Sahu, R. Kumar and B. Patnaik, "Inter-satellite optical wireless communication system design using diversity techniques," in 2015 *international conference on microwave, optical and communication engineering (ICMOCE)*, 250–253.

[107] D. Dardari, M. Luise and E. Falletti, “Satellite and terrestrial radio positioning techniques: a signal processing perspective,” *Academic Press*, 2011.

[108] Y. Wei, C. Arnold and J. Hong, "Multiport beamforming system based on reconfigurable waveguide phased antenna array for satellite communication applications," *IEEE Access*, vol.11, no.3, 29909–29917, 2023.

[109] R.D. Gaudenzi, F. Giannetti and M. Luise, "Advances in satellite CDMA transmission for mobile and personal communications," in 1996 *Proceedings of the IEEE*, vol.84, no.1, 18–39.

[110] A.L. Swindlehurst, "Applications of array signal processing," *Academic Press Library in Signal Processing*, vol.3, 859–953, 2014.

[111] N. Purswani, H. Singh and R. M. Jha, "Active cancellation of probing in the presence of multiple coherent desired radar sources," in 2009 *Applied Electromagnetics Conference (AEMC)*, 1–4.

[112] H. Singh and R.M. Jha, "Algorithm for suppression of wideband probing in adaptive array with multiple desired signals," *Defence Science Journal*, vol.61, no.4, 325–330, 2011.

[113] J. Liu et al., "Adaptive beamforming with sidelobe control: A second-order cone programming approach," *IEEE Signal Processing Letters*, vol.10, no. 11, 331–334, 2003.

[114] S.K. Goudos, "Pareto optimal design of dual-band base station antenna arrays using multi-objective particle swarm optimization with fitness sharing," *IEEE Transactions on Magnetics*, vol.45, no.3, 1522–1525, 2009.

[115] Z.D. Zaharis, C. Skeberis and T. Xenos, "Improved antenna array adaptive beamforming with low side lobe level using a novel adaptive invasive weed optimization method," *Progress In Electromagnetics Research*, vol.124, 137–150, 2012.

[116] Z.D. Zaharis, K. Gotsis and J. Sahalos, "Adaptive beamforming with low side lobe level using neural networks trained by mutated boolean PSO," *Progress In Electromagnetics Research*, vol.127, 139–154, 2012.

[117] Z.D. Zaharis et al., "Design of a novel antenna array beamformer using neural networks trained by modified adaptive dispersion invasive weed optimization based data," *IEEE Transactions on Broadcasting*, vol.59, no. 3, 455–460, 2013.

[118] K. Yang et al., "Robust adaptive beamforming using an iterative FFT algorithm," *Signal processing*, vol.96, 253–260, 2014.

[119] A. Sharma and S. Mathur, "A novel adaptive beamforming with reduced side lobe level using GSA," *COMPEL-The international journal for computation and mathematics in electrical and electronic engineering*, vol. 37, no.6, 2263–2278, 2018.

[120] K. Yang et al., "Robust adaptive beamforming with low sidelobe levels," in 2013 *IEEE Antennas and Propagation Society International Symposium (APSURSI)*, 872–873.

[121] P. Li et al., "Robust adaptive beamforming with sidelobe controlled based on improved objective function," in 2019 *International Applied Computational Electromagnetics Society Symposium-China (ACES)*, vol.1, 1–2.

[122] I.P. Gravas et al., "Adaptive beamforming with sidelobe suppression by placing extra radiation pattern nulls," *IEEE Transactions on Antennas and Propagation*, vol.67, no.6, 3853–3862, 2019.

[123] M. Zhou, "Weighted subspace-constrained adaptive beamforming for sidelobe control," *IEEE Communications Letters*, vol.23, no.3, 458–461, 2019.

[124] A.F. Gemechu et al., "Beampattern synthesis with sidelobe control and applications," *IEEE Transactions on Antennas and Propagation*, vol.68, no.1, 297–310, 2020.

[125] S. A. Hamza and M.G. Amin, "Hybrid sparse array beamforming design for general rank signal models," *IEEE Transactions on Signal Processing*, vol.67, no.24, 6215–6226, 2019.

[126] S.A. Hamza,"Sparse Array Beamformer Design for Active and Passive Sensing," Ph.D. dissertation, Villanova University, 2020.

[127] D.Ghosh et al., "Dictionary design for sparse signal representations using K-SVD with sparse bayesian learning," in 2012 *IEEE 11th International Conference on Signal Processing*, vol.1, 21–25.

[128] A. Deligiannis, M. Amin, S. Lambotharan and G. Fabrizio, "Optimum sparse subarray design for multitask receivers," *IEEE Transactions on Aerospace and Electronic Systems*, vol.2, 939–950, 2018.

[129] A.F. Molisch & Z.M Win,"MIMO systems with antenna selection," *IEEE microwave magazine*, vol.5, no.1, 46–56, 2004.

[130] S. Sanayei, S. & A. Nosratinia," Antenna selection in MIMO systems," *IEEE Communications magazine*, vol. 42, no. 10, 68–73, 2004.

[131] S.R. Shebert et al., "Multi- signal classification using deep learning and sparse arrays," in 2022 *IEEE Military Communications Conference (MILCOM)*, 1-–6.

[132] R. Cohen and Y.C. Eldar, "Sparse array design via fractal geometries," *IEEE transactions on signal processing*, vol.68, 4797–4812, 2020.

[133] M. Wax & Y. Anu,"Performance analysis of the minimum variance beamformer". *IEEE Transactions on Signal Processing*, vol. 44, no. 4, 928–937,2004.

[134] A. Gorokhov, D.A. Gore & A.J. Paulraj, "Receive antenna selection for MIMO spatial multiplexing: theory and algorithms," *IEEE Transactions on Signal Processing*, vol. 51, no. 11, 2796–2807, 2003.

[135] S.E. Nai et al.,"Beampattern synthesis for linear and planar arrays with antenna selection by convex optimization," *IEEE Transactions on Antennas and Propagation*, vol. 58, no. 12, 3923–3930, 2010.

[136] X. Wang, M.S. Greco & F. Gini, "Adaptive sparse array beamformer design by regularized complementary antenna switching", *IEEE Transactions on Signal Processing*, vol. 69, 2302–2315, 2021.

[137] N.B. Mehta, S. Kashyap, & A.F. Molisch, "Antenna selection in LTE: From motivation to specification," *IEEE Communications Magazine*, vol. 50, no. 10, 144–150, 2012.

[138] X. Wang, M. Amin, & X. Wang, "Robust sparse array design for adaptive beamforming against DOA mismatch,"*Signal Processing*, vol. 146, 41–49, 2018.

[139] X. Wang, M. Amin, & X. Cao, "Analysis and design of optimum sparse array configurations for adaptive beamforming," *IEEE Transactions on Signal Processing*, vol. 66, no. 2, 340–351, 2017.

[140] Z. Zheng et al., "Sparse Array Design for Adaptive Beamforming via Semidefinite Relaxation," *IEEE Signal Processing Letters*, vol. 27, 925–929, 2020.

[141] R. Compton, "The bandwidth performance of a two-element adaptive array with tapped delay-line processing," *IEEE Transactions on Antennas and Propagation*, vol.36, no.1, 5–14, 1988.

[142] F. Vook and R. Compton, "Bandwidth performance of linear adaptive arrays with tapped delay-line processing," *IEEE Transactions on Aerospace and Electronic Systems*, vol.28, no.3, 901–908, 1992.

[143] O. L. Frost, "An algorithm for linearly constrained adaptive array processing," *Proceedings of the IEEE*, vol. 60,no. 8, 926–935,1972.

[144] Y. Zhao , W. Liu, and R.J. Langley, "Adaptive wideband beamforming with frequency invariance constraints," *IEEE Transactions on Antennas and Propagation*, vol. 59, no. 4, 1175–1184, 2011.

[145] Y. Zhao and W. Liu, "Robust wideband beamforming with frequency response variation constraint subject to arbitrary norm-bounded error," *IEEE Transactions on Antennas and Propagation*, vol. 60, no. 5, 2566–2571,2012.

[146] B. K. Mathai, S. Gopi, and R. Pradeepa, "A recursive algorithm for robust wideband adaptive beamforming," *in 2013 International Conference on Communication and Signal Processing*, 1043–1047, 2013.

[147] D. B. Fogel, "The advantages of evolutionary computation," in *Biocomputing and Emergent Computation (BCEC)*, 1003–1005, 1997.

[148] A. Khunteta and D. Ghosh, "Edge detection via fuzzy rule-based edge strength estimation and optimal threshold selection using PSO," in 2013 *8th International Conference on Industrial and Information Systems*, 560–565, 2013.

[149] M. K. Khawaldeh and D. I. Abu-Al-Nadi, "Design of wideband beamforming using particle swarm optimization," in *International Multi-Conference on Systems, Signals & Devices*, 1–5, 2012.

[150] M. K. Khawaldeh and S. Khawaldeh, "Design of optimal beamforming using particle swarm optimization," *International Journal of Computer Applications*, vol. 174, 1–8, 2017.

[151] R. Eberhart and J. Kennedy, "Particle swarm optimization," in *Proceedings of the IEEE international conference on neural networks*, 1942–1948, 1995.

[152] Z.H. Zhan, J. Zhang, Y. Li, and Y.-H. Shi, "Orthogonal learning particle swarm optimization," *IEEE transactions on evolutionary computation*, vol. 15, no. 6, 832–847, 2010.

[153] Z.S.Y. Ho, H.S. Lin, W.H. Liauh and S.J. Ho, "OPSO: Orthogonal particle swarm optimization and its application to task assignment problems," *IEEE Transactions on Systems, Man, and Cybernetics-Part A: Systems and Humans*, vol. 38, no. 2, 288–298, 2008.

[154] S. A. Dianat and E. Saber, "Advanced linear algebra for engineers with Matlab," *CRC Press*, ch. 3-4, 2009.

[155] L. T. Al Bahrani, J. C. Patra, and R. Kowalczyk, "Orthogonal PSO algorithm for optimal dispatch of power of large-scale thermal generating units in smart power grid under power grid constraints," in *International Joint Conference on Neural Networks (IJCNN)*, 660–667, 2016.

[156] Y. Wei, C. Arnold, J. hong and J. Rao, "Reconfigurable wideband linear-polarized and dual left/right-hand circularly-polarized waveguide antennas for beamforming antenna array," in *2022 16th European Conference on Antennas and Propagation (EuCAP)*, 1–5, 2022.

[157] R. Xu, Z. Shen and S.S. Gao, "Compact-size ultra-wideband circularly polarized antenna with stable gain and radiation pattern," *IEEE Transactions on Antennas and Propagation*, vol. 70, no. 2, 943–952, 2021.